Tuned to Perfection: Ironing Out the Defects in Metal-Organic Framework UiO-66

Supporting information

Tuned to Perfection: Ironing out the Defects in Metal-Organic Framework UiO-66

Greig C. Shearer, † Sachin Chavan, † Jayashree Ethiraj, ‡ Jenny G. Vitillo, ‡ Stian Svelle, † Unni Olsbye, † Carlo Lamberti, ‡ Silvia Bordiga, ‡ Karl Petter Lillerud*.†

† inGAP Center of Research Based Innovation, Department of Chemistry, University of Oslo, P.O. Box 1033, Blindern, 0315 Oslo

‡ Department of Chemistry, NIS - INSTM Reference Center, University of Turin, Via G. Quarello 15 I-10135 Torino, Italy

Table of Content

A) Details of Synthesis, Washing, and Exchange procedures

The crude UiO-66 samples were synthesized by sequentially adding 3.78 g $ZrCl_4$ (16.2 mmol), 2.86 ml 35 % HCl (32.4 mmol), and H_2BDC (quantities in next sentence) to a 250 ml conical flask containing 97.4 ml of N,N'-dimethyl formamide (1260 mmol). Five different masses of H_2BDC (2.70, 3.37, 4.04, 4.72, and 5.39 g, corresponding to 16.3, 20.3, 24.3, 28.4, and 32.4 mmol respectively) were used in this work, such that the respective BDC:Zr molar ratios in the synthesis solutions were 1:1, 5:4, 3:2, 7:4, or 2:1. **Table S1** summarizes the quantities of each reagent used for each BDC:Zr ratio. The synthesis mixtures were stirred until the solutions were completely transparent before being transferred to 200 mL Teflon liners and sealed in stainless steel autoclaves where they were heated to either 100, 160, or 220 °C for 20 hours. The resulting microcrystalline powders were separated from the solvent by centrifugation and dried overnight in an oven set to 60 °C. The resulting, unwashed material is hereafter labelled as "crude".

Table S1: Molar ratios and gram quantities of the synthesis reagents used. All five synthesis mixtures (each differing only by their BDC:Zr molar ratio) were used at three different temperatures (100 °C, 160 °C, and 220 °C).

	Molar Equivalents (w.r.t $ZrCl_4$) / Mass added (g)			
BDC : Zr	**$ZrCl_4$**	**H_2BDC**	**35 % HCl**	**DMF**
1 : 1	1 / 3.78	1.00 / 2.70	2 / 3.38	77.5 / 91.9
5 : 4	"	1.25 / 3.37	"	"
3 : 2	"	1.50 / 4.04	"	"
7 : 4	"	1.75 / 4.72	"	"
2 : 1	"	2.00 / 5.39	"	"

DMF washes were typically performed on 3-5 grams of crude material. Samples were stirred in 120 mL DMF at 100 °C for 150 minutes, separated from the solvent by centrifugation, and dried overnight in an oven set to 60 °C. A small portion of the resulting material (labelled with suffix – DMF) was submitted for TGA characterization, while the rest was washed a second time by the same procedure, yielding the materials labelled with the suffix -2DMF.

Methanol exchange was performed on 1-1.5 grams of 2xDMF washed material. In separate experiments, samples were added to extraction thimbles which were subsequently placed in the main chamber of a soxhlet extractor. The extractor was then connected to a condenser and a 250 mL round bottom flask containing 200 mL of methanol. The round bottom flask was immersed

in an oil bath and heated to 130 °C for 18 hours, while cold water flowed through the condenser. After the extraction period, the thimble was removed from the extractor and the material was allowed to dry in air.

B) Further Methods and Characterization Details

Thermal Stability Tests

In each test, 30 mg of MOF sample was added to an alumina crucible and placed in a regular muffle furnace where they were heated (1 °C/min) at the desired temperature for 12 hours in air before being allowed left to cool to room temperature. After treatment, the entire remains of the sample (always less than the 30 mg starting weight) was then placed on a flat glass plate PXRD sample holder of 2.5 cm diameter. The material was then flattened, spread, and sealed with plastic film before PXRD measurement. The film is evident in the PXRD patterns, diffracting at $2\theta = 20\text{-}25$.

PXRD

PXRD patterns not related to thermal stability tests (e.g. those presented in the study of the forbidden reflections (section D) and in part 2 of the appendix) were collected on samples prepared on a different type of sample holder. These sample holders are also of 2.5 cm diameter but with a 1mm hollow, such that a substantial amount of material is required to fill them.

All powder X-ray diffraction patterns were collected on a Bruker D8 Discovery diffractometer equipped with a focusing Ge-monochromator, using Cu-K_α radiation(xx=1.5418 Å) and Bruker LYNXEYE detector. Patterns were collected in reflectance Bragg-Brentano geometry in the 2θ range from 2 to 50°.

TGA-DSC

Measurements were made with a Stanton Redcroft TGA-DSC, in which ca. 30 mg of powdered sample was loaded inside a platinum crucible. Samples were heated to 900 °C at a rate of 5 °C per minute while exposed to a continuous flow of both N_2 (20 mL/min) and O_2 (5 mL/min).

Nitrogen Sorption Measurements

Nitrogen sorption measurements were performed on a BelSorp mini II instrument at 77 K. All samples were measured in 9.001 cm^3 glass cells. Prior to adsorption measurements the (methanol exchanged) samples were pretreated (activated) under vacuum for 1h at 60°C and 2 h at 150°C. Brunauer–Emmett–Teller (BET) and Langmuir surface areas were calculated by fitting the isotherm data in the p/p_0 range 0 - 0.1, meeting the consistency criteria outlined by Watson and Snurr.[1]

Simulations of Nitrogen Adsorption Isotherms

Adsorption isotherms are calculated with the "Sorption tool" in Accelrys Materials Studio version 7.01. The adsorptive is a geometry optimized N_2 molecule and the temperature used is 77 K. The method is set to Metropolis, we use the COMPASS force field and charges are force field assigned. Summation methods used; electrostatic is Ewald & group based while van der Waals forces are calculated atom based. No constraints are assigned. The isotherms are calculated from 0.1 to 100 kPa with 50 fugacity steps distributed logarithmically to have more points in the steep initial portion of the isotherm. The overall quality was calculated with both "Normal" and "Fine" settings. The "Normal" setting uses 10,000 equilibration steps and 100,000 production steps while the "Fine" setting uses 100,000 equilibration steps and 1,000,000 production steps. Using the "Fine" settings invariably provides a higher calculated surface area due to the fact that there are more attempts to add a new nitrogen molecule. Due to the statistical nature of the calculations, we observe a small spread in the calculated values when they are repeated. Brunauer–Emmett–Teller (BET) surface areas were calculated from the simulated isotherms by fitting them in the p/p_0 range 0 - 0.1.

Dissolution / Liquid ^{1}H NMR Spectroscopy

Prior to measurement, samples were digested over a period of 24 hours by adding 600 uL of a 1M NaOH in D_2O solution to an NMR tube containing 20 mg of MOF. This hydroxide based procedure dissolves only the organic portion of the material (linker and pore filling solvent), while the inorganic component of the MOF sinks to the bottom as ZrO_2 and is not measured. The liquid ^{1}H NMR spectra were recorded on a Bruker Avance DPX-300 NMR Spectrometer (300 MHz). The relaxation delay (d1) was set to 20 seconds to ensure that reliable integrals were obtained, allowing for the relative concentrations of the various organic species to be accurately determined. The number of scans was 64.

In situ DRIFTS

Prior to measurement, the powdered samples were mixed with KBr before being pressed and ground and passed through sieves in order to obtain particle sizes which ranged 212-425 μm. Approximately 30 mg of these particles were used for measurement.

In situ DRIFTS was performed at 2 cm^{-1} resolution using a Bruker Vertex 70 FTIR spectrometer equipped with an MCT detector and a Praying Mantis high temperature reaction chamber (Harrick Scientific pro.). Samples were heated to 250 °C (5 °C/minute) under a continuous 40 ml min^{-1} N_2 flow while spectra were recorded *in situ*. The background spectrum was obtained using KBr as a non-absorbing standard.

Elemental Analysis via EDS

EDS was performed on a FEI Quanta 200 FEG-ESEM equipped with an EDAX Na EDS detector. Samples were prepared by smearing them onto carbon tape. Spectra were acquired for 100 seconds at an accelerating voltage of 20 keV.

Raman Spectroscopy

Samples were prepared as self supporting wafers which were then loaded in a homemade Raman cell equipped with quartz windows, where they were activated at 150 °C for 2h under vacuum before measurement. Raman spectra were recorded on a Renishaw inVia Raman microscope spectrometer. A diode laser emitting 785 nm was used, photons scattered by the sample were dispersed by a 1200 lines/mm grating monochromator and were simultaneously collected on a CCD camera; the collection optic was set at 20X objective. Raman spectrum was collected in range of 3200-100 cm^{-1}. The spectra were collected at 1% Laser power with 100 acquisitions of 20 seconds each.

Simulation of the Raman Spectrum of ideal UiO-66

Simulation of the Raman spectrum was performed with the CRYSTAL ab initio code.[2] The Hamiltonian is B3LYP. All electron basis sets were used for Zr, O, C, and H atoms; they consist of (8s)-(7631sp)-(621d), (8s)-(411sp)-(1d), (6s)-(31sp)- (1d), and (31s)-(1p), respectively. All parameters except shrinking factor (here raised to 3 from the original value of 2) are the same as in the previous work of Valenzano et al.[3] Raman intensities have been computed through a newly implemented, entirely analytical procedure.[4] A Lorentzian broadening of 5 cm^{-1} has been adopted. Frequencies have been shifted by a factor of 0.98 to compensate for the well known DFT overestimation effect.

C) Thermal Stability Test Results of Entire Series

Used as an explanation of how the data in **Figure S2** is derived, **Figure S1** displays the results of the thermal stability tests performed on UiO-66-220-2:1-2DMF. The "% Crystallinity" presented on the y-axis of **Figure S1b** was derived by taking the area of the (111) peak (highlighted on **Figure S1a**) at each treatment temperature. The data was then normalized such that the (111) peak area of the pattern collected on the untreated sample (top curve in **Figure S1a**) equated to "100 % crystallinity", representing the initial crystallinity of the material.

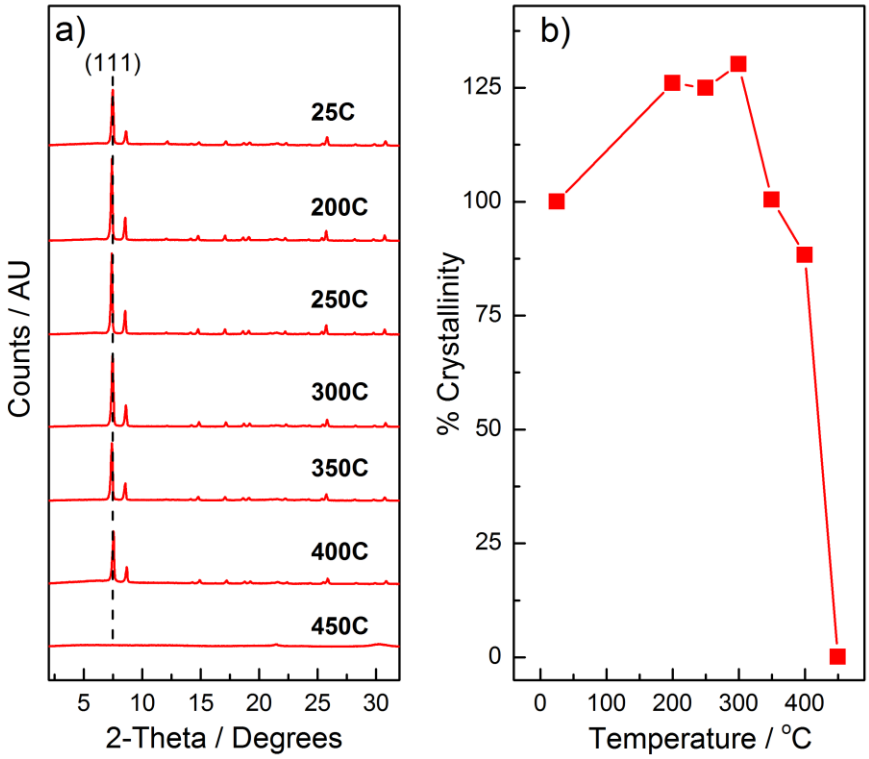

Figure S1: a) Thermal stability tests of UiO-66-220-2:1-2DMF (same data as presented in **Figure 1c** in the main article); b) plot (derived from the data presented in part a) of the normalized peak area of the (111) reflection (denoted as "% Crystallinity") against the treatment temperature. The (111) reflection is highlighted on part a) of the figure.

Visual comparison with the raw PXRD data in **Figure S1** shows that the method of representation used in part b essentially condenses said data while preserving the information. The evolution of the crystallinity of the sample is in fact even more obvious in **Figure S1b**: it can clearly be seen that the crystallinity of the sample improves at moderate temperatures, diminishes slightly in the 350-400 °C range, and completely collapses at 450 °C. The increase in crystallinity at moderate temperatures was not mentioned in the main article and is believed to be due to the loss of disordered solvent which ordinarily occupies a significant portion of the electron density of the material.

The method used to plot **Figure S1b** was employed for all 45 (15 crude, 15 twice DMF washed, and 15 methanol exchanged) samples studied, allowing their thermal stabilities to be easily compared in a single figure, **Figure S2**. The 45 individual PXRD thermal stability plots (resembling **Figure S1a**) from which **Figure S2** is derived are available as **Figures S23-67** in the appendix.

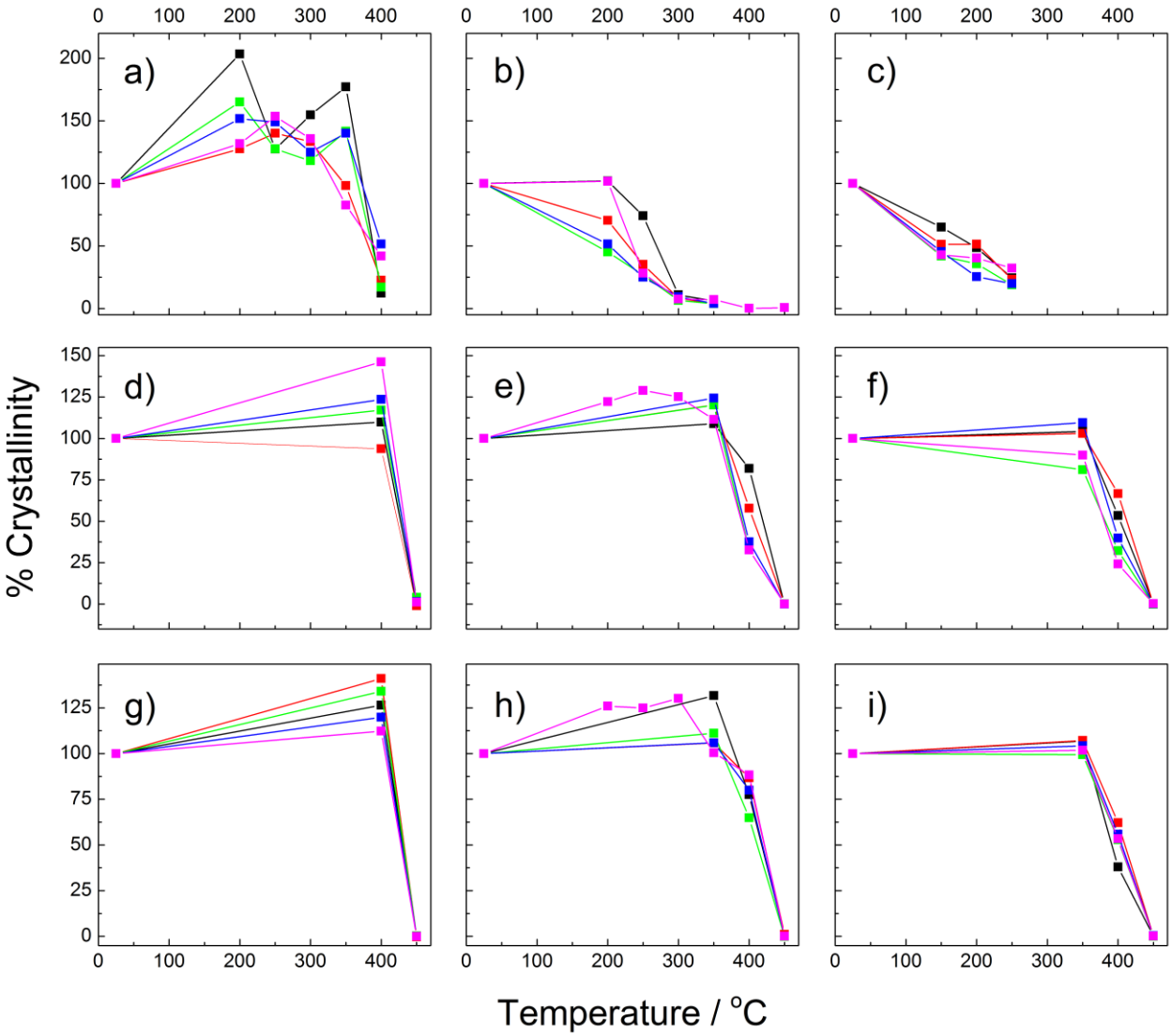

Figure S2: % Crystallinity vs Temperature plots of: UiO-66 samples synthesized at 100 °C; a) Crude, b) Twice DMF washed, c) Methanol exchanged. Synthesized at 160 °C; d) Crude, e) Twice DMF washed, f) Methanol exchanged. Synthesized at 220 °C: g) Crude, h) Twice DMF Washed, i) Methanol exchanged. Throughout the figure, the BDC:Zr ratio used in the synthesis is represented by the color of the line/points: 1:1 (black), 5:4 (red), 3:2 (green), 7:4 (blue), and 2:1 (magenta). See **Figure S1** and associated text for an explanation of how these plots were derived from PXRD data.

The figure is organized such that if the materials are washed increasingly thoroughly when observing the plots from left to right. Data recorded on crude, twice DMF washed, and methanol exchanged samples are shown in the left, middle, and right columns respectively. The synthesis temperature increases down the column such that the top, middle, and bottom rows represent samples synthesized at 100, 160, and 220 °C respectively. The BDC:Zr ratio used in the synthesis mixture is represented by the same color code throughout the figure: black, red, green, blue, and magenta curves correspond to samples synthesized with BDC:Zr ratios of 1:1, 5:4, 3:2, 7:4, and 2:1 respectively.

Figure S2 evidences the three conclusions presented in the main article:

1) Samples synthesized at higher synthesis temperatures are more thermally stable.

2) The materials become increasingly unstable with washing.

3) The thermal stability of the samples does not vary significantly or systematically with the BDC:Zr ratio used in the synthesis.

Conclusion 1) can be arrived at when viewing the plots from top to bottom, where it is seen that the stability of the samples gradually improves. Conclusion 2) is reached by viewing the plots from left to right where the stability of the samples is found to gradually worsen. Conclusion 3) is evidenced by the lack of significant or systematic spread in the paths of the different colored lines.

D) PXRD - Forbidden Reflections

The forbidden reflection region of PXRD patterns recorded on all the crude UiO-66 samples is displayed in **Figure S3**:

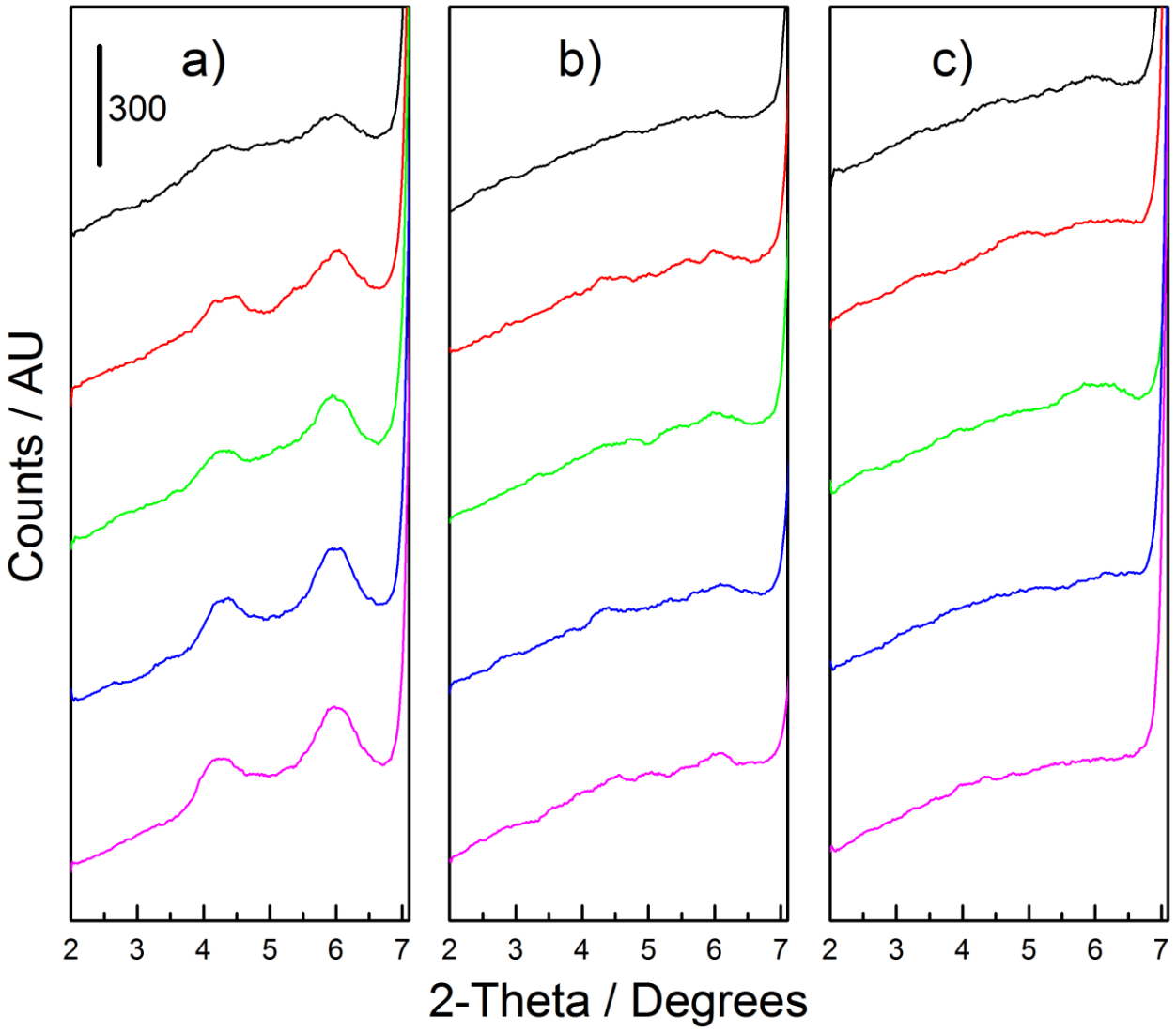

Figure S3: Forbidden reflection region of PXRD patterns recorded on crude (unwashed) UiO-66 samples synthesized at: a) 100 °C, b) 160 °C, and c) 220 °C. Throughout the figure, the BDC:Zr ratio used in the synthesis is represented by the color of the curve: 1:1 (black), 5:4 (red), 3:2 (green), 7:4 (blue), and 2:1 (magenta). The same y-scale is applied to all three plots.

Part a) of the figure demonstrates that the forbidden reflections (appearing at 2θ = 4.2, and 6.0) are prominent in the PXRD patterns of the samples synthesized at 100 °C, and that they are essentially non-existent in the samples synthesized at higher temperatures.

The following three figures demonstrate how the forbidden reflections are affected as the materials are increasingly thoroughly washed. Data related to samples synthesized at 100 °C, 160 °C, and 220 °C is displayed in **Figures S4, S5, and S6** respectively:

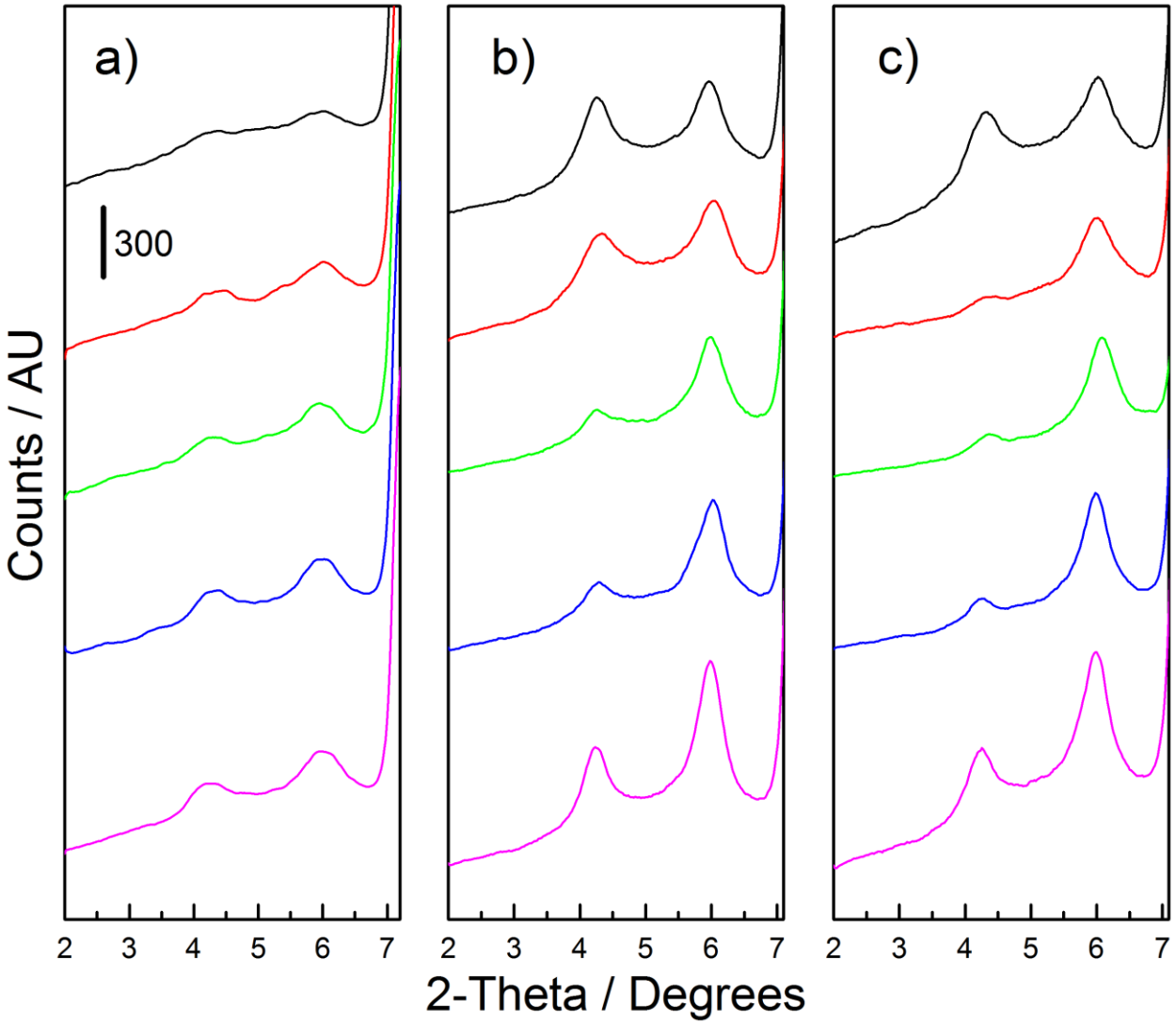

Figure S4: Forbidden reflection region of PXRD patterns recorded on UiO-66 samples synthesized at 100 °C: a) Crude (unwashed), b) Twice DMF washed, and c) Methanol Exchanged. Throughout the figure, the BDC:Zr ratio used in the synthesis is represented by the color of the curve: 1:1 (black), 5:4 (red), 3:2 (green), 7:4 (blue), and 2:1 (magenta). The same y-scale is applied to all three plots.

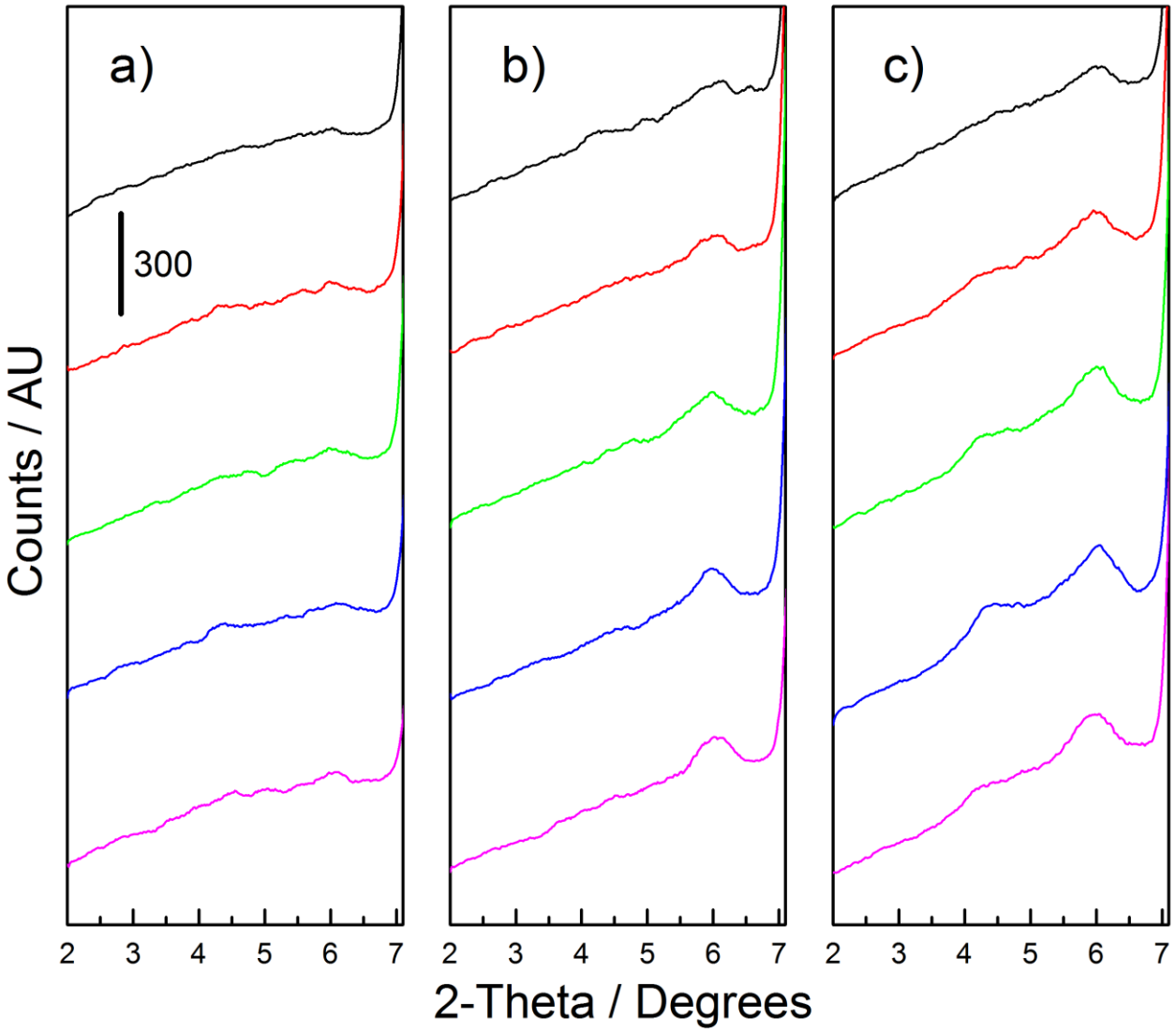

Figure S5: Forbidden reflection region of PXRD patterns recorded on UiO-66 samples synthesized at 160 °C: a) Crude (unwashed), b) Twice DMF washed, and c) Methanol Exchanged. Throughout the figure, the BDC:Zr ratio used in the synthesis is represented by the color of the curve: 1:1 (black), 5:4 (red), 3:2 (green), 7:4 (blue), and 2:1 (magenta). The same y-scale is applied to all three plots.

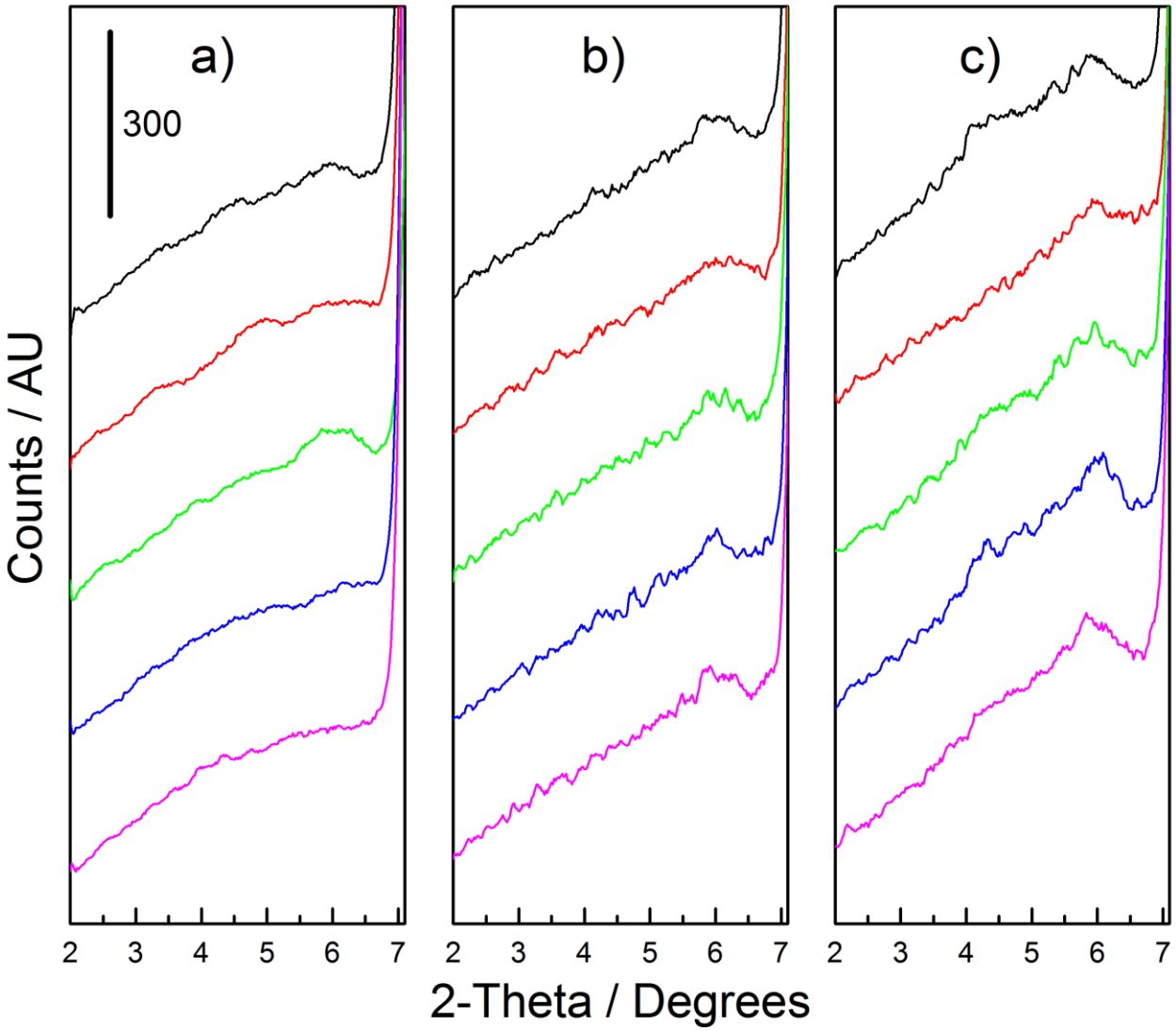

Figure S6: Forbidden reflection region of PXRD patterns recorded on UiO-66 samples synthesized at 220 °C: a) Crude (unwashed), b) Twice DMF washed, and c) Methanol Exchanged. Throughout the figure, the BDC:Zr ratio used in the synthesis is represented by the color of the curve: 1:1 (black), 5:4 (red), 3:2 (green), 7:4 (blue), and 2:1 (magenta). The same y-scale is applied to all three plots.

The three figures (**S4-S6**) afford the conclusion that the prominence of the forbidden reflections increases as the samples are more thoroughly washed. This observation is independent of the synthesis temperature used. However, it must be noted that even after methanol exchange, the peaks are only very weakly evident in the samples synthesized at 220 °C. For the sake of completeness, comparisons of the forbidden reflection regions of PXRD patterns collected on twice DMF washed (**Figure S7**) and methanol exchanged (**Figure S8**) materials are also presented:

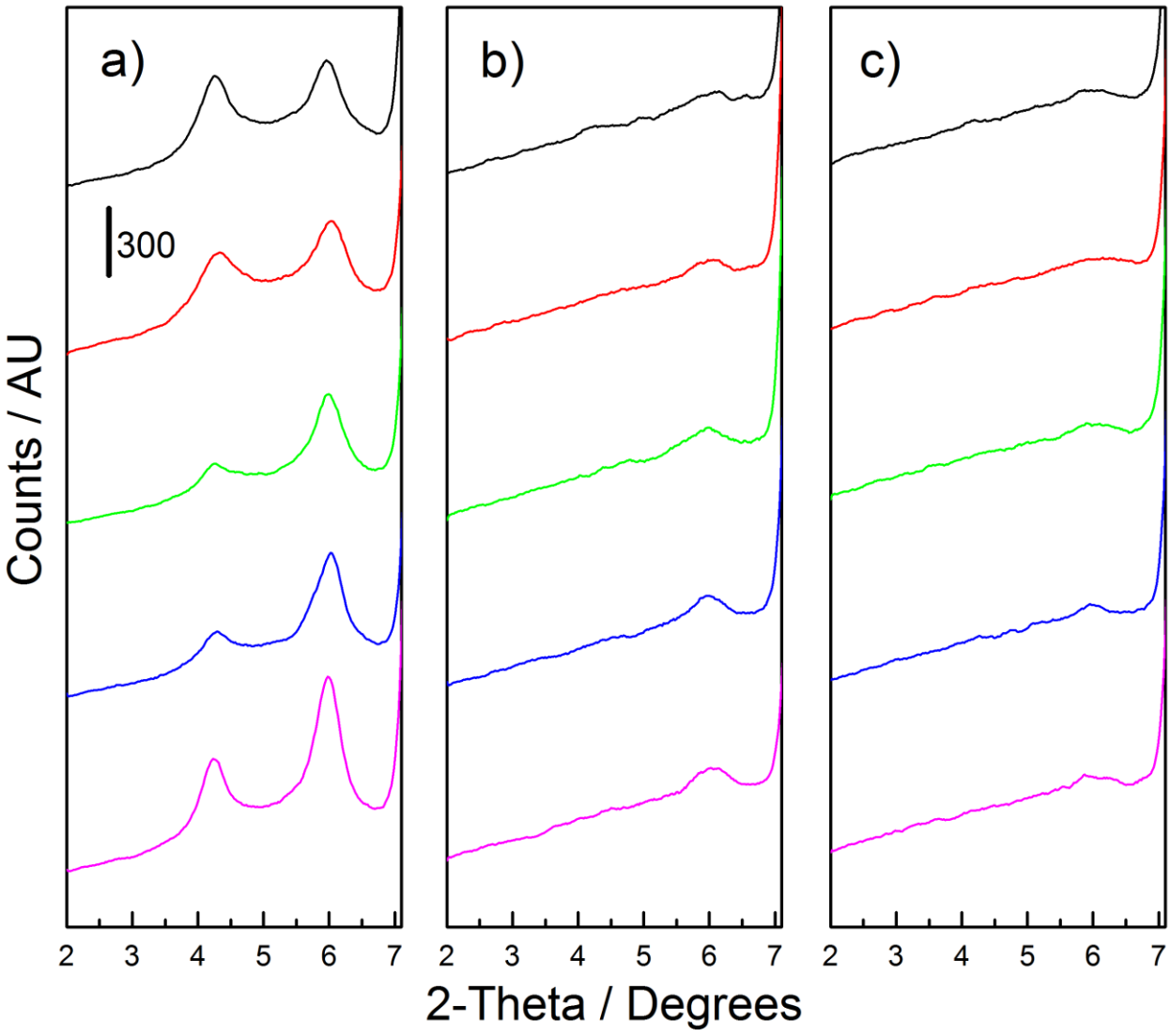

Figure S7: Forbidden reflection region of PXRD patterns recorded on twice DMF washed UiO-66 samples synthesized at: a) 100 °C, b) 160 °C, and c) 220 °C. Throughout the figure, the BDC:Zr ratio used in the synthesis is represented by the color of the curve: 1:1 (black), 5:4 (red), 3:2 (green), 7:4 (blue), and 2:1 (magenta). The same y-scale is applied to all three plots.

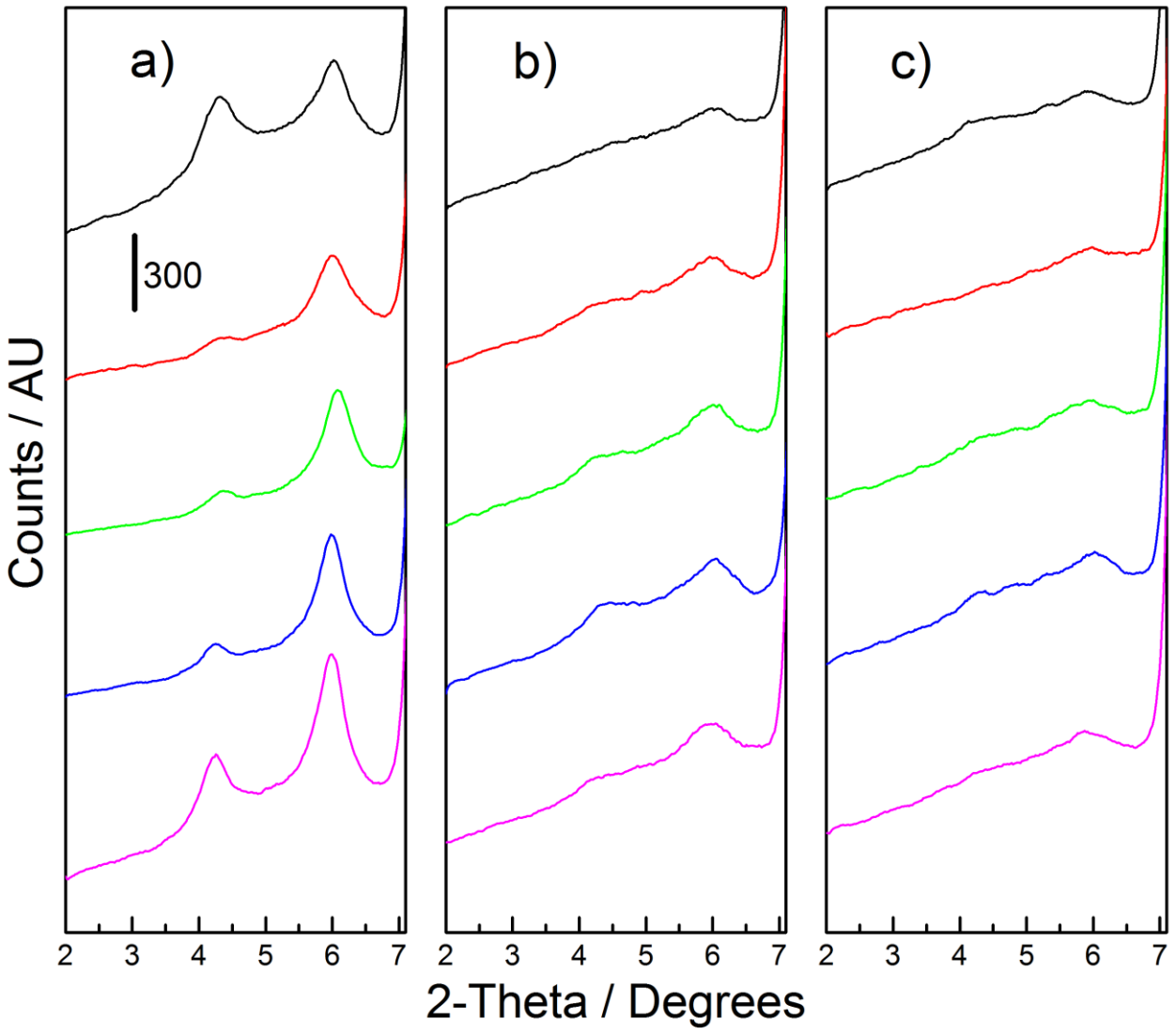

Figure S8: Forbidden reflection region of PXRD patterns recorded on methanol exchanged UiO-66 samples synthesized at: a) 100 °C, b) 160 °C, and c) 220 °C. Throughout the figure, the BDC:Zr ratio used in the synthesis is represented by the color of the curve: 1:1 (black), 5:4 (red), 3:2 (green), 7:4 (blue), and 2:1 (magenta). The same y-scale is applied to all three plots.

The two figures (**S7-S8**) demonstrate that when the materials have been washed to an equivalent extent, the forbidden reflections are always much more prominent in the PXRD patterns recorded on the samples synthesized at 100 °C. On samples synthesized at either 160 °C or 220 °C, the reflections are substantially less visible. However, one can say that they are slightly more evident on those synthesized at 160 °C. There is therefore an overall trend, affording the conclusion that the reflections become less prominent as the synthesis temperature increases.

A final conclusion is arrived at by considering the data from all six figures (**S3-S8**). When considering the 5 different colored PXRD patterns (representing UiO-66 samples synthesized with 5 different BDC:Zr ratios) within any individual plot, it can be seen that there is no systematic or significant spread in the prominence of their forbidden reflections. This allows us to conclude that the prominence of the forbidden reflections does not change significantly or systematically with the BDC:Zr ratio used in the synthesis.

To summarize, three conclusions have been reached regarding forbidden reflections on the PXRD patterns of the UiO-66 samples:

1) They become increasingly less prominent on samples synthesized at higher temperatures.

2) They become increasingly prominent as the material is more thoroughly washed.

3) Their prominence does not significantly or systematically depend on the BDC:Zr ratio used in the synthesis.

These 3 conclusions correlate strongly with those regarding the thermal stabilities of the samples:

1) Samples synthesized at higher synthesis temperatures are more thermally stable.

2) The materials become increasingly unstable with washing.

3) The thermal stability of the samples does not vary significantly or systematically with the BDC:Zr ratio used in the synthesis.

Comparing the two sets of conclusions, one can see the strong correlation between poor thermal stability and the extent to which the forbidden reflections are evident in the PXRD patterns of the materials. As mentioned in the main article, this makes sense if one accepts the assignment (made by Cliffe and Goodwin) of the forbidden reflections to defect regions of composition $Zr_6O_4(OH)_4(BDC)_4(HCOO)_4$.

The PXRD patterns presented in this section are available in their full (2θ = 2-50) range in **Figures S68-73** in the appendix. The patterns show that there is little variance in the overall crystallinity of the samples.

E) In Depth TGA-DSC Studies

Displayed in **Figure S9, S10, and S11** are the TGA-DSC results obtained on the crude (unwashed) UiO-66 samples synthesized at 100 °C, 160 °C, and 220 °C respectively:

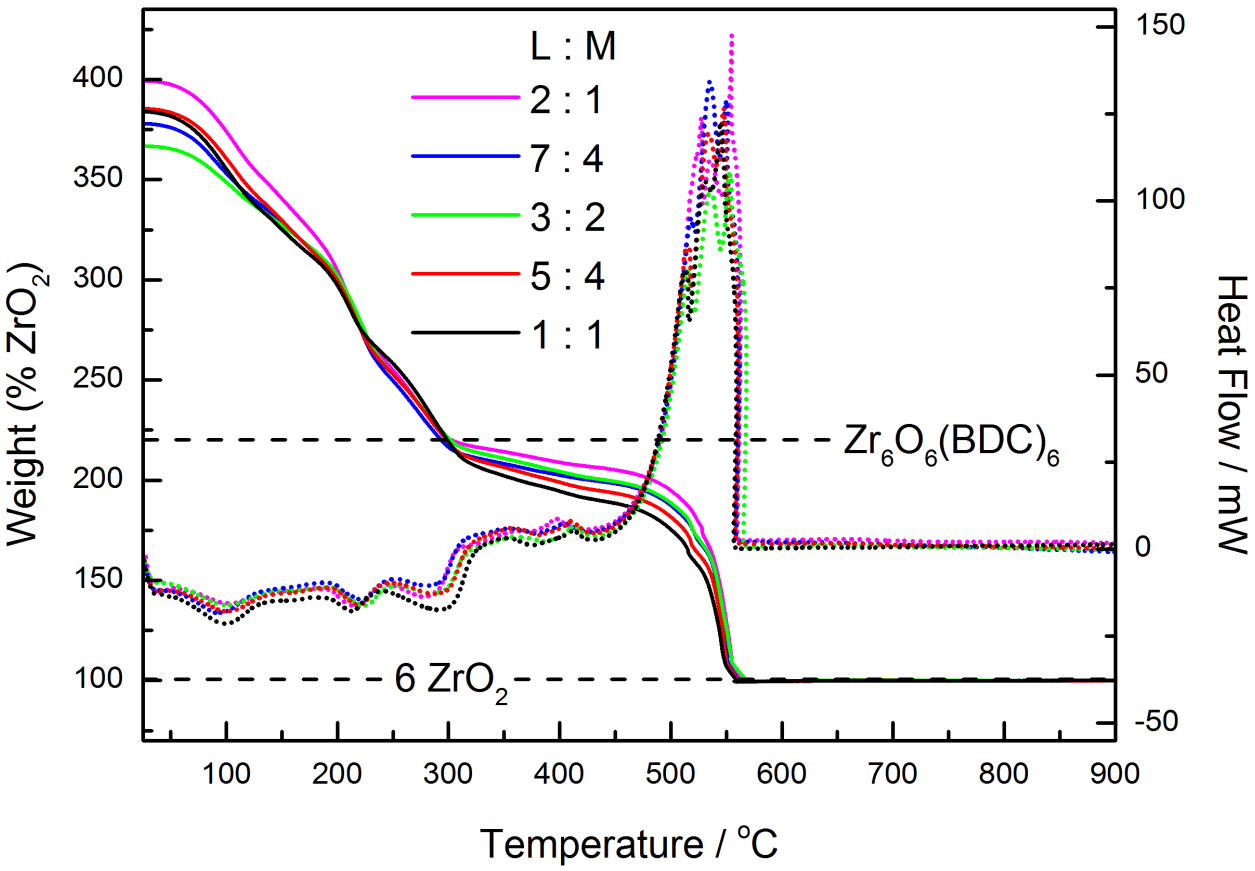

Figure S9: TGA curves (relative to ZrO_2, solid lines) and DSC signals (dotted lines) obtained on crude (unwashed) samples synthesized at 100 °C. Each color represents a sample synthesized with a different BDC:Zr (displayed as L:M) ratio. The on figure legend explains the color code. The position of the theoretical TGA plateau is marked by the horizontal dashed line labelled "Zr_6O_6 $(BDC)_6$".

Figure S9 shows that the TGA plateau systematically increases with increasing BDC:Zr ratio in the synthesis mixture. This makes sense if one interprets this as the insertion of increasing amounts of BDC into the linker deficient structure. At this synthesis temperature (100 °C) it can be seen that even when a BDC:Zr ratio is used, the TGA plateau is still far from that theoretically expected.

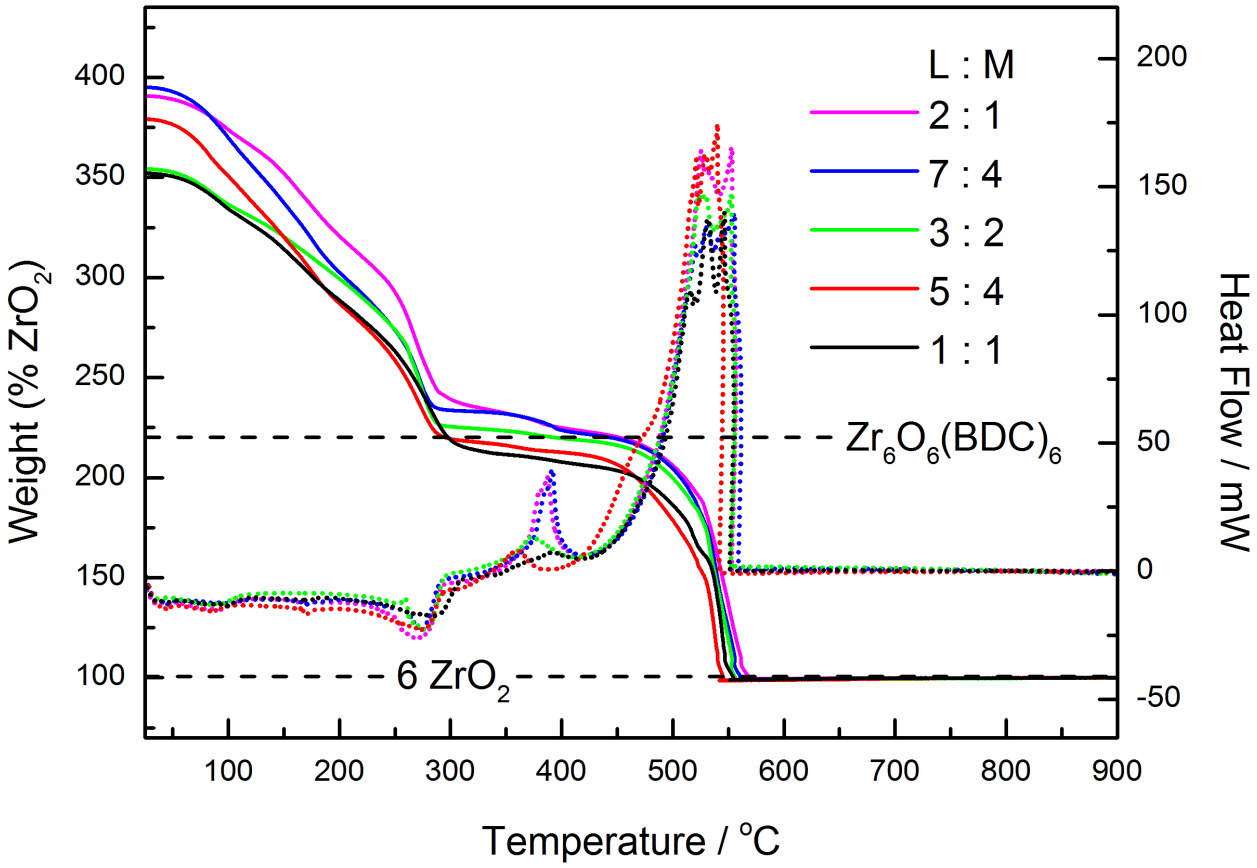

Figure S10: TGA curves (relative to ZrO_2, solid lines) and DSC signals (dotted lines) obtained on crude (unwashed) samples synthesized at 160 °C. Each color represents a sample synthesized with a different BDC:Zr (displayed as L:M) ratio. The on figure legend explains the color code. The position of the theoretical TGA plateau is marked by the horizontal dashed line labelled "Zr_6O_6 $(BDC)_6$".

Figure S10 shows the same trend observed in **Figure S9**. There are however, two further observations which cannot be made on **Figure S9**: 1) There is now a third well defined weight loss step occurring in the temperature range 290-400 °C; and 2) There is an extra exothermic heat signal which peaks at around 380 °C. These two further observations appear to be related due to the fact that: 1) They appear in the same temperature range; and 2) Their prominence both increase as the BDC:Zr ratio used to make the sample increases. All evidence considered, the new weight loss and heat signal is assigned to the burning of "excess linkers"; unbound BDC molecules which likely reside in the pores of the samples. This makes sense when one considers that the new weight loss step and its corresponding heat signal is systematically more prominent on samples synthesized with a greater and greater excess of BDC. Furthermore, the only material on which the weight loss step and heat signal is not observed is that syntheses with a 1:1 BDC:Zr

ratio, the only sample which would be expected to be free of "excess linkers" in the crude, unwashed state. After the "excess linker" burning step, it can be seen that the materials synthesized with BDC:Zr ratios of 7:4 and 2:1 both reach the ideal TGA plateau. However, their plateaus were found to decrease with washing, as demonstrated later in **Figure S13**.

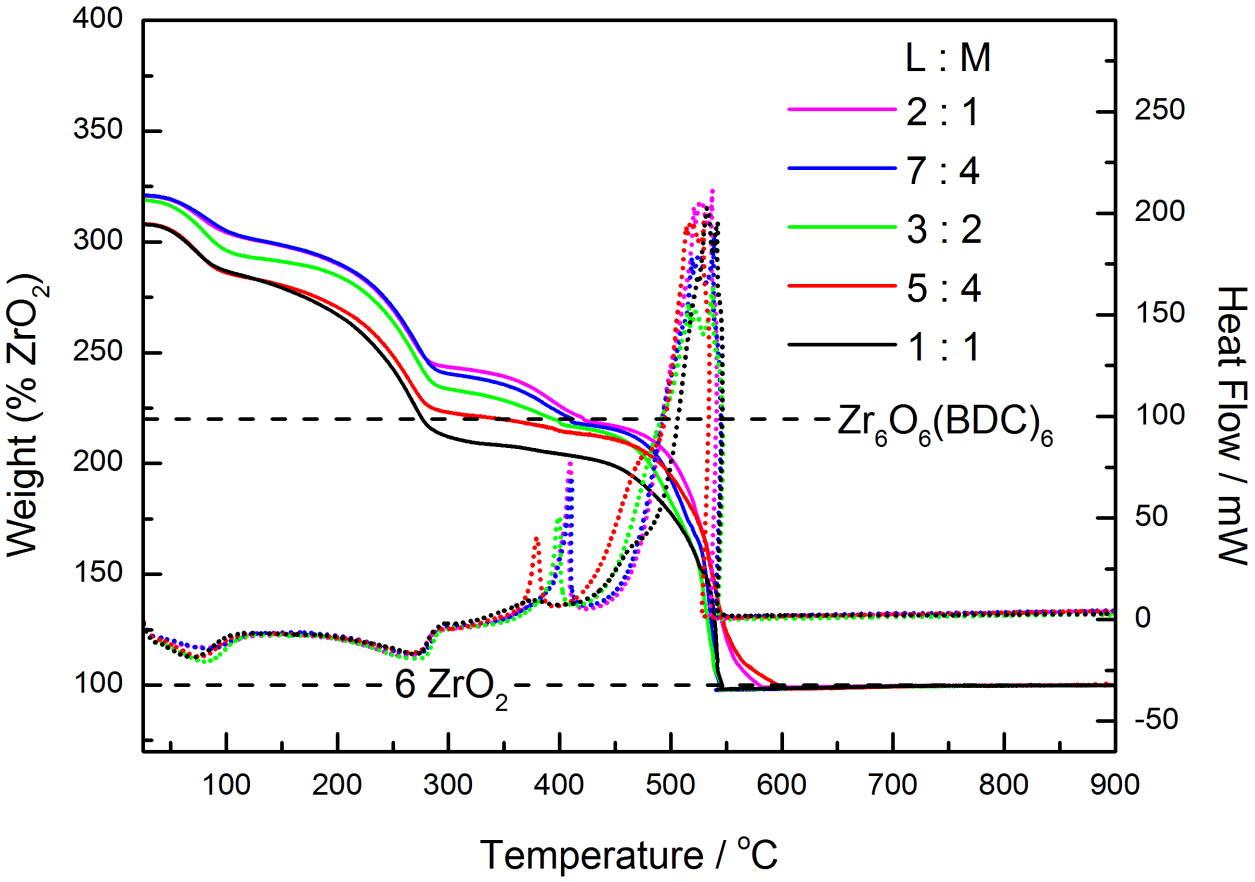

Figure S11: TGA curves (relative to ZrO_2, solid lines) and DSC signals (dotted lines) obtained on crude (unwashed) samples synthesized at 220 °C. Each color represents a sample synthesized with a different BDC:Zr (displayed as L:M) ratio. The on figure legend explains the color code. The position of the theoretical TGA plateau is marked by the horizontal dashed line labelled "Zr_6O_6 $(BDC)_6$".

In general, the previous discussion of **Figures S9** and **S10** also applies to **Figure S11**. Again the materials synthesized with BDC:Zr ratios of 7:4 and 2:1 attain the ideal TGA plateau after the "excess linker" burning step. Of more importance is that in this case their plateaus do not decrease with washing (see **Figure S12**). Also noteworthy is the fact that the trend of the "excess linker" burning weight loss step and heat signal is emphasized to a greater extent in **Figure S11**.

Both features are clearly progressively more prominent on samples synthesized with an increasingly large BDC:Zr ratio. A final observation is that the first weight loss step is substantially lower than that seen on the TGA curves of the previous 2 figures, indicating that the samples synthesized at 220 °C contain considerably less pore filling solvent than those synthesized at the two lower temperatures. This is reflected in the crude synthesis yields, which ranged from 6 to 8 grams (theoretical yield of empty MOF was 4.5 grams). The crude yields of samples synthesized at lower temperatures were generally towards the upper end of the scale, whereas those synthesized at 220 °C were at the lower extremity. The large difference in the amount of pore filling solvent accounts for this observation.

Figure S12 shows the evolution; of the TGA-DSC results obtained on UiO-66-220-2:1 as it is increasingly thoroughly washed:

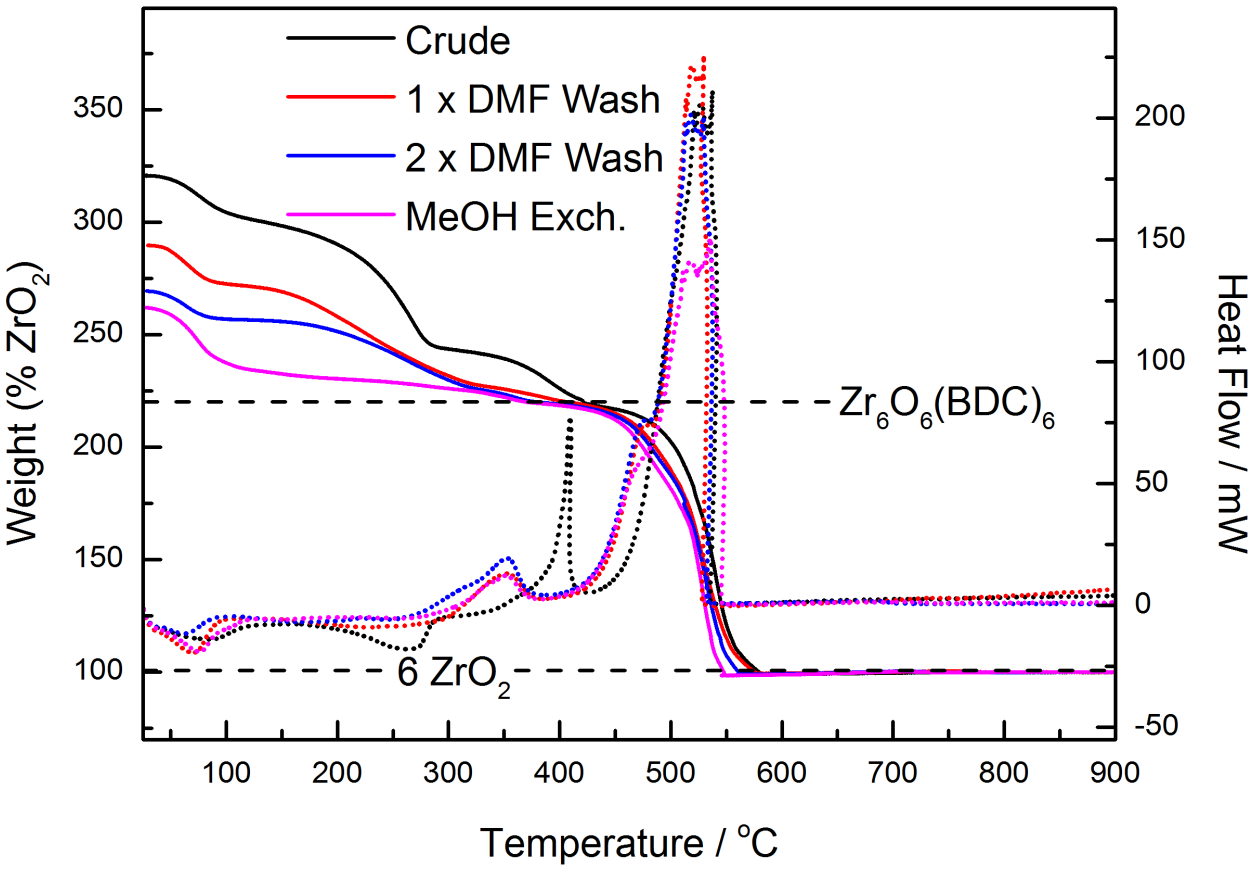

Figure S12: TGA curves (relative to ZrO_2, solid lines) and DSC signals (dotted lines) obtained on UiO-66-220-2:1 at various states of washing (explained on the legend). The position of the theoretical TGA plateau is marked by the horizontal dashed line labelled "Zr_6O_6 $(BDC)_6$".

Figure S12 demonstrates that:

1) The TGA plateau of UiO-66-220-2:1 is not affected by washing.

2) Exchanging DMF (b.p = 153 °C) for methanol (b.p. = 65) substantially lowers the temperature required for activation (solvent removal).

3) The "excess linker" burning weight loss step and heat signal progressively decrease in prominence as the sample is increasingly thoroughly washed.

Point 3) is interpreted as the removal of the excess linkers, and provides a final piece of strong evidence for their existence in these samples. It can however be seen (and is pointed out in the main article) that there is still a considerable amount of excess linker in the material even after methanol exchange. It is for this reason that we recommend an alternative activation method for thermally stable UiO-66 samples:

1) Wash the material thoroughly in DMF.

2) Heat the sample in air at 400 °C for a prolonged period. This method not only burns off the excess linkers but also removes the DMF, such that the material is subsequently filled by atmospheric water vapor, allowing the sample to be activated at a moderate temperature.

This method was employed on the UiO-66-220-2:1 sample measured by DRIFTS (section H).

Figure S13 shows the evolution of the TGA-DSC results obtained on UiO-66-160-2:1 as it is increasingly thoroughly washed:

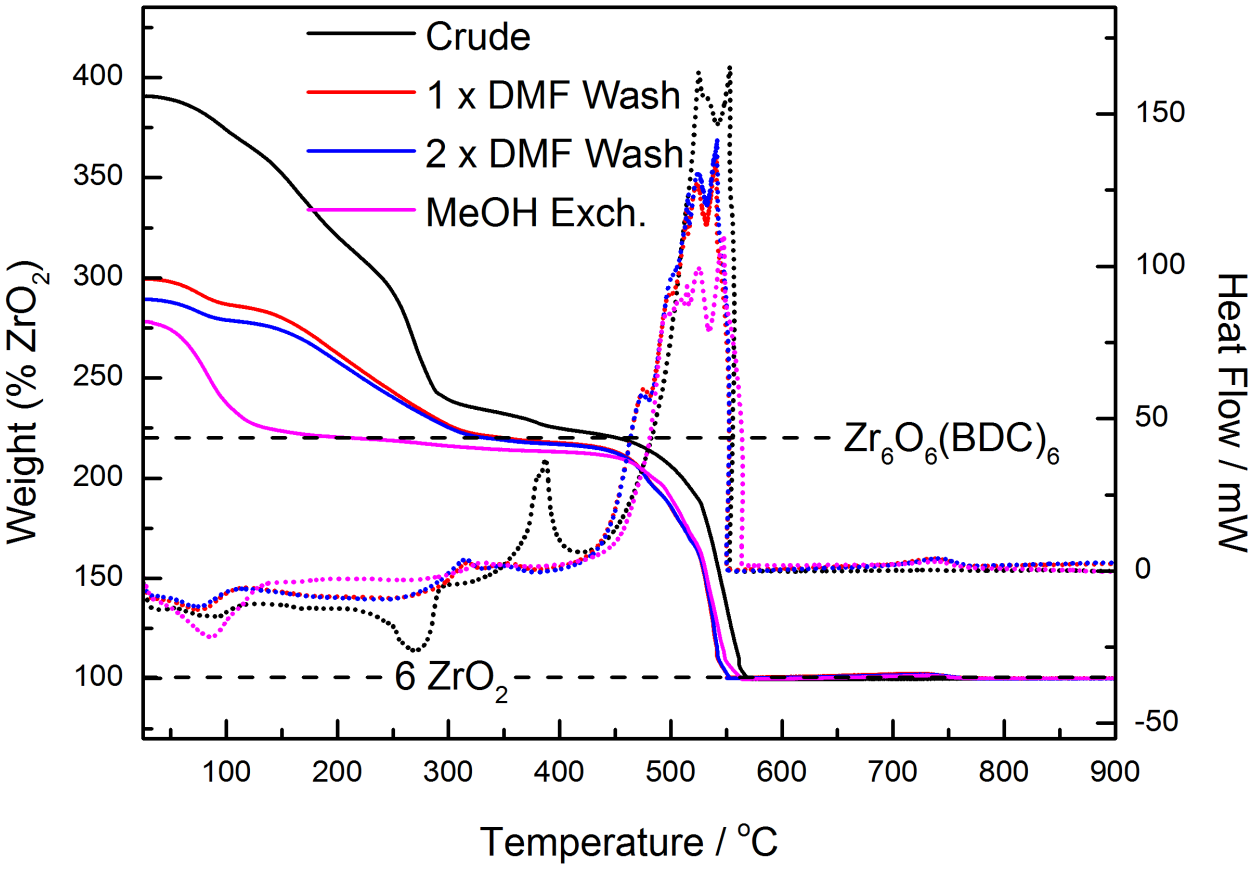

Figure S13: TGA curves (relative to ZrO_2, solid lines) and DSC signals (dotted lines) obtained on UiO-66-160-2:1 at various states of washing (explained on the legend). The position of the theoretical TGA plateau is marked by the horizontal dashed line labelled "Zr_6O_6 $(BDC)_6$".

Figure S13 illustrates the same points as **Figure S12** but also shows that the initially ideal TGA plateau of this sample (UiO-66-160-2:1) is found to decrease with progressing extent of washing. This is an effect which randomly occurs on some samples and not on others (see **Figures S74-S88** in the appendix for similar TGA plots which follow the washing on all 15 samples). The end (perhaps coincidental) result is that at each synthesis temperature, the TGA plateaus of the methanol exchanged samples are found to converge somewhat, meaning that the significant and systematic trend between the plateau and the BDC:Zr ratio is less well observed (see **Figure S14** in the following section).

F) Experimental and Simulated N_2 Adsorption Isotherms: Trend Between Porosity (BET SA, Langmuir SA, and Pore Volume), TGA plateau, and Missing Linkers

Figure S14 compares the TGA-DSC results to the nitrogen adsorption isotherms obtained on all 15 methanol exchanged UiO-66 samples studied:

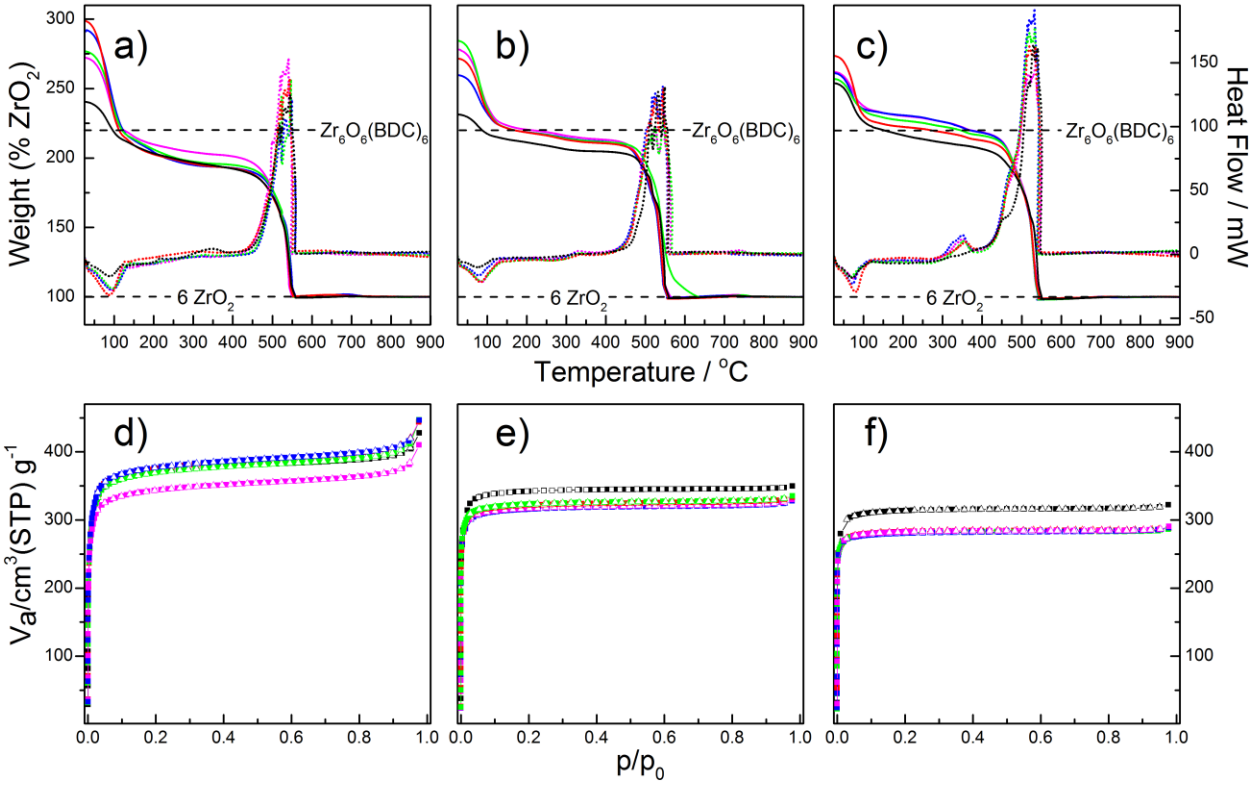

Figure S14: Comparison between the TGA-DSC (top) results and the nitrogen adsorption isotherms (bottom) obtained on all 15 methanol exchanged UiO-66 samples studied. Shown in parts a), b), and c) are the TGA curves (relative to ZrO_2, solid lines) and the DSC signals (dotted lines) obtained of UiO-66 samples synthesized at 100, 160, and 220 °C respectively. The same y-scales are applied to all three plots. Parts d), e), and f) display the nitrogen adsorption isotherms obtained on the same UiO-66 samples, synthesized at 100, 160, and 220 °C respectively. Adsorption represented by filled squares, desorption by open triangles. The same y-scale is applied to all three plots. Throughout all six parts of the figure, the BDC:Zr ratio used in the synthesis is represented by the color of the curve: 1:1 (black), 5:4 (red), 3:2 (green), 7:4 (blue), and 2:1 (magenta).

The TGA-DSC results presented in parts a), b), and c) of the figure demonstrate how the methanol exchange procedure has affected the materials as a whole. The first observation of note is that the progressive increase in the TGA plateau with increasing synthesis temperature has been preserved after methanol exchange. That is, the plateaus of the TGA curves in part a) (synthesis temperature = 100 °C) are still generally lower than those in part b) (synthesis temperature = 160 °C) which are subsequently lower than those in part c) (synthesis temperature = 220 °C). However, with the exception of the samples synthesized at 220 °C, the highly systematic and progressive tendency towards ideality with increasing BDC:Zr synthesis ratio (observed on the crude materials, **Figures S9-S11** in the previous section) is no longer evident. This is due to the fact that the methanol exchange procedure was found to reduce the TGA plateau of some samples but not others, with no clear indicator as to which samples would be affected. For more information, see **Figures S74-S88** in the appendix for TGA-DSC results which follow the washing and methanol exchange of each sample individually.

Observing the results in greater detail, one can see that rather than following a systematic and progressive trend, the TGA plateaus of the methanol exchanged materials synthesized at 100 and 160 °C (parts a and b of the figure) are now seen to converge into two groups based on the BDC:Zr ratio used in their syntheses. Of those synthesized at 100 °C, the TGA plateau of the material synthesized with BDC:Zr = 2:1 (magenta curve) is significantly higher than that seen for the other samples, which all have very similar TGA plateaus. A similar observation is made for the materials synthesized at 160 °C, albeit with the outlier (BDC:Zr = 1:1, black curve) having a lower plateau than the others. Methanol exchange was found not to affect any of the samples synthesized at 220 °C and as a result, the progressive trend between the BDC:Zr ratio and the TGA plateau remains intact. The interested reader is again directed to **Figures S74-S88** in the appendix to see how the TGA-DSC results of each individual sample were affected by the washing and methanol exchange procedures.

Shown in parts d), e), and f) of the figure are the nitrogen adsorption isotherms obtained on methanol exchanged samples synthesized at 100, 160, and 220 °C respectively. Upon visual comparison with the TGA data, it is immediately evident that the nitrogen uptake has a strong inverse relation with the TGA plateau. That is, a material with a relatively high TGA plateau has a relatively low nitrogen uptake and vice versa. As mentioned in the main article, this observation makes sense if one accepts the hypothesis that a lower than ideal TGA plateau is indicative of missing linker defects.

Indeed, nitrogen adsorption isotherms simulated from models of UiO-66 in which 0-6 linkers are missing per unit cell (part a of **Figure S15**) show that the nitrogen uptake systematically increases as the number of linker deficiencies increases, as previously demonstrated by Katz and coworkers.[5] Moreover, BET analysis of the simulated isotherms affords the observation of the strong linear relationship between the number of missing linkers per unit cell and the surface area of the material (part b of **Figure S15**).

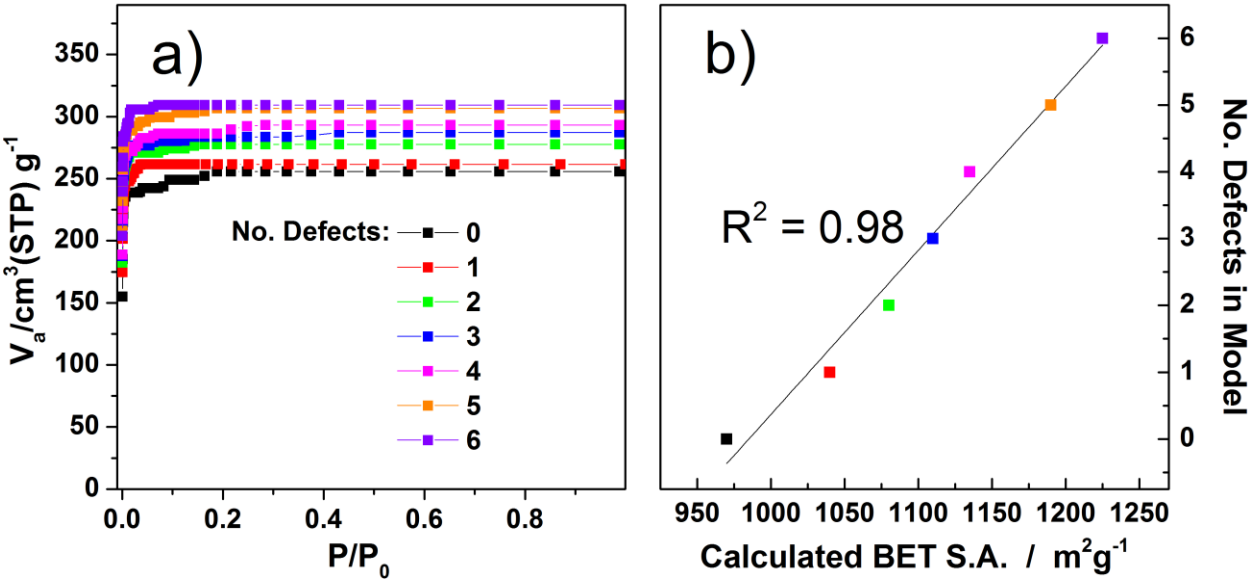

Figure S15: a) Nitrogen adsorption isotherms simulated from models of UiO-66 in which 0-6 linkers are missing per unit cell; b) Linear fit obtained when the number of missing linkers per unit cell is plotted against calculated BET surface areas. See the legend on part a) for explanation of the color scheme. No. Defects = number of linkers missing per unit cell.

Figure S16 presents the linear fits obtained experimentally when the TGA plateau (% ZrO_2) of the methanol exchanged samples (from the data presented in **Figure S14** parts a-c) is plotted against porosity descriptors derived from their nitrogen adsorption isotherms (**Figure S14** parts d-f). Plots of TGA plateaus against the BET surface area, the Langmuir surface area, and the pore volume of the materials are presented in parts a), b), and c) respectively. The raw dataset used for these plots is presented in **Table S2**.

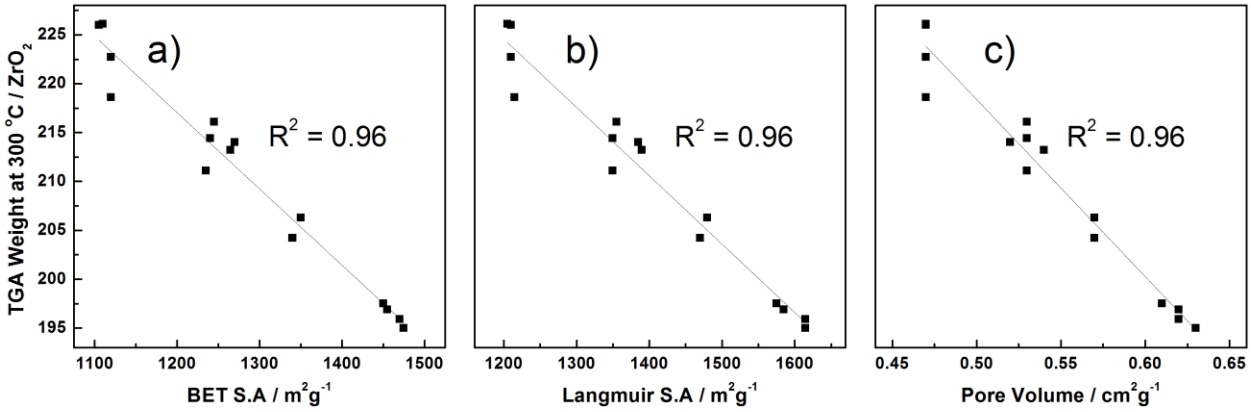

Figure S16: Linear fits obtained when the TGA plateaus (% ZrO_2) of all 15 methanol exchanged samples are plotted against their respective: a) BET surface areas (the same plot is presented in the main article as the inset of **Figure 2b**), b) Langmuir surface areas, and c) Pore volumes derived from their nitrogen adsorption isotherms. See **Table S2** for the raw dataset used in the plots. The same y-scale is applied throughout all three parts.

One can see that very good linear fits are obtained on all three plots. Combining this observation with that obtained via simulations (**Figure S15b**) affords the conclusion that the relationship between the number of missing linkers and the TGA plateau is also linear (and inverse), and that the conventional "missing linker" interpretation of the TGA plateau is thus solid.

Note however, that due to the discrepancy between the calculated (970 m^2g^{-1}) and experimental (UiO-66-220-2:1 = 1105 m^2g^{-1}) BET surface area of ideal UiO-66, we are unable to estimate the number of missing linkers on each sample. This discrepancy is due to the use of the relatively quick "normal" method used to simulate the isotherms displayed here. Employing the much more time consuming "fine" method gives a BET surface area of 1125 m^2g^{-1}, a value very close to that obtained experimentally (thus demonstrating the ideality of UiO-66-220-2:1) and to that previously calculated by Katz and coworkers.[5] See Section B for full details of the simulations.

Table S2: Raw dataset (derived from the data presented in **Figure S14**) used to plot the linear fits presented in **Figure S16**.

Sample (Methanol Exchanged)	TGA Wt. At 300 °C (% ZrO_2)*	BET SA (m^2g^{-1})	Langmuir SA (m^2g^{-1})	Pore Volume (cm^3g^{-1})
UiO-66-100-1:1	196.9	1455	1585	0.62
UiO-66-100-5:4	195.9	1470	1615	0.62
UiO-66-100-3:2	197.5	1450	1575	0.61
UiO-66-100-7:4	195.0	1475	1615	0.63
UiO-66-100-2:1	204.2	1340	1470	0.57
UiO-66-160-1:1	206.3	1350	1480	0.57
UiO-66-160-5:4	213.2	1265	1390	0.54
UiO-66-160-3:2	214.0	1270	1385	0.52
UiO-66-160-7:4	214.4	1240	1350	0.53
UiO-66-160-2:1	216.1	1245	1355	0.53
UiO-66-220-1:1	211.1	1235	1350	0.53
UiO-66-220-5:4	218.6	1120	1215	0.47
UiO-66-220-3:2	222.7	1120	1210	0.47
UiO-66-220-7:4	226.1	1110	1205	0.47
UiO-66-220-2:1	226.0	1105	1210	0.47

* The mild activation conditions used in the adsorption measurements do not remove excess linkers from the samples. The most relevant plateau temperature is thus 300 °C, where the excess linkers (where applicable) are still present.

G) MOF Dissolution / Liquid ^{1}H NMR Spectroscopy – Assessing the Efficiency of Methanol Exchange and Activation Procedures

The ^{1}H NMR spectrum of a solution in which a MOF has been digested contains signals due not only to the linkers but also to the pore filling solvent. It is thus a powerful method for the quantitative determination of the efficiency of solvent exchange and activation procedures. To the best of the authors' knowledge, such an application of the technique has not been demonstrated before.

In this work, 1M NaOH in D_2O was used as the digestion media. DMF is the solvent which is used in the synthesis (and thus fills the pores) of UiO-66. Under the basic conditions employed in the digestion method, DMF hydrolyses to formic acid (as formate) and dimethylamine:

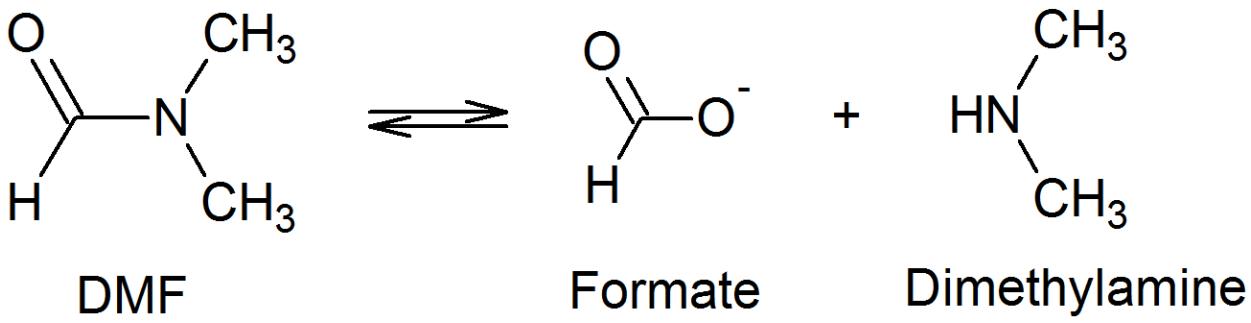

This does not prevent DMF from being quantified due to the fact that:

1) Dimethylamine and formic acid are the only products.

2) The reaction goes to completion on the timescale of the digestion method (24 hours).

3) Both formic acid and dimethyl amine may be quantified by ^{1}H NMR.

Quantification of either of the two products is thus equivalent to quantifying DMF. In this work, dimethylamine was used to quantify DMF due to the fact that it has 6 equivalent protons and can thus be quantified with greater sensitivity than formate, which only has 1 proton.

Figure S17 demonstrates how the liquid ^{1}H NMR spectrum of UiO-66-220-2:1 (digested in 1M NaOH in D_2O) is affected by methanol exchange and activation:

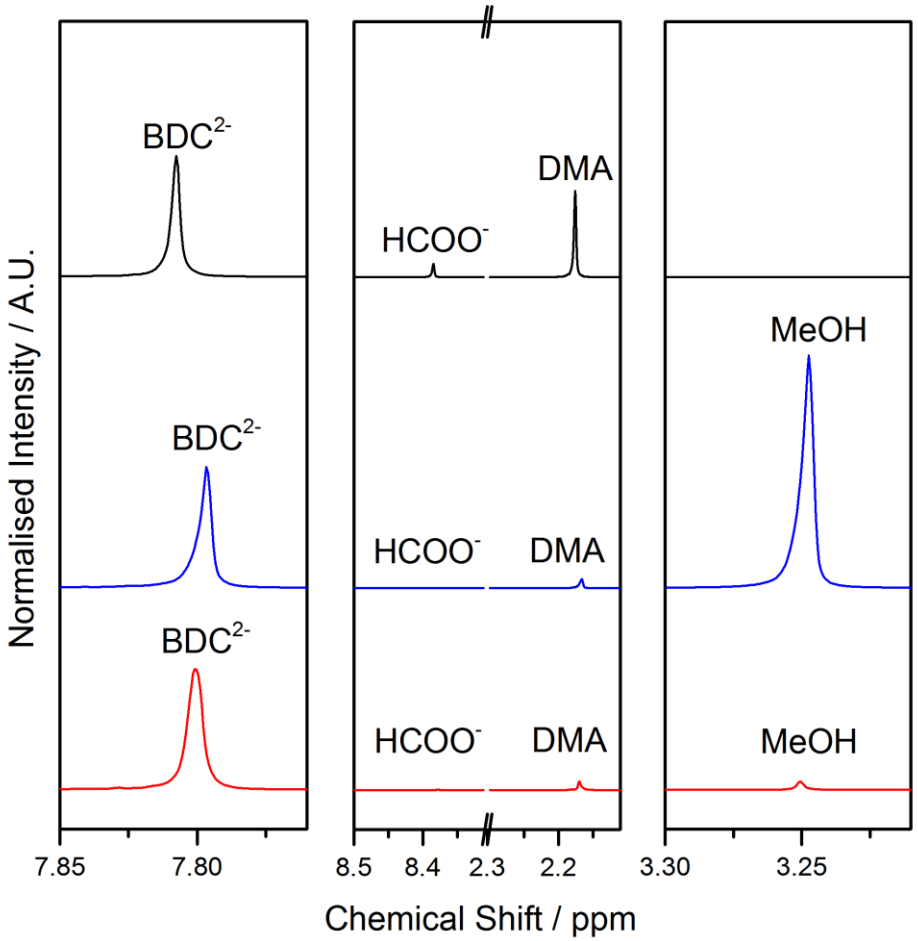

Figure S17: Liquid ^{1}H NMR spectra of digested (1M NaOH in D_2O for 24 hours) samples of UiO-66-220-2:1. Black: 2xDMF washed; blue: methanol exchanged; red: methanol exchanged sample after activation at 150 °C for 2 hours under vacuum. All normalized to the BDC^{2-} signal. Legend: BDC^{2-} = benzene-1,4-dicarboxylate, $HCOO^{-}$ = Formate, DMA = dimethylamine, MeOH = Methanol. The instability of chemical shifts is due to the use of the HDO signal as reference.

The black and blue curves on **Figure S17** represent the sample before and after methanol exchange respectively. Observing the two curves in sequence reveals that methanol exchange has removed almost all the DMF (represented by the near disappearance of both its decomposition products). Furthermore, a highly significant amount of methanol is now found in the material. Both these observations demonstrate the efficiency of the methanol exchange procedure.
The blue and red curves represent the methanol exchanged sample before and after activation (150 °C for 2 hours) respectively. It is immediately striking that methanol has been almost completely removed by the activation, proving the high efficiency of the method employed in this work.

The dissolution/ liquid ^{1}H NMR spectra (presented in the same theme as **Figure S17**) obtained on the rest of the materials in the series can be found in the appendix. Such figures are effective in qualitatively illustrating the efficiency of the exchange and activation procedures. However, the real strength of ^{1}H NMR spectroscopy in this application is that the signals may be integrated, allowing the efficiency of these procedures to be quantified. To this end, the following method was used:

First of all, the number of BDC molecules was set:

$$No.BDC\ molecules = \frac{BDC\ integral}{No.\ H\ Rep.(=4)}$$

In this work, the BDC integral was set to 4, such that the value for the number of BDC molecules is normalized to 1. All further integrations are relative to this value, allowing for facile quantification of the solvent molecules with respect to the amount of BDC.

The number of DMF molecules relative to BDC was then calculated:

$$DMF\ molecules\ per\ BDC\ Molecule = \frac{DMA\ Integral}{No.\ H\ Rep\ (=6)}\ /\ No.BDC\ Molecules$$

As was the number of methanol molecules:

$$Methanol\ molecules\ per\ BDC\ Molecule = \frac{MeOH\ Integral}{No.\ H\ Rep\ (=3)}\ /\ No.BDC\ Molecules$$

Calculating the number of DMF molecules before and after methanol exchange allowed for the efficiency of DMF removal to be determined:

$$\%\ DMF\ Removed = 100 - \frac{DMF\ molecules\ per\ BDC\ Molecule\ after\ MeOH\ Exch.}{DMF\ molecules\ per\ BDC\ Molecule\ before\ MeOH\ Exch.} \times 100\ \%$$

Similarly, calculating the number of methanol molecules before and after activation allows for the efficiency of the activation procedure to be calculated:

$$\%\ Methanol\ Removed = 100 - \frac{MeOH\ molecules\ per\ BDC\ Molecule\ after\ Activation}{MeOH\ molecules\ per\ BDC\ Molecule\ before\ Activation} \times 100\ \%$$

Applying the above method to the 3 ^{1}H NMR spectra of all 15 samples afforded the results presented in Table S3:

Table S3: The efficiency (determined by integrating ^{1}H NMR spectra of digested samples, see method above) of the methanol exchange and activation procedures on all UiO-66 samples.

	DMF Molecules Per BDC Molecule			**Methanol Molecules Per BDC Molecule**		
Sample	**Before MeOH Exch.**	**After MeOH Exch.**	**% DMF Removed**	**After MeOH Exch.**	**After Activation**	**% MeOH Removed**
UiO-66-100-1:1	1.53	0.01	99.7	1.15	0.20	82.9
UiO-66-100-5:4	0.97	0.00	99.7	4.03	0.01	99.8
UiO-66-100-3:2	1.28	0.00	99.9	2.67	0.12	95.4
UiO-66-100-7:4	1.35	0.00	99.9	3.86	0.13	96.7
UiO-66-100-2:1	0.68	0.01	99.3	1.77	0.02	98.9
UiO-66-160-1:1	1.04	0.00	99.7	7.33	0.05	99.4
UiO-66-160-5:4	0.89	0.01	99.4	5.35	0.06	98.8
UiO-66-160-3:2	0.91	0.01	99.5	4.50	0.05	98.8
UiO-66-160-7:4	0.91	0.01	99.5	2.31	0.07	97.1
UiO-66-160-2:1	0.92	0.01	99.3	1.92	0.04	97.7
UiO-66-220-1:1	0.57	0.03	95.3	2.48	0.07	97.3
UiO-66-220-5:4	0.67	0.03	95.5	0.98	0.01	99.0
UiO-66-220-3:2	0.85	0.05	94.1	1.42	0.04	97.4
UiO-66-220-7:4	0.32	0.06	81.5	0.78	0.03	96.6
UiO-66-220-2:1	0.45	0.05	88.6	2.40	0.05	98.1

As one can see, the exchange and activation procedures were generally highly efficient in removing DMF and methanol respectively. However, methanol exchange was slightly less efficient on the samples synthesized at 220 °C, while the activation procedure was significantly less efficient on UiO-66-100-1:1. The interested reader is directed to **Figures S89-103** in the appendix, where the dissolution / liquid ^{1}H NMR spectra of the whole series of samples can be found.

H) *In situ* DRIFTS – Desolvation and ν(OH) Stretching Region Studies

The *in situ* DRIFTS results obtained on UiO-66-100-5:4-2DMF and UiO-66-220-2:1-2DMF are presented in **Figure S18** (over the page). Prior to measurement, the materials were calcined for 12 hours at 200 °C (UiO-66-100-5:4-2DMF) and 400 °C (UiO-66-220-2:1-2DMF) respectively. This treatment served two purposes:

1) To remove DMF, which is subsequently replaced by atmospheric water (allowing for solvent removal at a lower temperature). UiO-66-100-5:4-2DMF was chosen over UiO-66-100-1:1-2DMF due to the fact that DMF was not sufficiently removed via calcination. This is in accordance with the poor activation efficiency of UiO-66-100-1:1-MeOH (see previous section), an observation which also suggests that solvent is strongly bound to the sample.

2) To burn off "excess linkers" (see section E for more on this) which we have found to perturb the hydroxyl groups and thus obscures their observation in the spectrum. This requires treatment at 400 °C and thus is only applicable to the most thermally stable UiO-66 samples.

Since methanol exchange does not completely remove "excess linkers", we suggest the use of the above 400 °C pre calcination method for the activation of UiO-66, provided the sample is thermally stable. We reiterate that the only reason methanol exchange was used in this work was to allow the thermally unstable materials to be emptied prior to nitrogen adsorption measurements. Thermally stable materials were also methanol exchanged simply in order to obtain comparable data.

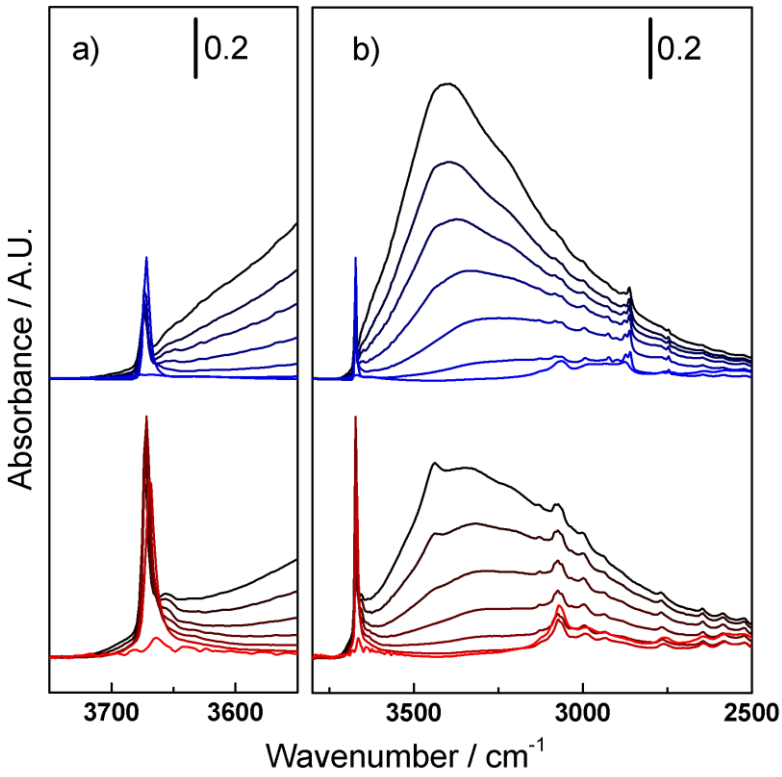

Figure S18: a) ν(OH) stretching region and b) Hydrogen bonded physisorbed solvent region of in situ DRIFT spectra obtained by progressively heating (5 °C/min) samples from room temperature (black) to 250 °C (colored) under 40 mL/min N_2 flux. Top, blue = UiO-66-100-5:4-2DMF; bottom, red = UiO-66-220-2:1-2DMF. UiO-66-100-5:4-2DMF and UiO-66-220-2:1-2DMF were pre calcined for 12 hours at 200 and 400 °C respectively.

The DRIFTS results presented in the figure were obtained by gradually (5 °C/min) heating the samples to 250 °C under N_2 flux. Part b) focusses on the desolvation of the frameworks, a process which (in accordance with previous studies[3,6]) is clearly represented by the gradual erosion of the broad band which initially dominates the spectrum of both materials. Of greater importance to this work is part a) where the ν(OH) stretching region is emphasized, highlighting the isolated structural hydroxyl groups.

On both samples it is clear that there exists a single intense, sharp ν(OH) band after the desolvation, appearing at 3672 cm^{-1}. This band represents the μ^3 hydroxyl groups on the inorganic cornerstone of the materials and is removed after prolonged heating at 250 °C, indicating dehydroxylation.[3] The appearance of a single isolated ν(OH) band is the result expected of ideal UiO-66, where all the structural μ^3 hydroxyl groups are chemically equivalent.[6b]

The fact that even the defective UiO-66-100-5:4 is ideal in this respect indicates that linker deficiencies are not responsible for the hydroxyl based defects observed in previous work, and that their origin is thus still unknown. However, we note that they have only been observed on samples synthesized in the presence of a large excess of modulator.[5,6b] Further studies are required to fully comprehend this issue.

I) Elemental Analysis (via EDS) – Chlorine Content Studies

Figure S19 follows the evolution of the EDS spectra of the materials at the two extremities of the series (part a, grey curves = UiO-66-100-1:1; part b, red curves = UiO-66-220-2:1) as they are increasingly thoroughly washed. Crude, 1 x DMF washed, 2 x DMF washed, and Methanol exchanged samples are displayed from top to bottom (and thick to thin) respectively. The quantitative data derived from these spectra is displayed in **Table S4**, where the concentration of chlorine relative to zirconium in the samples is provided. Although carbon and oxygen peaks are shown on the figure, these light elements cannot be reliably quantified due to the fact that the low energy X-rays that they emit do not efficiently penetrate the beryllium detector windows.

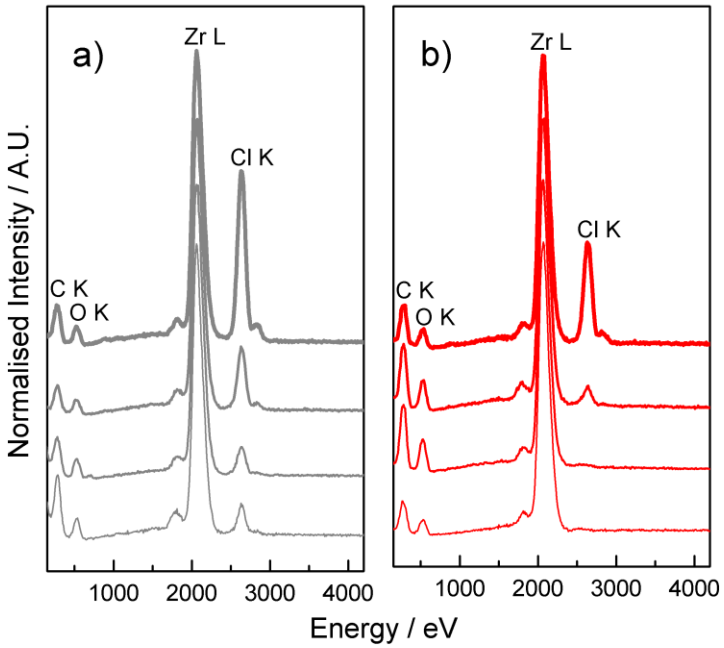

Figure S19: EDS spectra of a) UiO-66-100-1:1, and b) UiO-66-220-2:1. Crude, 1 x DMF washed, 2 x DMF washed, and Methanol exchanged materials are displayed from top to bottom (and thick to thin) respectively. Spectra are normalized by their Zr L peak.

Table S4: Quantitative data derived from the spectra presented in **Figure S19**.

	Cl : Zr Atomic Ratio	
Washing Extent	**UiO-66-100-1:1**	**UiO-66-220-2:1**
Crude (Unwashed)	1.41	0.90
1 x DMF Washed	0.57	0.16
2 x DMF Washed	0.26	0
MeOH Exchanged	0.25	0

Both the spectra and the table show that there is a significant amount of chlorine in both materials in the crude, unwashed state. However, the chlorine content significantly and systematically decreases as the samples are increasingly thoroughly washed. We propose that any chlorine which may be removed by washing is simply due to HCl adsorbed in the pores, where they may be further solvated by DMF molecules. The presence of adsorbed HCl in the as synthesized materials is highly plausible due to the fact that:

1) 2 molar equivalents of HCl was added to the synthesis mixture (see section A).

2) 24 moles of HCl is formed per mole of UiO-66 produced by the idealized reaction equation:

$$\mathbf{6\ ZrCl_4 + 8H_2O + 6\ H_2BDC \rightarrow Zr_6O_4(OH)_4(BDC)_6 + 24\ HCl}$$

Of greater interest is the fact that even after 2 DMF washes and subsequent methanol exchange, significant (Cl/Zr = 0.25) chlorine remains in the UiO-66-100-1:1 sample, something which cannot be said for the UiO-66-220-2:1, where chlorine is completely removed after just 2 DMF washes, demonstrating the ideality of this sample.

The nature of the residual chlorine in samples such as UiO-66-100-1:1 cannot be determined by EDS results. However, one can speculate that it exists either on defect sites or as part of an amorphous impurity phase. An interesting possibility is that chlorine may compensate for the charge and coordination deficiencies of missing linker defects by bonding to the resultant open zirconium sites. In order to investigate the feasibility of this hypothesis, EDS data was collected on the entire series of washed samples. **Figures S20 and S21** (over the page) display the results obtained on the twice DMF washed and methanol exchanged samples respectively.

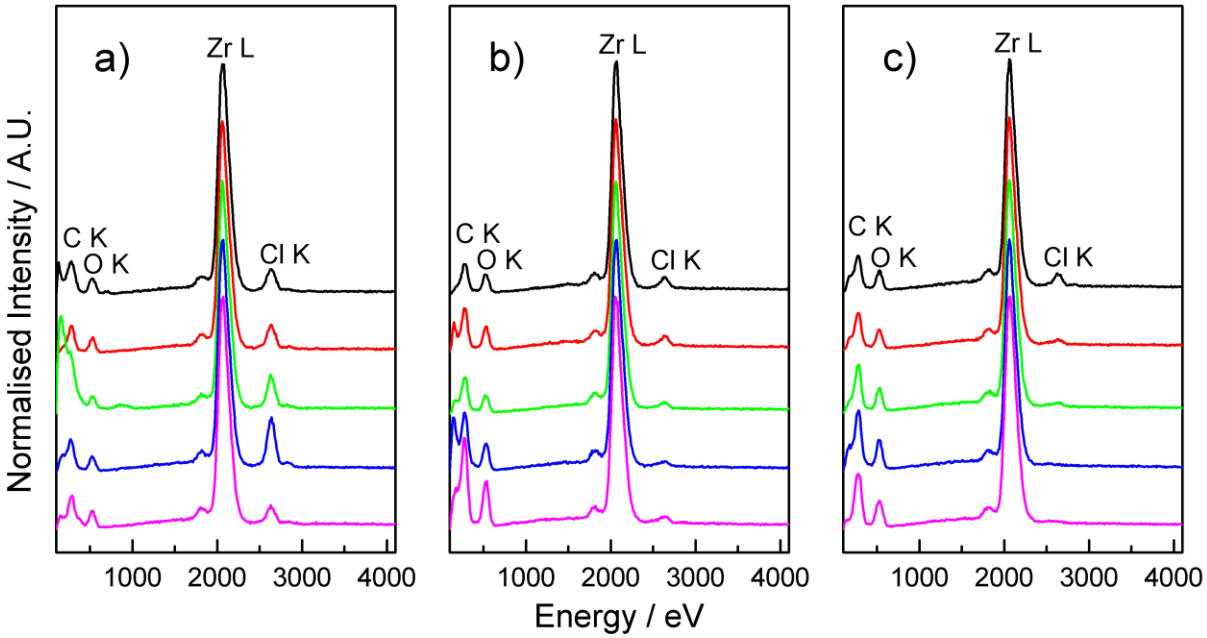

Figure S20: EDS spectra (normalized by Zr L peak) of twice DMF washed UiO-66 samples synthesized at a) 100; b) 160 and; c) 220 °C. Black, red, green, blue and magenta spectra were recorded on samples synthesized with BDC:Zr ratios of 1:1, 5:4, 3:2, 7:4, and 2:1 respectively.

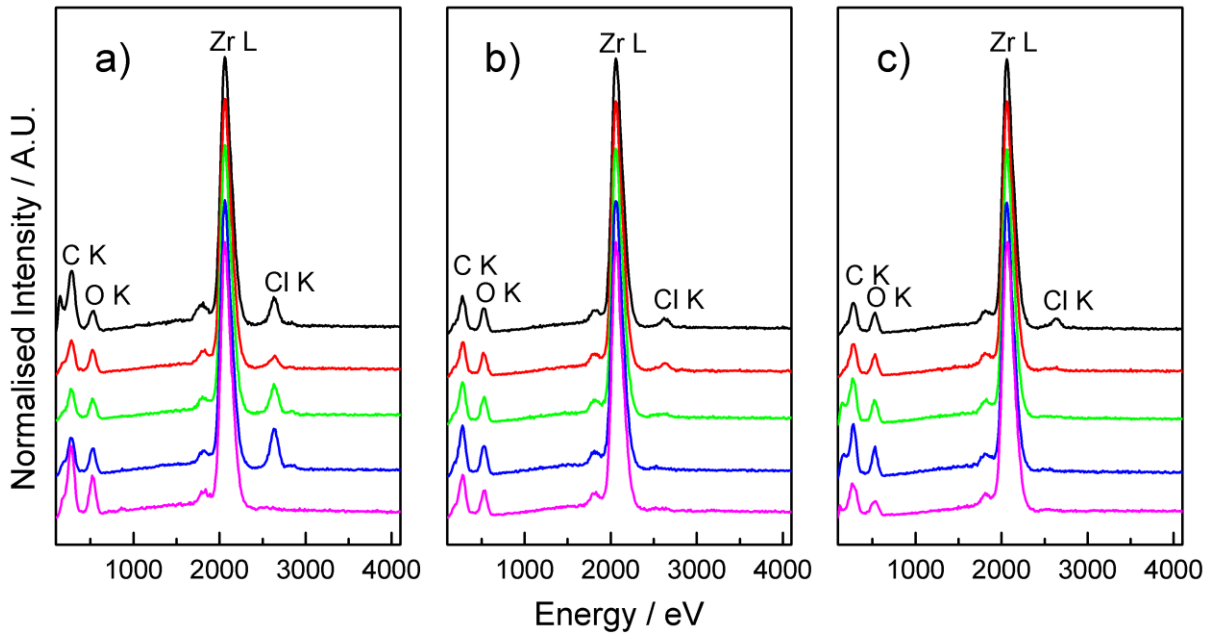

Figure S21: EDS spectra (normalized by Zr L peak) of methanol exchanged UiO-66 samples synthesized at a) 100; b) 160 and; c) 220 °C. Black, red, green, blue and magenta spectra were recorded on samples synthesized with BDC:Zr ratios of 1:1, 5:4, 3:2, 7:4, and 2:1 respectively.

The quantitative data derived from the spectra in **Figures S21** and **S22** is summarized in **Table S5**, where the concentration of chlorine relative to zirconium in the samples is presented. With only two significant outliers (UiO-66-100-3:2 and UiO-66-100-7:4), it can be seen that the chlorine content generally decreases with increasing synthesis temperature and BDC:Zr ratios. This is the inverse of what was found regarding the TGA plateaus of the materials (see section E). Since low TGA plateaus are indicative of missing linkers, there is therefore a correlation between the chlorine content and the number of linker deficiencies on the samples. Such a correlation is compelling evidence for the hypothesis that missing linker defects may be at least partially terminated by chloride.

Table S5: Quantitative data derived from the spectra presented in **Figures S20 and S21**.

	Cl : Zr Atomic Ratio	
Sample	**2 x DMF Washed**	**MeOH Exchanged**
UiO-66-100-1:1	0.26	0.25
UiO-66-100-5:4	0.25	0.11
UiO-66-100-3:2	0.34	0.27
UiO-66-100-7:4	0.50	0.36
UiO-66-100-2:1	0.18	0
UiO-66-160-1:1	0.12	0.08
UiO-66-160-5:4	0.11	0.07
UiO-66-160-3:2	0.07	0.07
UiO-66-160-7:4	0.05	0
UiO-66-160-2:1	0.07	0
UiO-66-220-1:1	0.13	0.09
UiO-66-220-5:4	0.05	0.03
UiO-66-220-3:2	0.05	0
UiO-66-220-7:4	0	0
UiO-66-220-2:1	0	0

J) Raman Spectroscopy – Comparison Between Simulated and Experimental Results

Figure S22 compares the Raman spectra recorded on the samples at the two extremities of the series (grey curve: UiO-66-100-1:1-MeOH; red curve: UiO-66-220-2:1-MeOH) with that simulated from a model of the ideal UiO-66 structure (green curve):

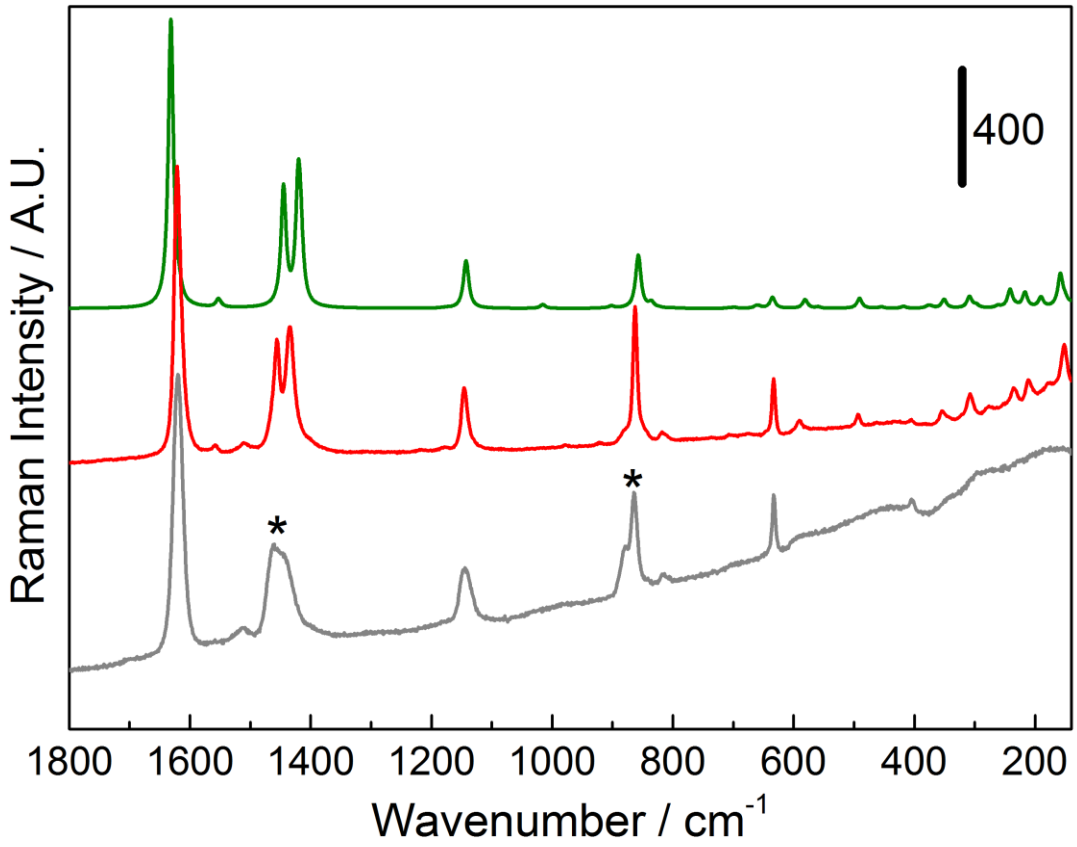

Figure S22: Raman spectra. From top to bottom: Simulated from a model of the ideal UiO-66 structure (green curves); Measured on UiO-66-220-2:1-MeOH (red curves); Measured on UiO-66-100-1:1-MeOH (grey curves). Before measurement, the samples were activated at 150 °C for 2h under vacuum. Spectral regions which deviate significantly from the model spectrum are marked by asterisks.

The close resemblance of the simulated Raman spectrum to that experimentally collected on UiO-66-220-2:1-MeOH is conspicuous, a finding which not only emphasizes the ideality of the sample, but also allows the synergistic power of the experimental/computational approach to be demonstrated. That is, the complete Raman spectrum of UiO-66-220-2:1 can now be assigned irrefutably by visualization of the relevant vibrational modes on the idealized model. Note that this is only possible due to the near equivalence of the experimental and simulated data. The assignment is presented in **Table S6**, whose caption contains a link to a web address where the vibrational modes of UiO-66 may be visualized via animations.

Table S6: Comparison and assignment of the vibrational frequencies in the simulated and experimental Raman spectra (green and red curves of **Figure S22**, respectively). Numbers in brackets are the values calculated before being shifted by a 0.98 scaling factor**.** Animations available at **http://www.crystal.unito.it/vibs/uio66_hydro/**

Vibrational Frequency / cm^{-1}		Assignment
Exp.	**Calc.**	
1621	1632 (1665)	C-C aromatic stretch in phase
1454	1445 (1474)	Carboxylate OCO symmetric stretch (C-C aromatic to carboxylate stretch)
1434	1420-(1449)	C-C aromatic to carboxylate stretch (Carboxylate OCO symmetric stretch)
1145	1143 (1166)	C-C symmetric ring breathing
862	858 (875)	OH bending + CC symmetric breathing
818	836 (853)	O-H bending
634	635 (648)	C-C-C aromatic ring in plane bending
589	581 (593)	C-C-C- Carboxylate to aromatic in plane bending
493	491 (501)	Zr-μ^3O symmetric stretching
353	351 (358)	Framework out of phase breathing
308	308 (314)	Out of plane, out of phase C-C-C bending
210	217 (221)	Zr-μ^3O asymmetric stretching
152	160 (163)	Cluster torsion mode

Returning attention to **Figure S22**, it can be seen that the spectrum of UiO-66-100-1:1 (grey curves) clearly deviates from the model. Several discrepancies are observed, with the most severe being accentuated by asterisks. To this end, the model once again proves useful in that it tells us that the two asterisked regions (appearing at ca. 1450 and 870 cm^{-1}) are associated with carboxylate based and O-H bending modes respectively. Carboxylate based modes are exactly those one would expect to be most affected by linker deficiencies. The observation of peculiarities in this region therefore provides compelling further evidence for the presence of missing linker defects on this sample.

Of further note is the distinct lack of bands below 500 cm^{-1} in the spectrum of this material, a region where several bands are expected to appear. The majority of the bands in this portion of the spectrum are associated with vibrations involving the Zr-O bonds of the inorganic cornerstones. The absence of these bands suggests that either the cornerstone vibrations are strongly affected by linker deficiencies or there are defects on the clusters themselves.

K) Appendix

Table of Content

1. Individual PXRD Thermal Stability Plots

Table of Content

1.1.1. Thermal Stability Tests - Crude (Unwashed) Samples Synthesized at 100 °C

Figures S23-S27 present the results of thermal stability tests performed on crude (unwashed) samples synthesized at 100 °C with BDC:Zr ratios of 1:1, 5:4, 3:2, 7:4, and 2:1 respectively:

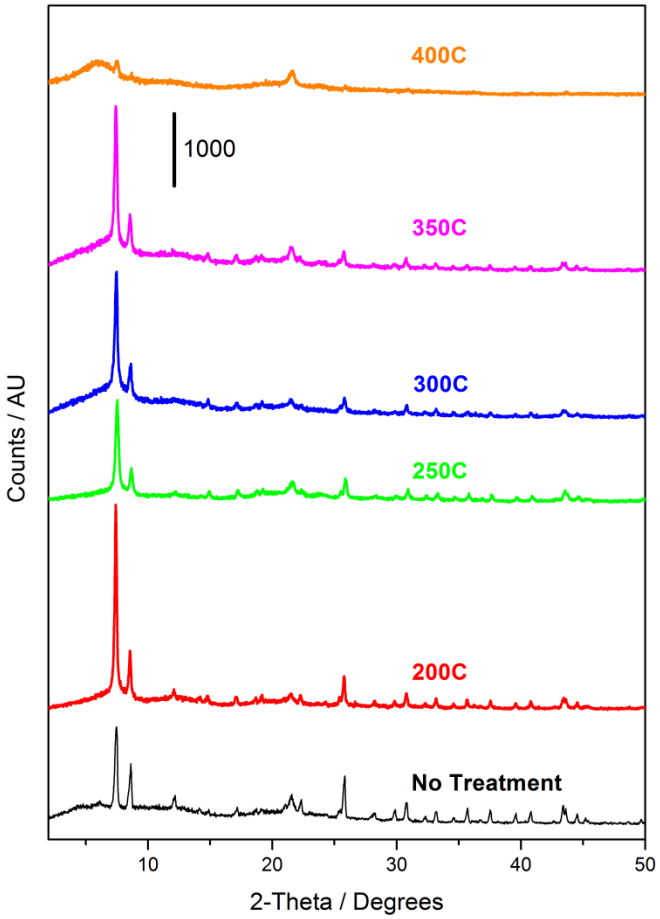

Figure S23: PXRD patterns recorded on crude (unwashed) UiO-66-100-1:1 after 12 hour exposures (in air) to the temperatures indicated on the figure.

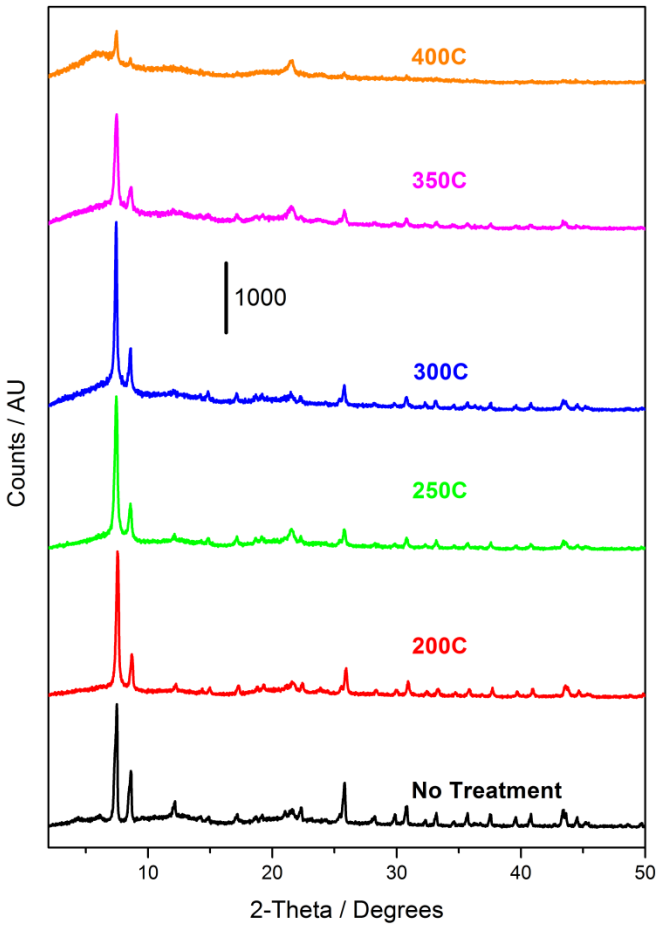

Figure S24: PXRD patterns recorded on crude (unwashed) UiO-66-100-5:4 after 12 hour exposures (in air) to the temperatures indicated on the figure.

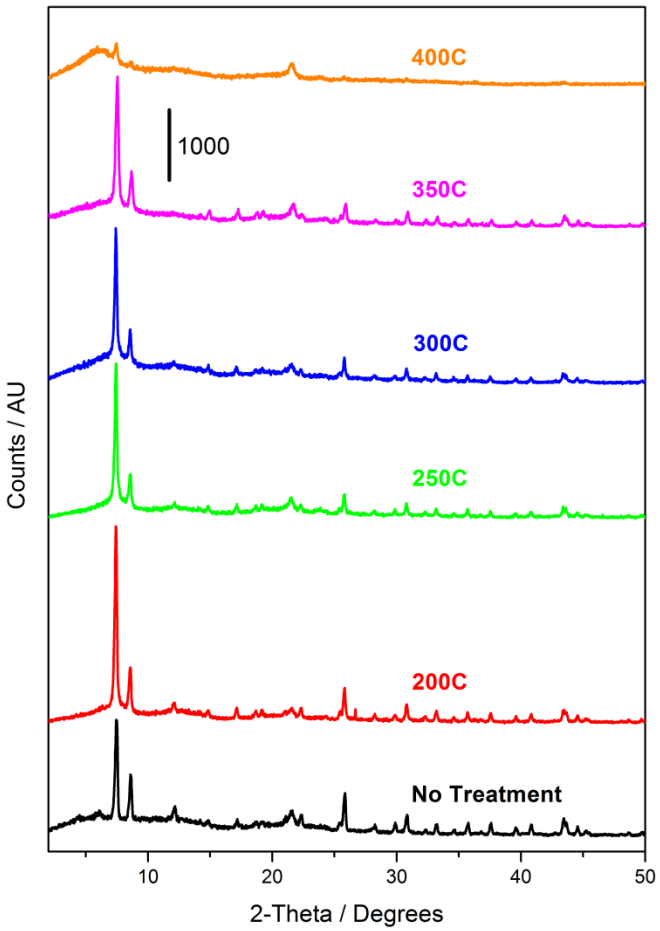

Figure S25: PXRD patterns recorded on crude (unwashed) UiO-66-100-3:2 after 12 hour exposures (in air) to the temperatures indicated on the figure.

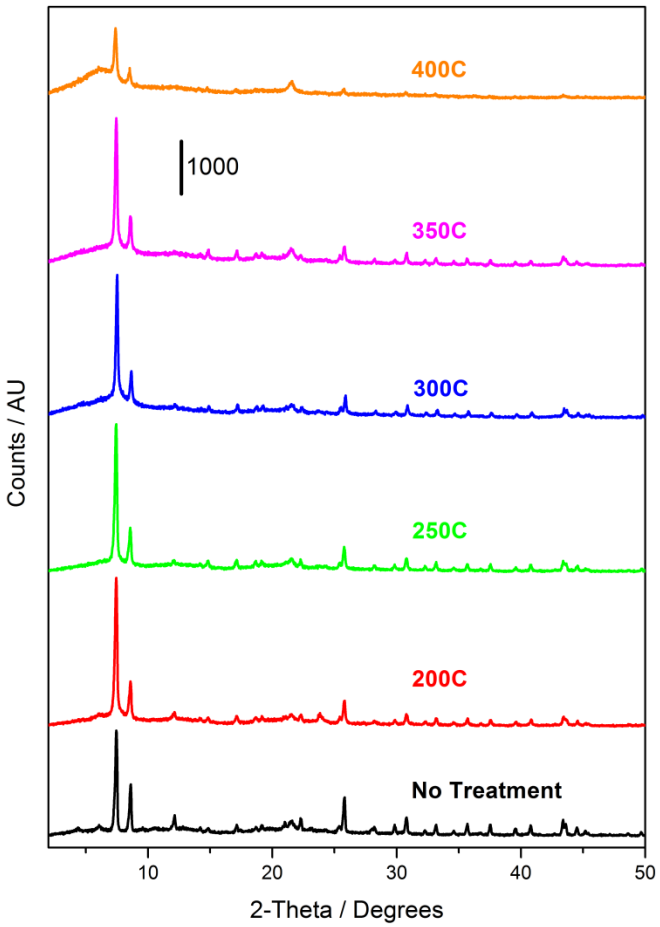

Figure S26: PXRD patterns recorded on crude (unwashed) UiO-66-100-7:4 after 12 hour exposures (in air) to the temperatures indicated on the figure.

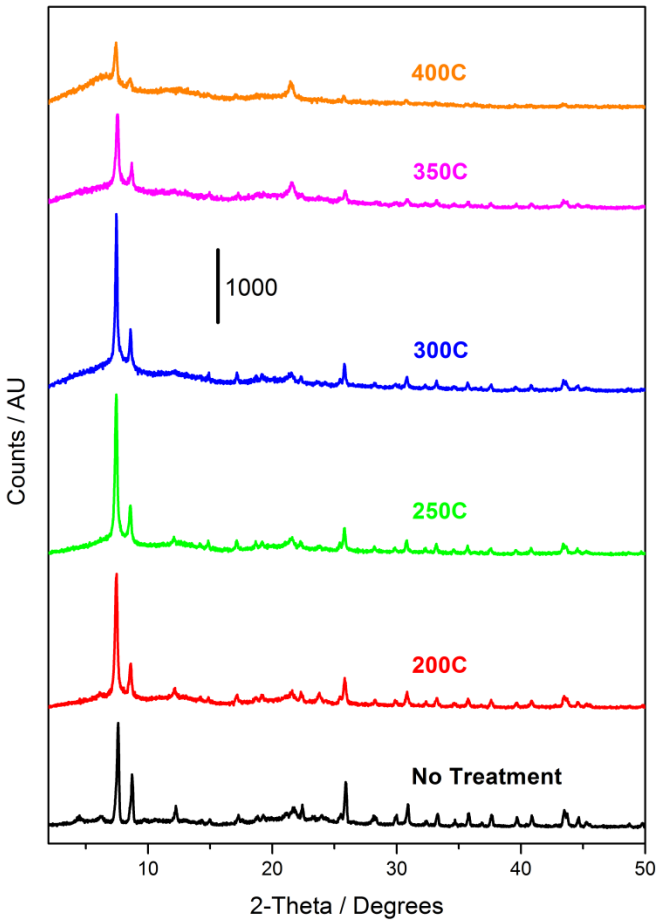

Figure S27: PXRD patterns recorded on crude (unwashed) UiO-66-100-2:1 after 12 hour exposures (in air) to the temperatures indicated on the figure.

1.1.2. Thermal Stability Tests - Twice DMF Washed Samples Synthesized at 100 °C

Figures S28-S32 present the results of thermal stability tests performed on twice DMF washed samples synthesized at 100 °C with BDC:Zr ratios of 1:1, 5:4, 3:2, 7:4, and 2:1 respectively:

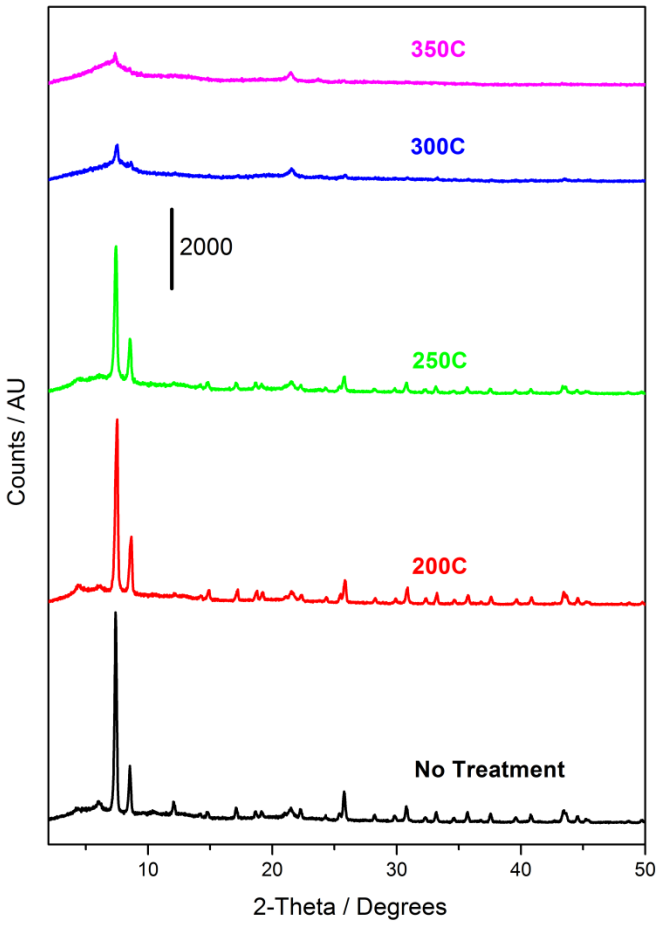

Figure S28: PXRD patterns recorded on UiO-66-100-1:1-2DMF after 12 hour exposures (in air) to the temperatures indicated on the figure.

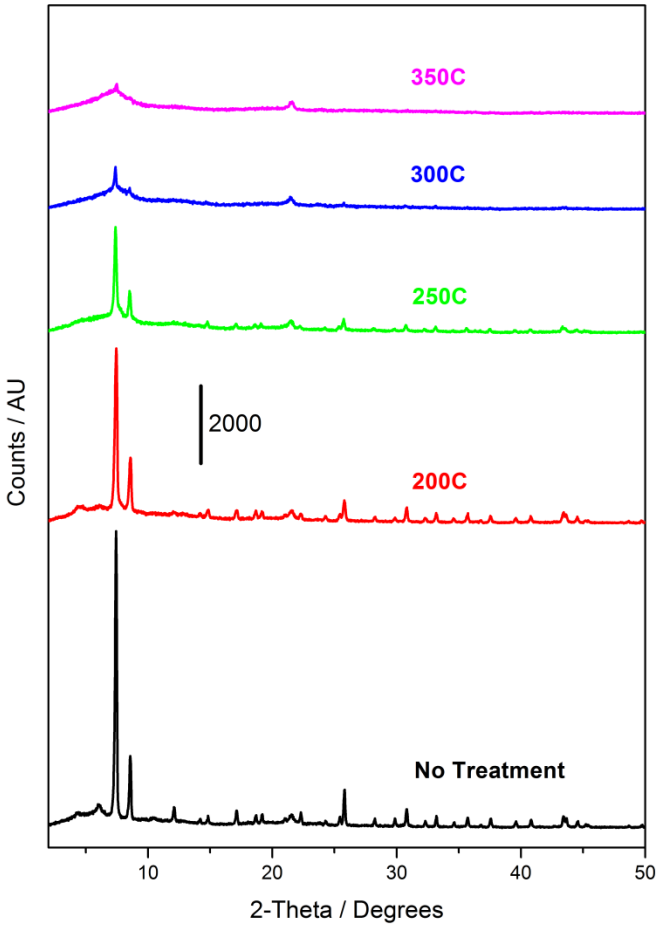

Figure S29: PXRD patterns recorded on UiO-66-100-5:4-2DMF after 12 hour exposures (in air) to the temperatures indicated on the figure.

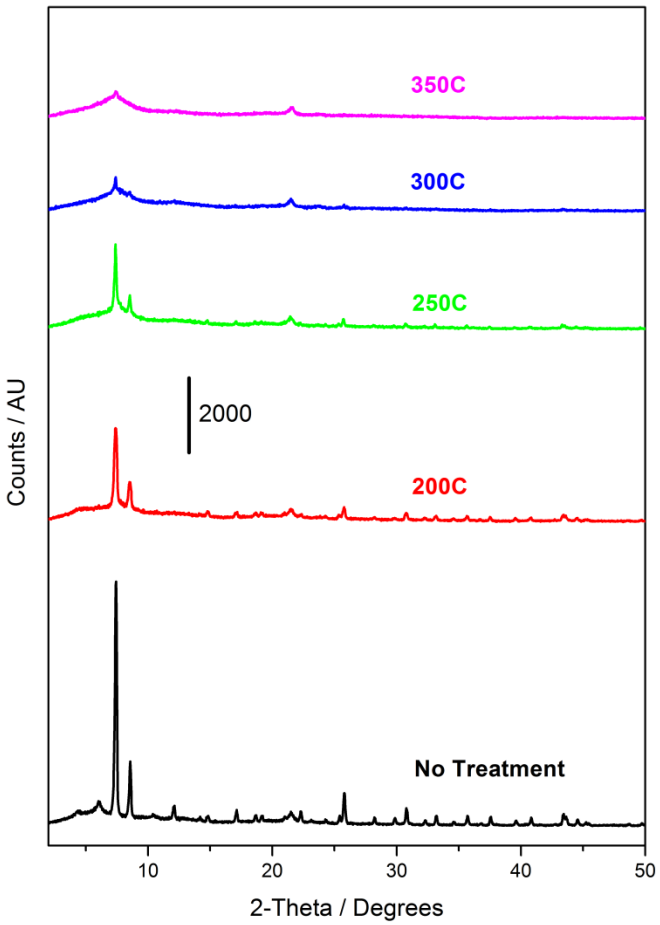

Figure S30: PXRD patterns recorded on UiO-66-100-3:2-2DMF after 12 hour exposures (in air) to the temperatures indicated on the figure.

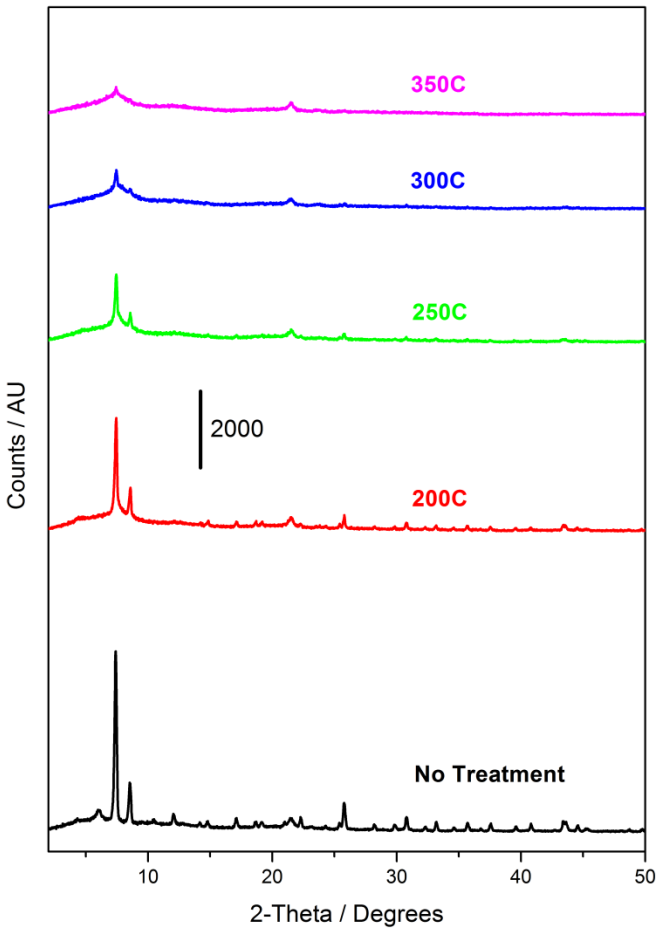

Figure S31: PXRD patterns recorded on UiO-66-100-7:4-2DMF after 12 hour exposures (in air) to the temperatures indicated on the figure.

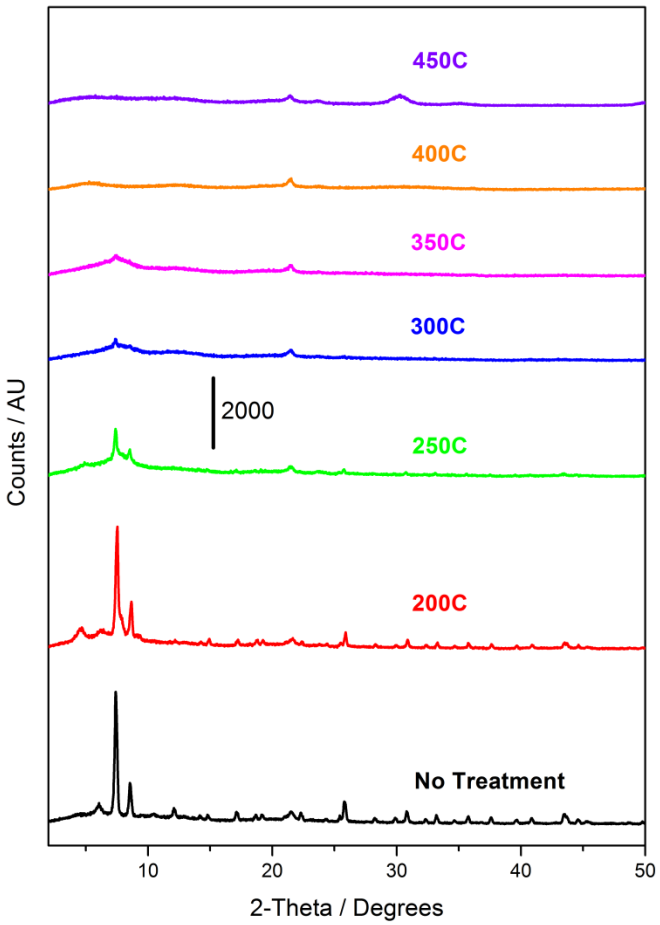

Figure S32: PXRD patterns recorded on UiO-66-100-2:1-2DMF after 12 hour exposures (in air) to the temperatures indicated on the figure. Monoclinic ZrO_2 begins to form after treatment at 450 °C, as evidenced by the emergence of broad and low intensity reflections at 30.3 and 35.1 2θ.

1.1.3. Thermal Stability Tests - Methanol Exchanged Samples Synthesized at 100 °C

Figures S33-S37 present the results of thermal stability tests performed on methanol exchanged samples synthesized at 100 °C with BDC:Zr ratios of 1:1, 5:4, 3:2, 7:4, and 2:1 respectively:

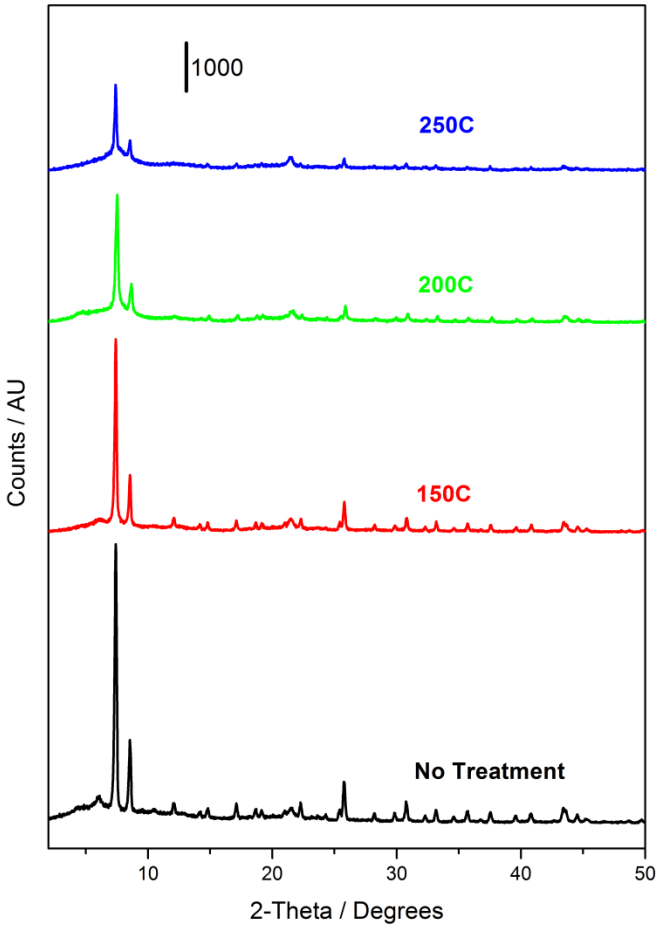

Figure S33: PXRD patterns recorded on UiO-66-100-1:1-MeOH after 12 hour exposures (in air) to the temperatures indicated on the figure.

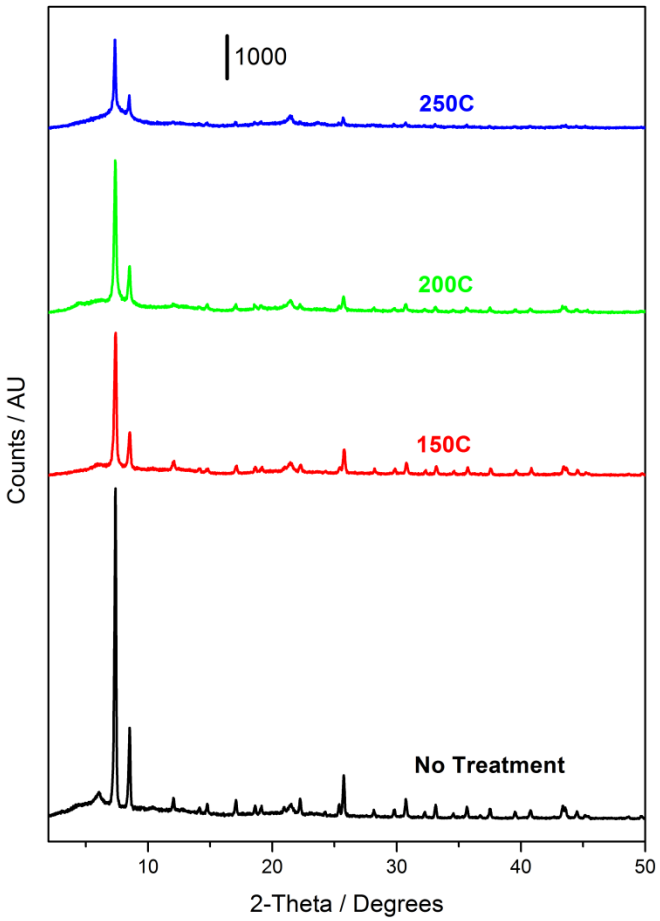

Figure S34: PXRD patterns recorded on UiO-66-100-5:4-MeOH after 12 hour exposures (in air) to the temperatures indicated on the figure.

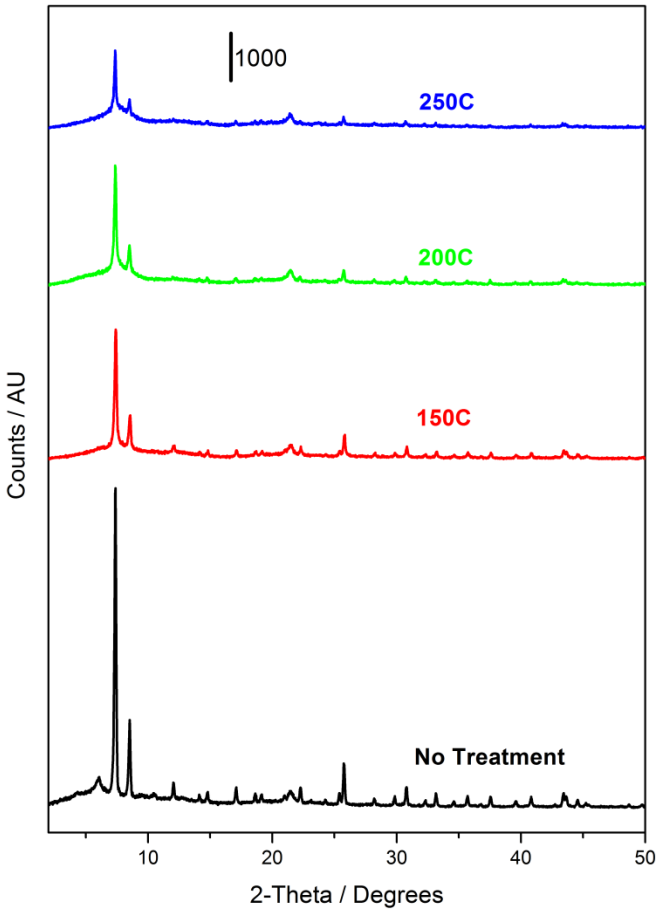

Figure S35: PXRD patterns recorded on UiO-66-100-3:2-MeOH after 12 hour exposures (in air) to the temperatures indicated on the figure.

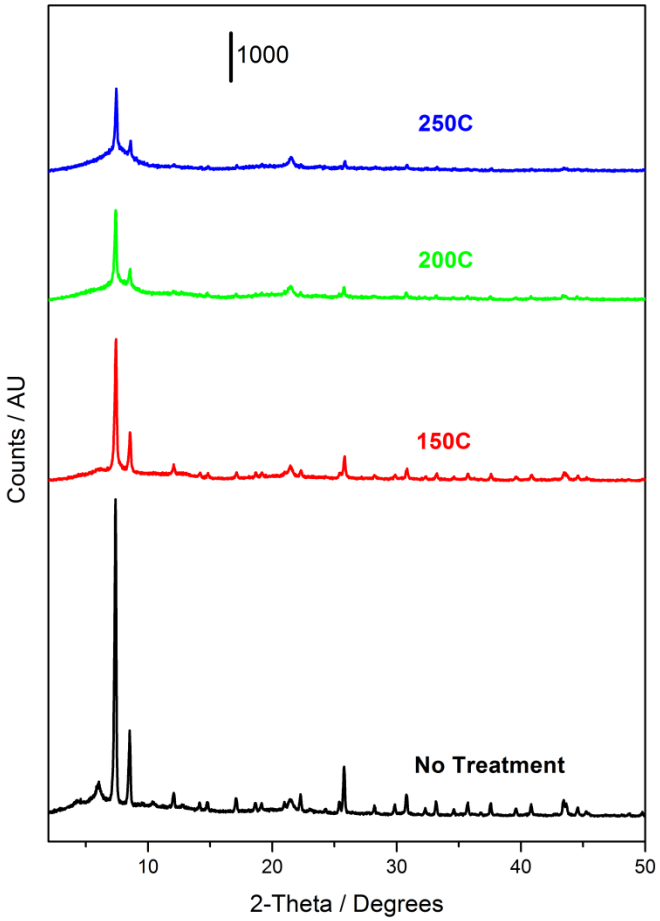

Figure S36: PXRD patterns recorded on UiO-66-100-7:4-MeOH after 12 hour exposures (in air) to the temperatures indicated on the figure.

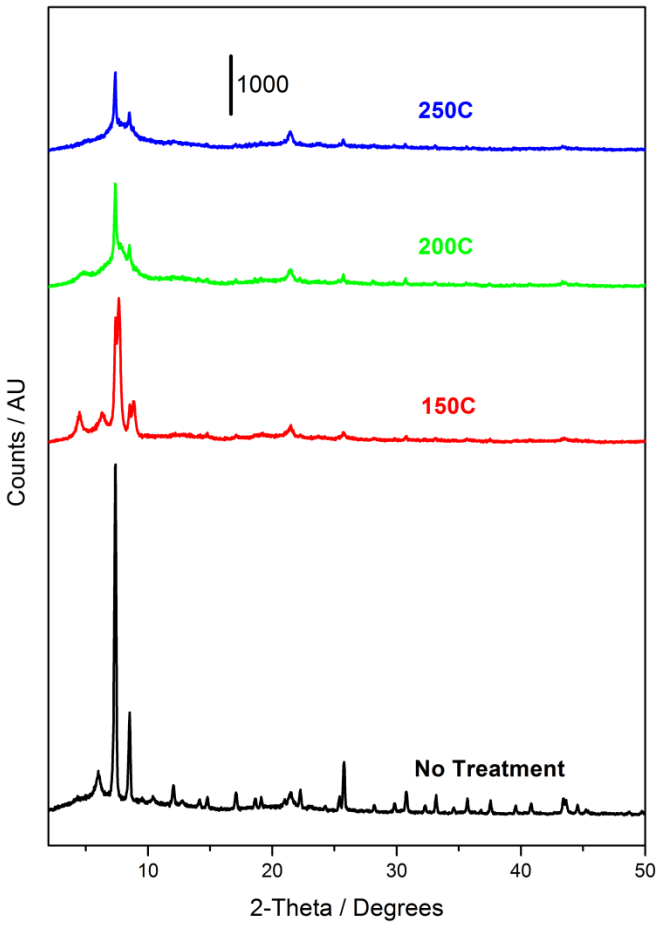

Figure S37: PXRD patterns recorded on UiO-66-100-2:1-MeOH after 12 hour exposures (in air) to the temperatures indicated on the figure.

1.2.1. Thermal Stability Tests - Crude (Unwashed) Samples Synthesized at 160 °C

Figures S38-S42 present the results of thermal stability tests performed on crude (unwashed) samples synthesized at 160 °C with BDC:Zr ratios of 1:1, 5:4, 3:2, 7:4, and 2:1 respectively:

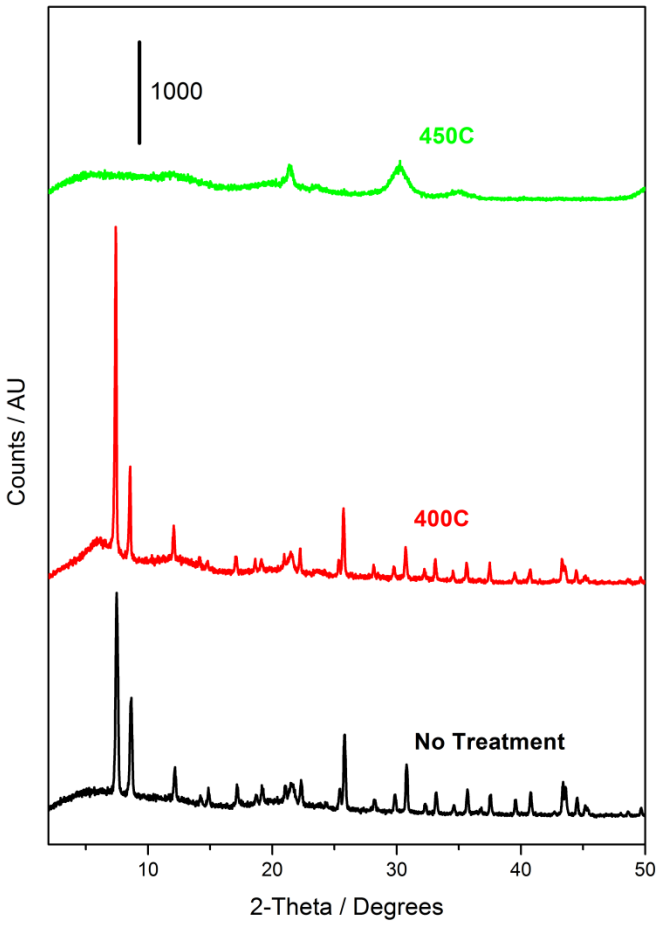

Figure S38: PXRD patterns recorded on crude (unwashed) UiO-66-160-1:1 after 12 hour exposures (in air) to the temperatures indicated on the figure. Monoclinic ZrO_2 begins to form after treatment at 450 °C, as evidenced by the emergence of broad and low intensity reflections at 30.3 and 35.1 2θ.

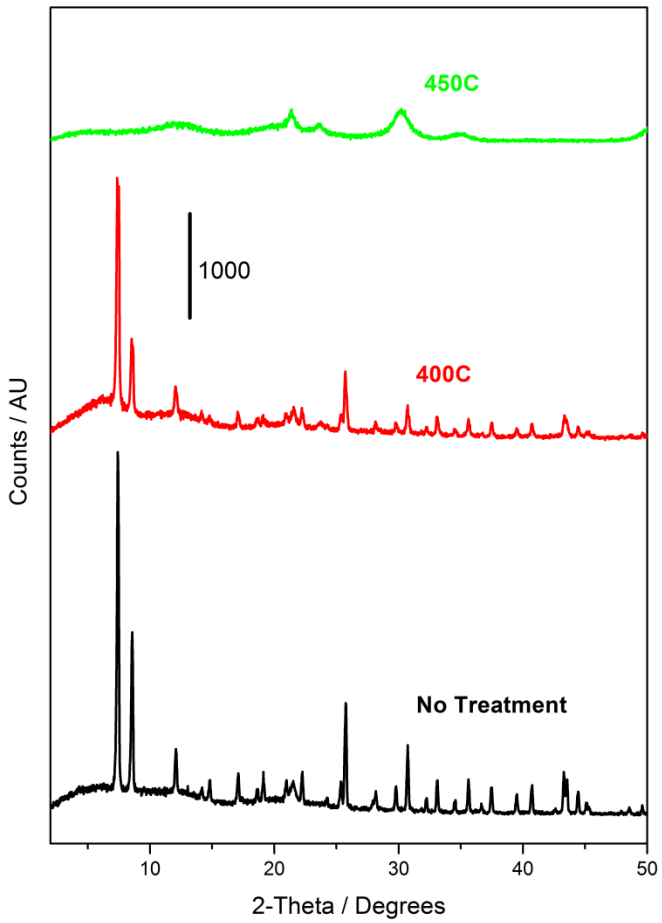

Figure S39: PXRD patterns recorded on crude (unwashed) UiO-66-160-5:4 after 12 hour exposures (in air) to the temperatures indicated on the figure. Monoclinic ZrO_2 begins to form after treatment at 450 °C, as evidenced by the emergence of broad and low intensity reflections at 30.3 and 35.1 2θ.

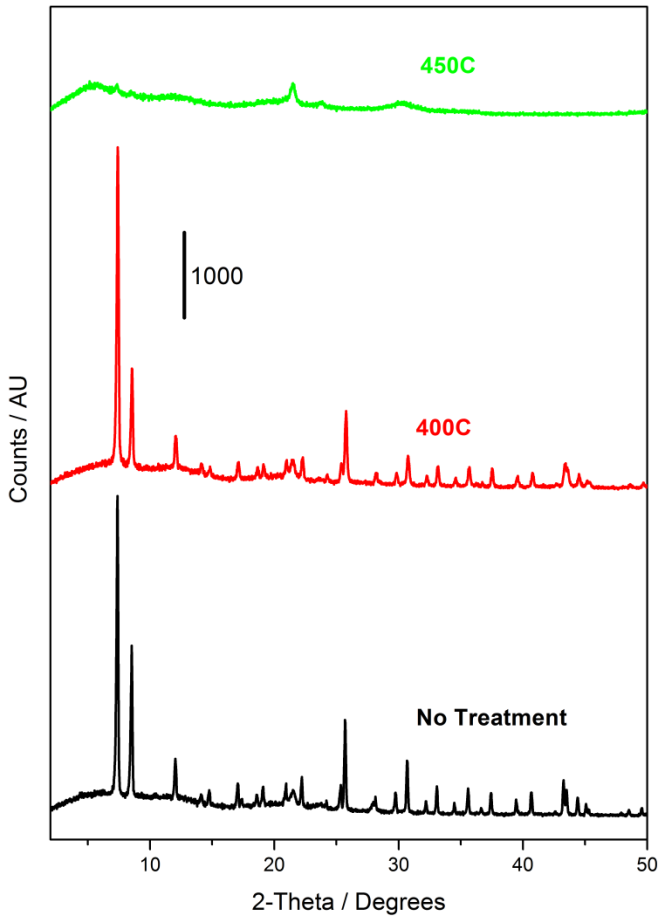

Figure S40: PXRD patterns recorded on crude (unwashed) UiO-66-160-3:2 after 12 hour exposures (in air) to the temperatures indicated on the figure. Monoclinic ZrO_2 begins to form after treatment at 450 °C, as evidenced by the emergence of broad and low intensity reflections at 30.3 and 35.1 2θ.

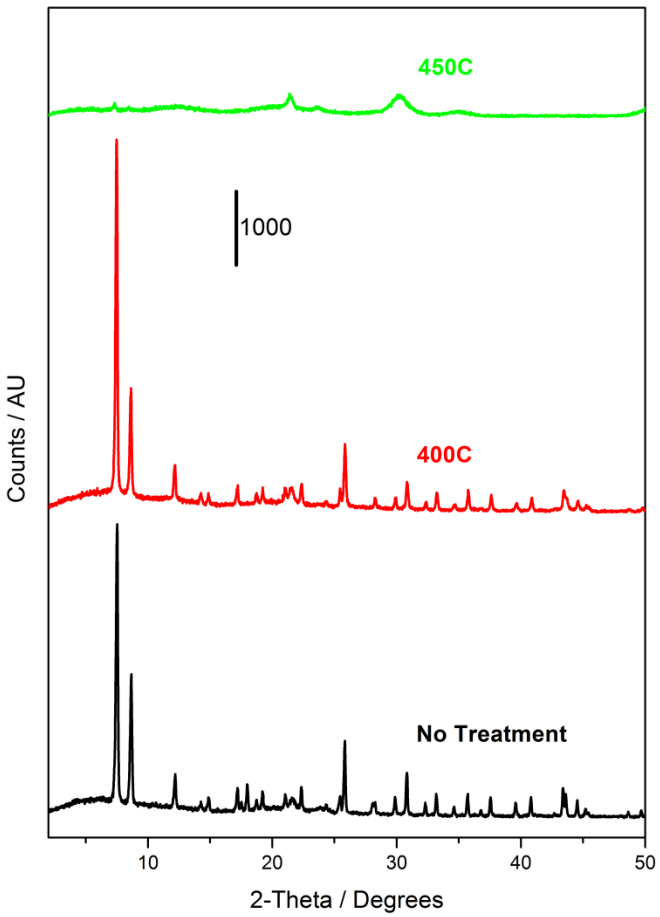

Figure S41: PXRD patterns recorded on crude (unwashed) UiO-66-160-7:4 after 12 hour exposures (in air) to the temperatures indicated on the figure. Monoclinic ZrO_2 begins to form after treatment at 450 °C, as evidenced by the emergence of broad and low intensity reflections at 30.3 and 35.1 2θ.

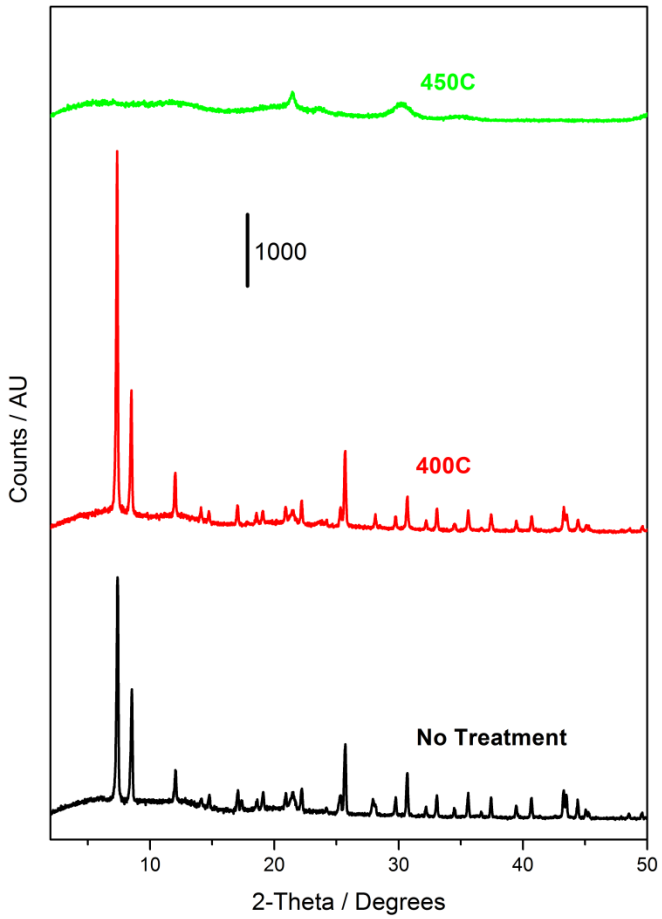

Figure S42: PXRD patterns recorded on crude (unwashed) UiO-66-160-2:1 after 12 hour exposures (in air) to the temperatures indicated on the figure. Monoclinic ZrO_2 begins to form after treatment at 450 °C, as evidenced by the emergence of broad and low intensity reflections at 30.3 and 35.1 2θ.

1.2.2. Thermal Stability Tests - Twice DMF Washed Samples Synthesized at 160 °C

Figures S43-S47 present the results of thermal stability tests performed on twice DMF washed samples synthesized at 160 °C with BDC:Zr ratios of 1:1, 5:4, 3:2, 7:4, and 2:1 respectively:

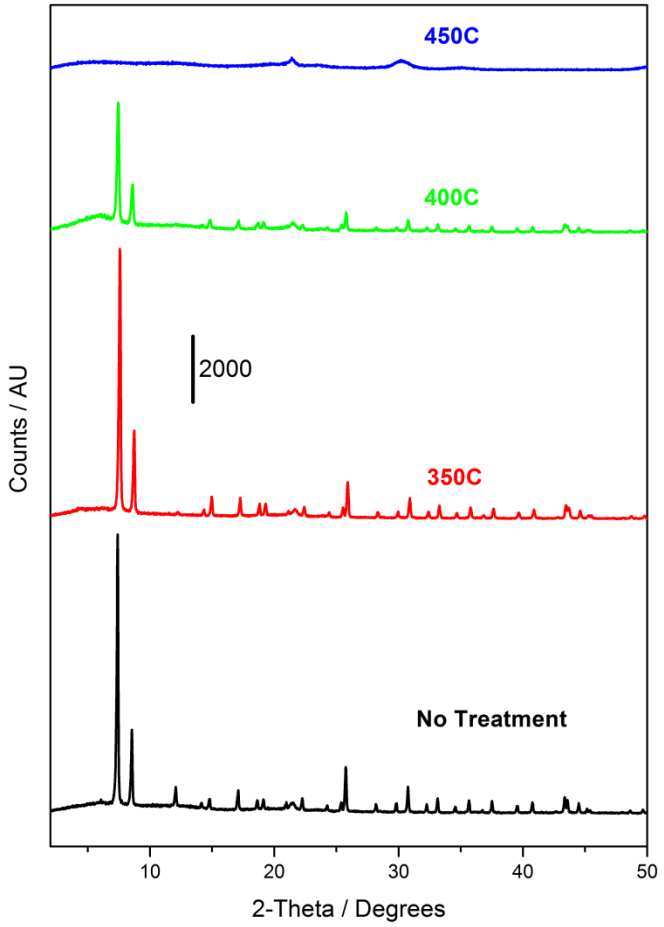

Figure S43: PXRD patterns recorded on UiO-66-160-1:1-2DMF after 12 hour exposures (in air) to the temperatures indicated on the figure. Monoclinic ZrO_2 begins to form after treatment at 450 °C, as evidenced by the emergence of broad and low intensity reflections at 30.3 and 35.1 2θ.

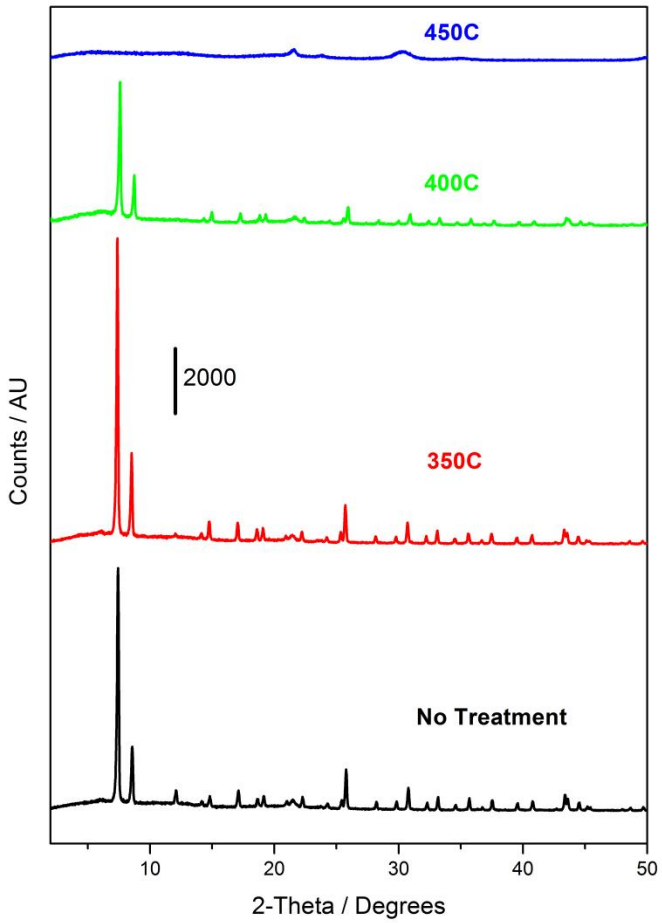

Figure S44: PXRD patterns recorded on UiO-66-160-5:4-2DMF after 12 hour exposures (in air) to the temperatures indicated on the figure. Monoclinic ZrO_2 begins to form after treatment at 450 °C, as evidenced by the emergence of broad and low intensity reflections at 30.3 and 35.1 2θ.

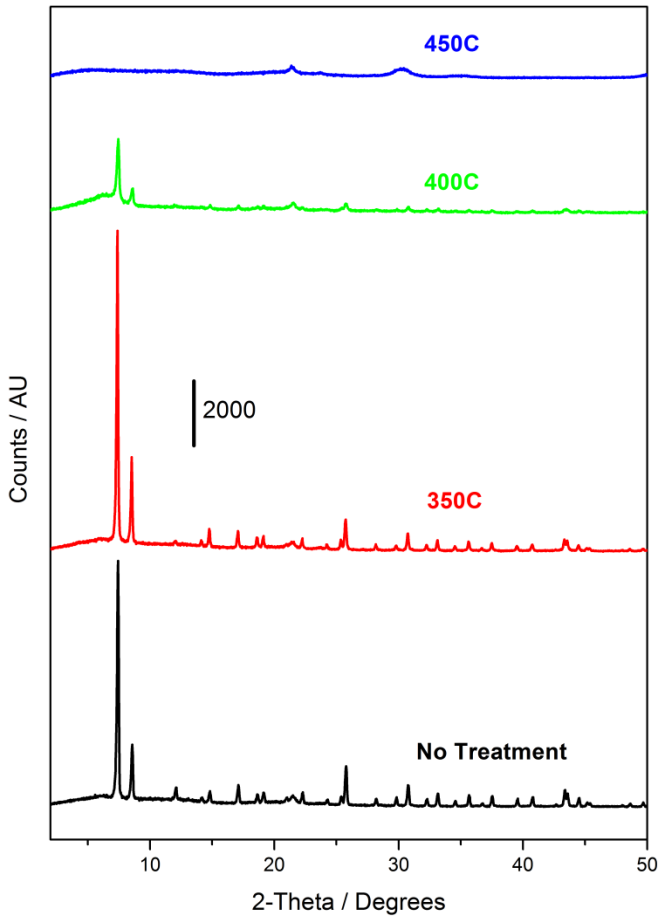

Figure S45: PXRD patterns recorded on UiO-66-160-3:2-2DMF after 12 hour exposures (in air) to the temperatures indicated on the figure. Monoclinic ZrO_2 begins to form after treatment at 450 °C, as evidenced by the emergence of broad and low intensity reflections at 30.3 and 35.1 2θ.

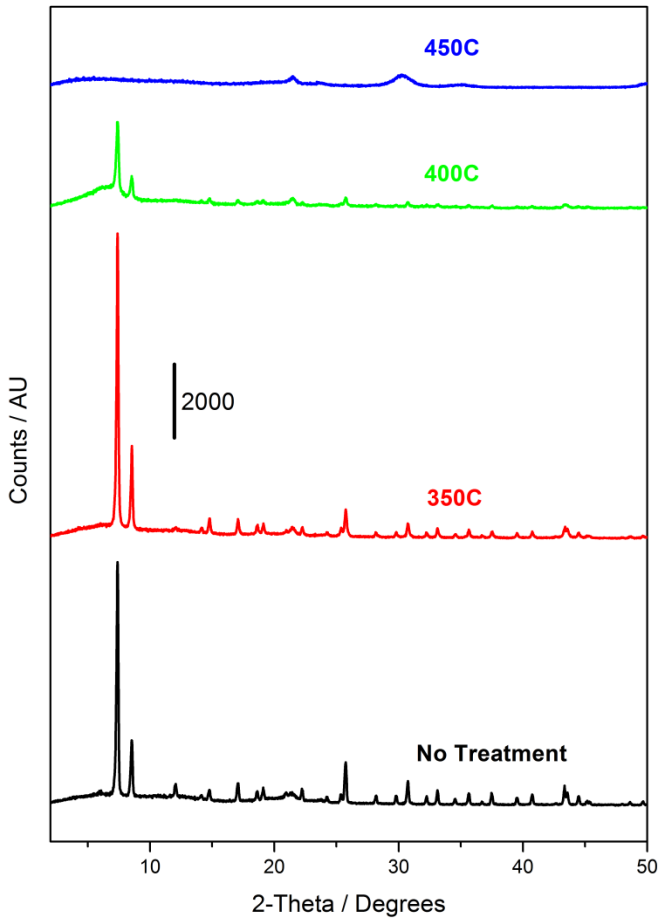

Figure S46: PXRD patterns recorded on UiO-66-160-7:4-2DMF after 12 hour exposures (in air) to the temperatures indicated on the figure. Monoclinic ZrO_2 begins to form after treatment at 450 °C, as evidenced by the emergence of broad and low intensity reflections at 30.3 and 35.1 2θ.

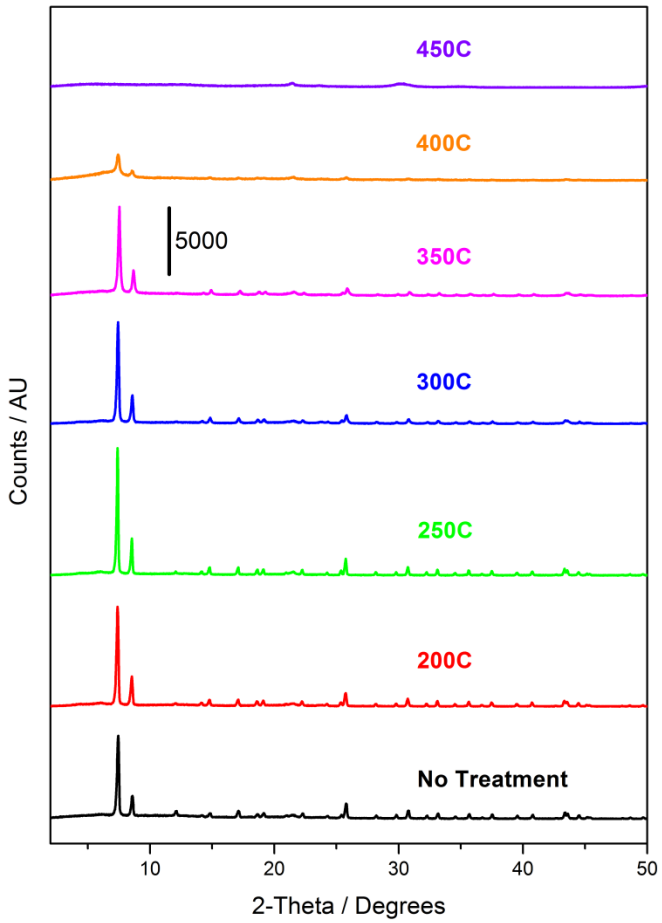

Figure S47: PXRD patterns recorded on UiO-66-160-2:1-2DMF after 12 hour exposures (in air) to the temperatures indicated on the figure. Monoclinic ZrO_2 begins to form after treatment at 450 °C, as evidenced by the emergence of broad and low intensity reflections at 30.3 and 35.1 2θ.

1.2.3. Thermal Stability Tests - Methanol Exchanged Samples Synthesized at 160 °C

Figures S48-S52 present the results of thermal stability tests performed on methanol exchanged samples synthesized at 160 °C with BDC:Zr ratios of 1:1, 5:4, 3:2, 7:4, and 2:1 respectively:

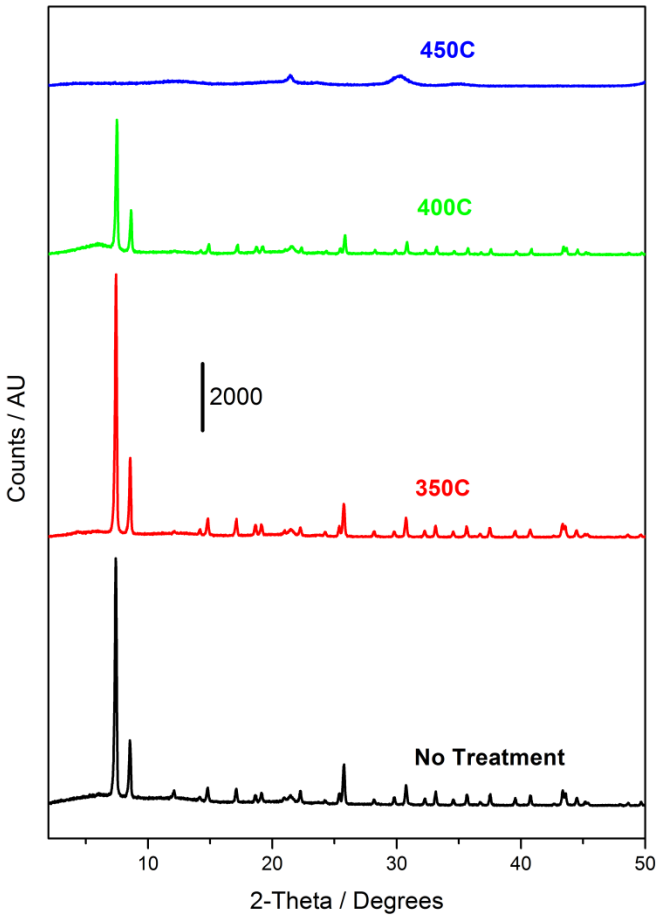

Figure S48: PXRD patterns recorded on UiO-66-160-1:1-MeOH after 12 hour exposures (in air) to the temperatures indicated on the figure. Monoclinic ZrO_2 begins to form after treatment at 450 °C, as evidenced by the emergence of broad and low intensity reflections at 30.3 and 35.1 2θ.

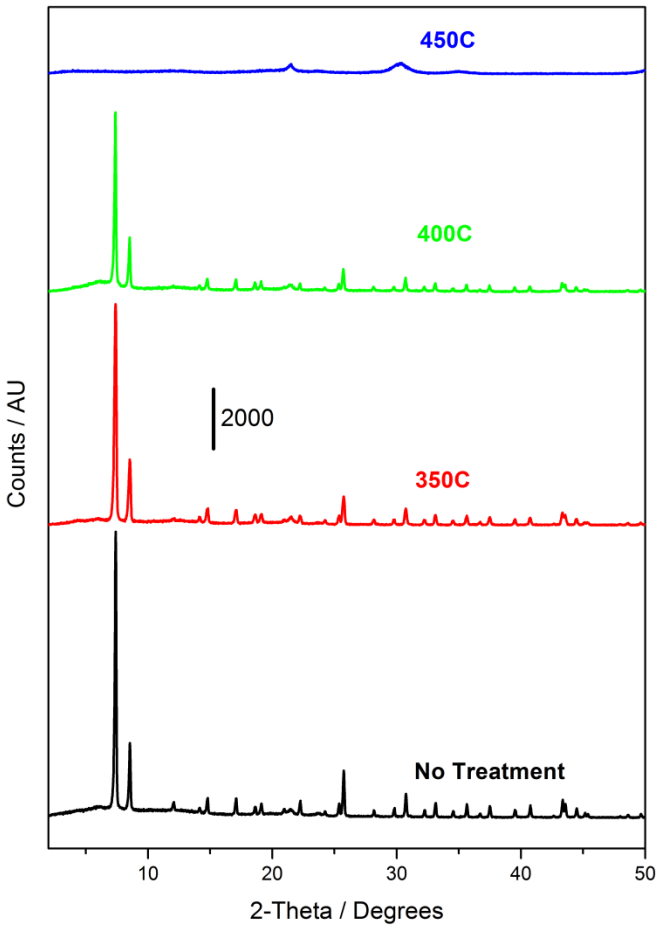

Figure S49: PXRD patterns recorded on UiO-66-160-5:4-MeOH after 12 hour exposures (in air) to the temperatures indicated on the figure. Monoclinic ZrO_2 begins to form after treatment at 450 °C, as evidenced by the emergence of broad and low intensity reflections at 30.3 and 35.1 2θ.

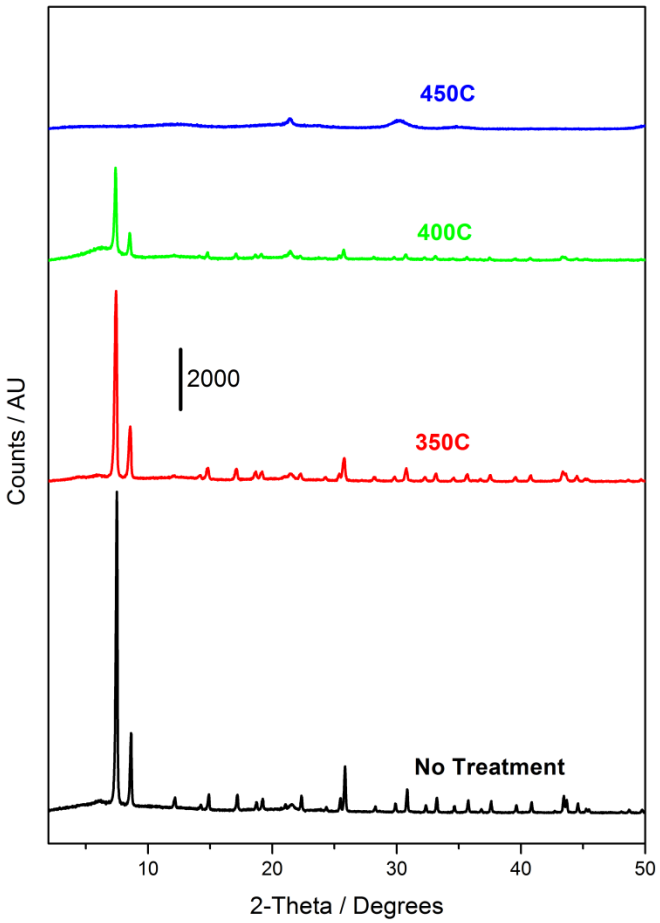

Figure S50: PXRD patterns recorded on UiO-66-160-3:2-MeOH after 12 hour exposures (in air) to the temperatures indicated on the figure. Monoclinic ZrO_2 begins to form after treatment at 450 °C, as evidenced by the emergence of broad and low intensity reflections at 30.3 and 35.1 2θ.

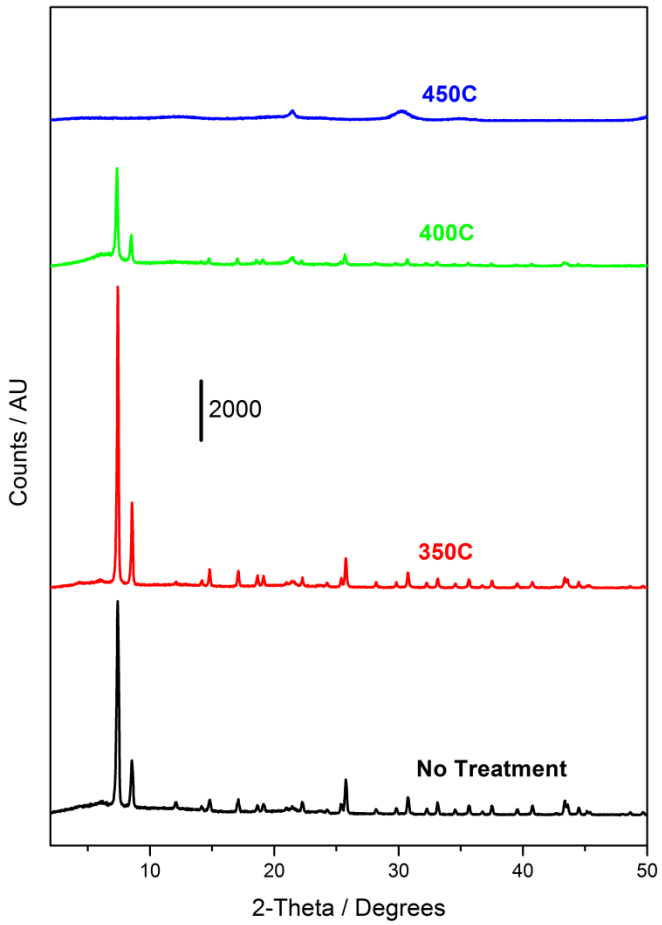

Figure S51: PXRD patterns recorded on UiO-66-160-7:4-MeOH after 12 hour exposures (in air) to the temperatures indicated on the figure. Monoclinic ZrO_2 begins to form after treatment at 450 °C, as evidenced by the emergence of broad and low intensity reflections at 30.3 and 35.1 2θ.

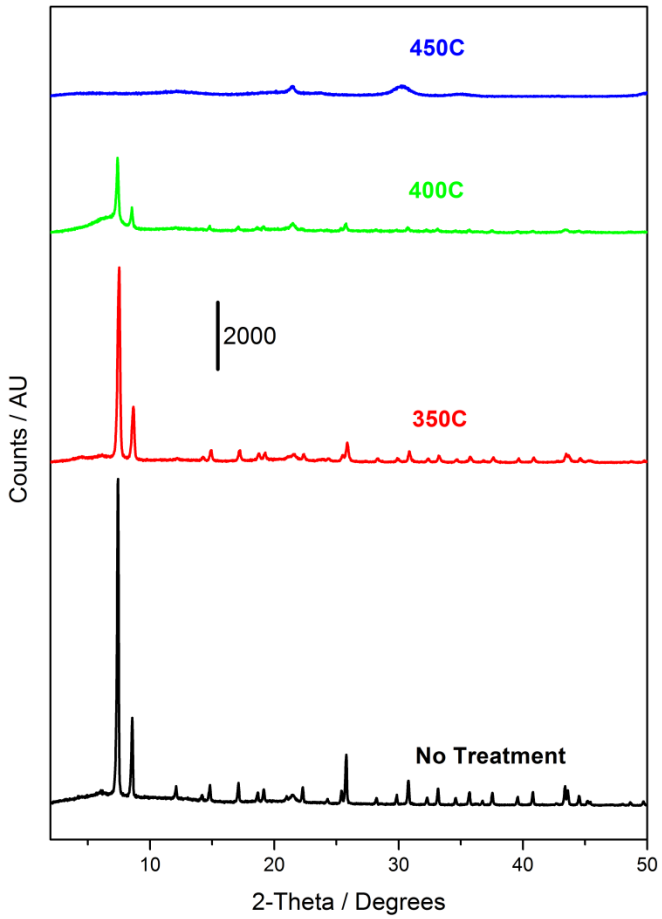

Figure S52: PXRD patterns recorded on UiO-66-160-2:1-MeOH after 12 hour exposures (in air) to the temperatures indicated on the figure. Monoclinic ZrO_2 begins to form after treatment at 450 °C, as evidenced by the emergence of broad and low intensity reflections at 30.3 and 35.1 2θ.

1.3.1. Thermal Stability Tests - Crude (Unwashed) Samples Synthesized at 220 °C

Figures S53-S57 present the results of thermal stability tests performed on crude (unwashed) samples synthesized at 220 °C with BDC:Zr ratios of 1:1, 5:4, 3:2, 7:4, and 2:1 respectively:

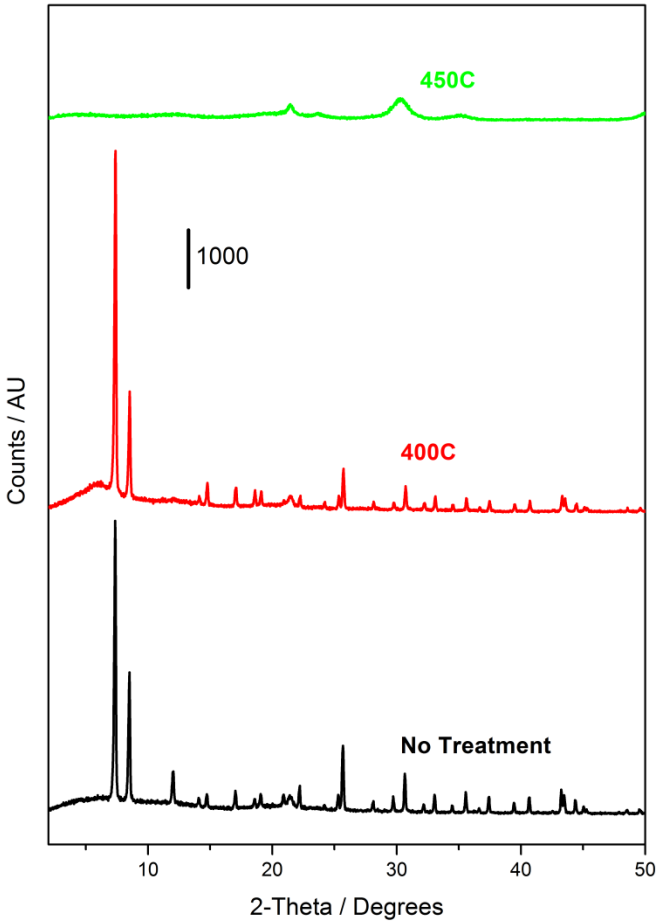

Figure S53: PXRD patterns recorded on crude (unwashed) UiO-66-220-1:1 after 12 hour exposures (in air) to the temperatures indicated on the figure. Monoclinic ZrO_2 begins to form after treatment at 450 °C, as evidenced by the emergence of broad and low intensity reflections at 30.3 and 35.1 2θ.

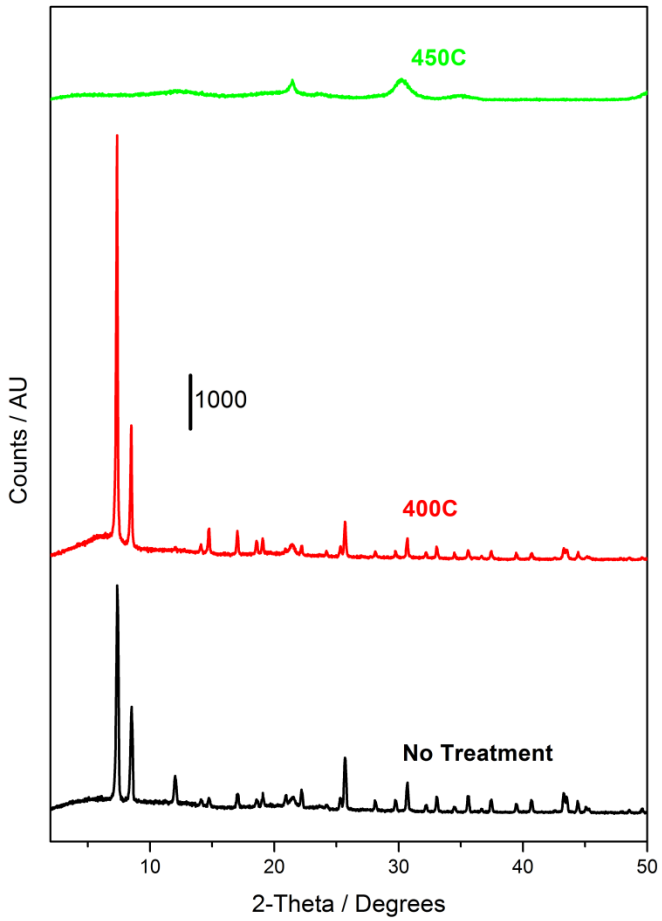

Figure S54: PXRD patterns recorded on crude (unwashed) UiO-66-220-5:4 after 12 hour exposures (in air) to the temperatures indicated on the figure. Monoclinic ZrO_2 begins to form after treatment at 450 °C, as evidenced by the emergence of broad and low intensity reflections at 30.3 and 35.1 2θ.

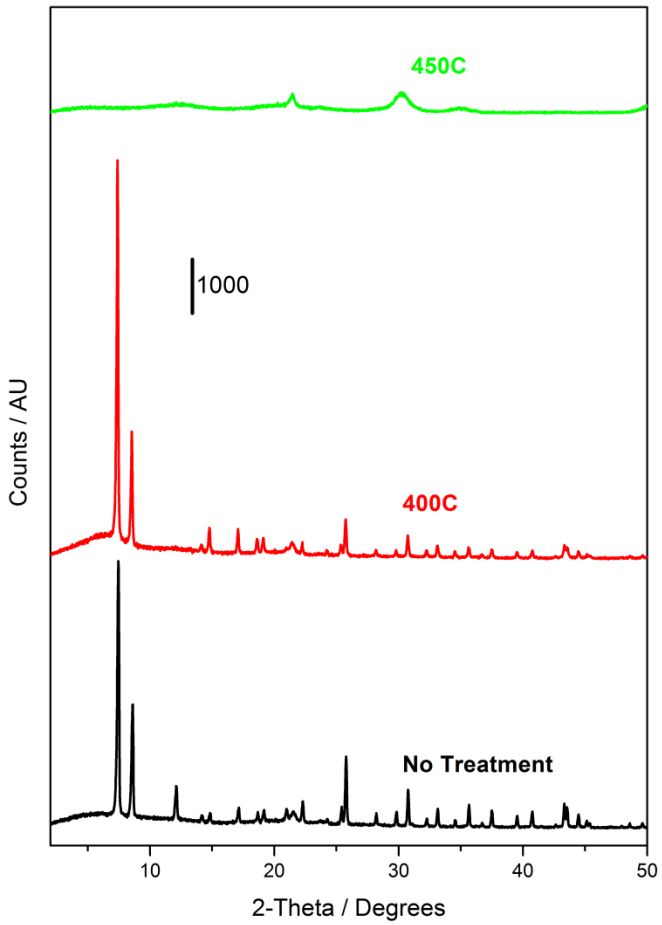

Figure S55: PXRD patterns recorded on crude (unwashed) UiO-66-220-3:2 after 12 hour exposures (in air) to the temperatures indicated on the figure.

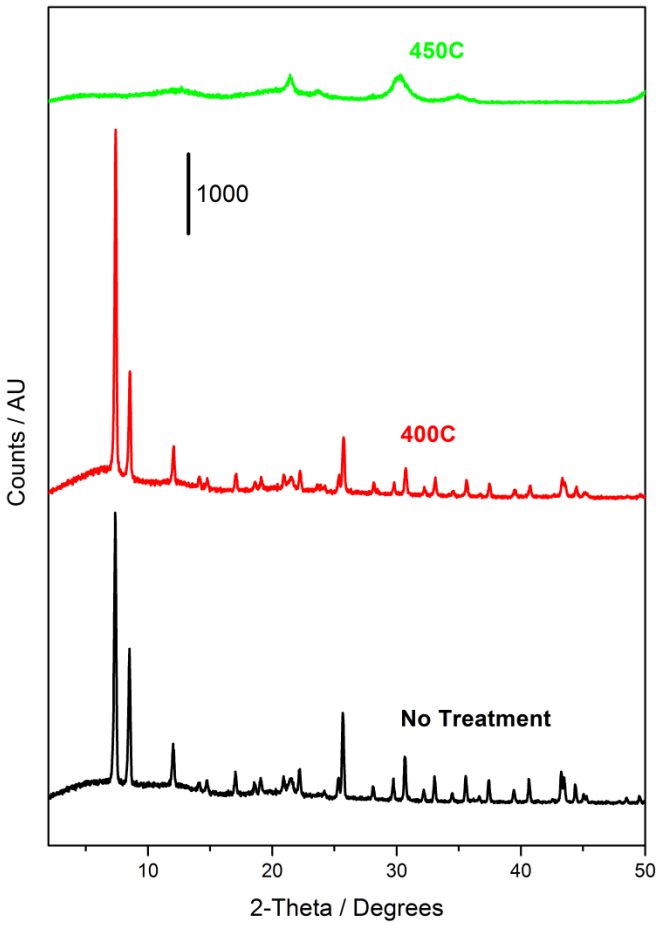

Figure S56: PXRD patterns recorded on crude (unwashed) UiO-66-220-7:4 after 12 hour exposures (in air) to the temperatures indicated on the figure. Monoclinic ZrO_2 begins to form after treatment at 450 °C, as evidenced by the emergence of broad and low intensity reflections at 30.3 and 35.1 2θ.

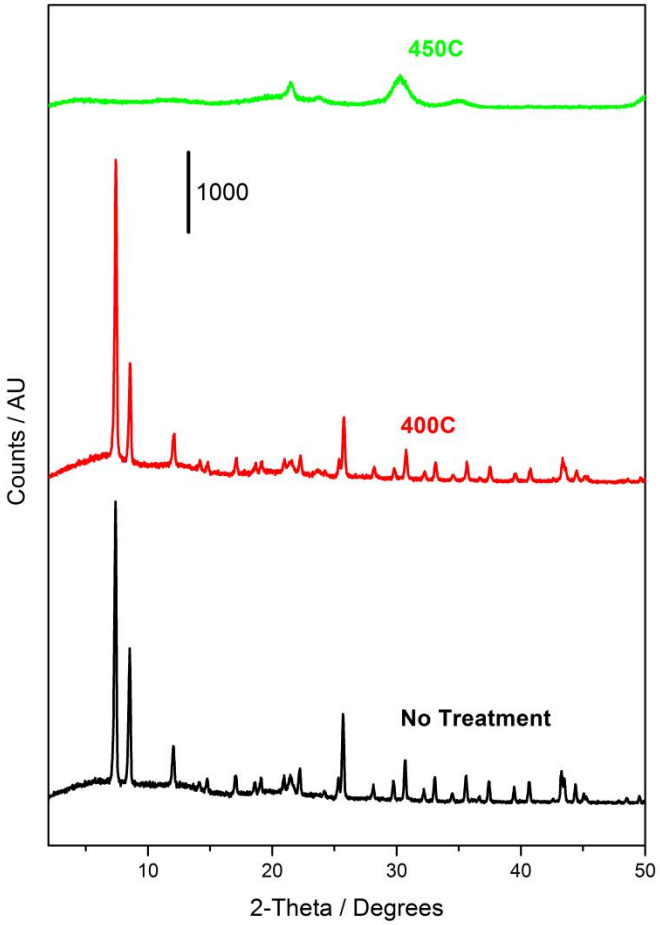

Figure S57: PXRD patterns recorded on crude (unwashed) UiO-66-220-2:1 after 12 hour exposures (in air) to the temperatures indicated on the figure. Monoclinic ZrO_2 begins to form after treatment at 450 °C, as evidenced by the emergence of broad and low intensity reflections at 30.3 and 35.1 2θ.

1.3.2. Thermal Stability Tests - Twice DMF Washed Samples Synthesized at 220 °C

Figures S58-S62 present the results of thermal stability tests performed on twice DMF washed samples synthesized at 220 °C with BDC:Zr ratios of 1:1, 5:4, 3:2, 7:4, and 2:1 respectively:

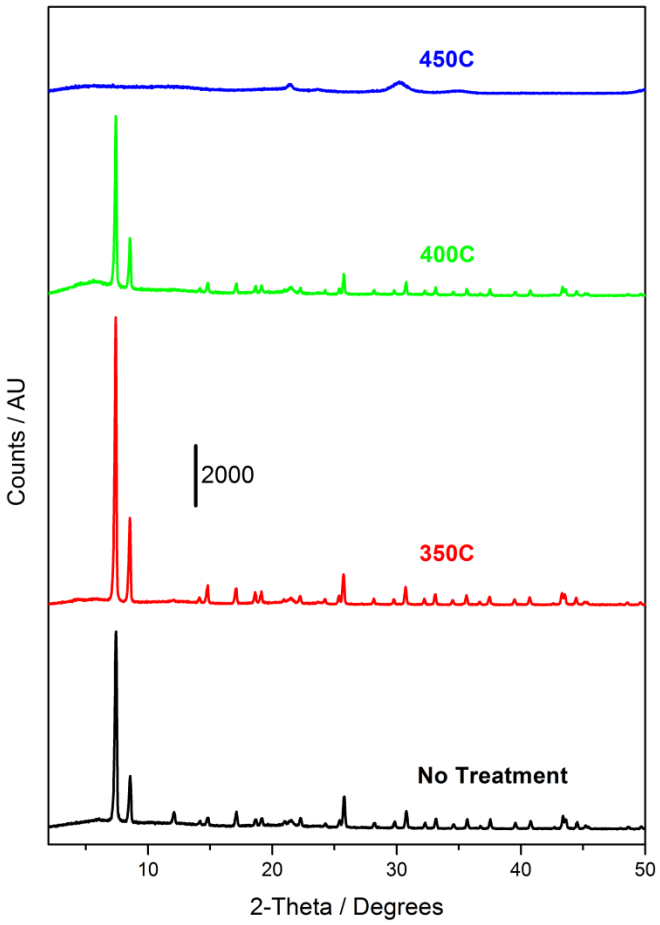

Figure S58: PXRD patterns recorded on UiO-66-220-1:1-2DMF after 12 hour exposures (in air) to the temperatures indicated on the figure. Monoclinic ZrO_2 begins to form after treatment at 450 °C, as evidenced by the emergence of broad and low intensity reflections at 30.3 and 35.1 2θ.

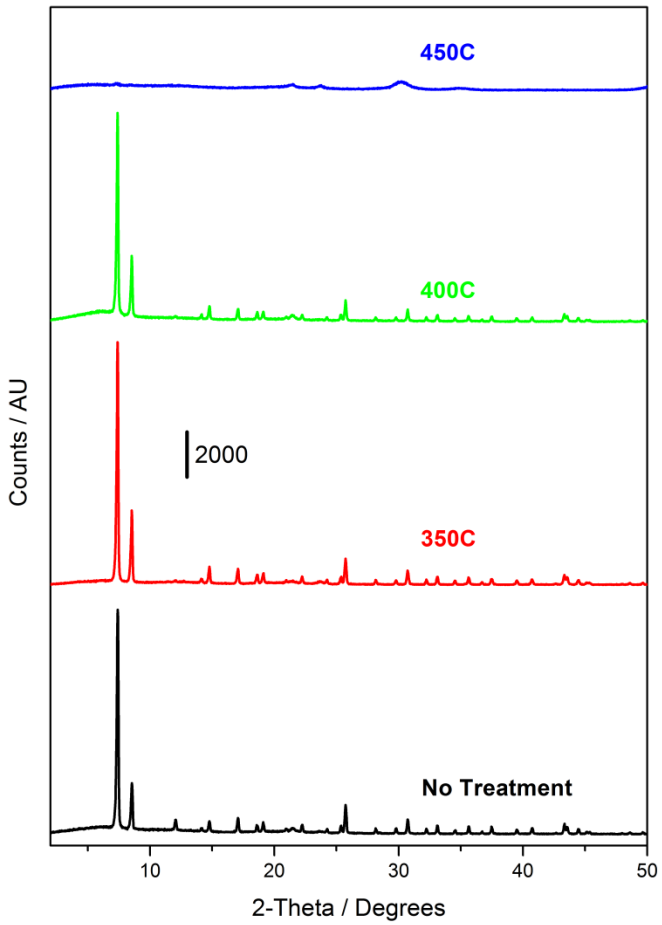

Figure S59: PXRD patterns recorded on UiO-66-220-5:4-2DMF after 12 hour exposures (in air) to the temperatures indicated on the figure. Monoclinic ZrO_2 begins to form after treatment at 450 °C, as evidenced by the emergence of broad and low intensity reflections at 30.3 and 35.1 2θ.

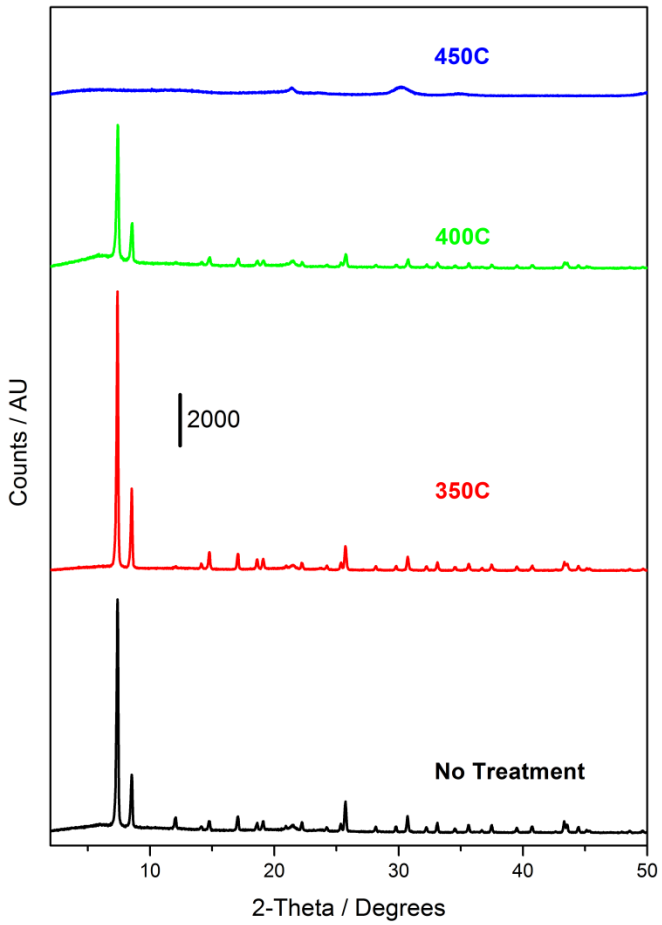

Figure S60: PXRD patterns recorded on UiO-66-220-3:2-2DMF after 12 hour exposures (in air) to the temperatures indicated on the figure. Monoclinic ZrO_2 begins to form after treatment at 450 °C, as evidenced by the emergence of broad and low intensity reflections at 30.3 and 35.1 2θ.

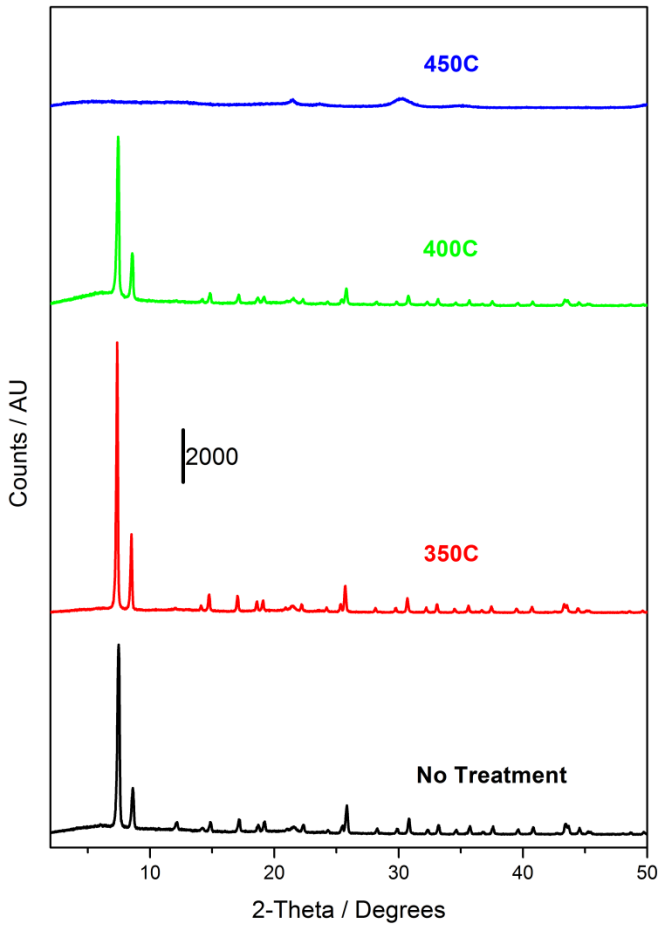

Figure S61: PXRD patterns recorded on UiO-66-220-7:4-2DMF after 12 hour exposures (in air) to the temperatures indicated on the figure. Monoclinic ZrO_2 begins to form after treatment at 450 °C, as evidenced by the emergence of broad and low intensity reflections at 30.3 and 35.1 2θ.

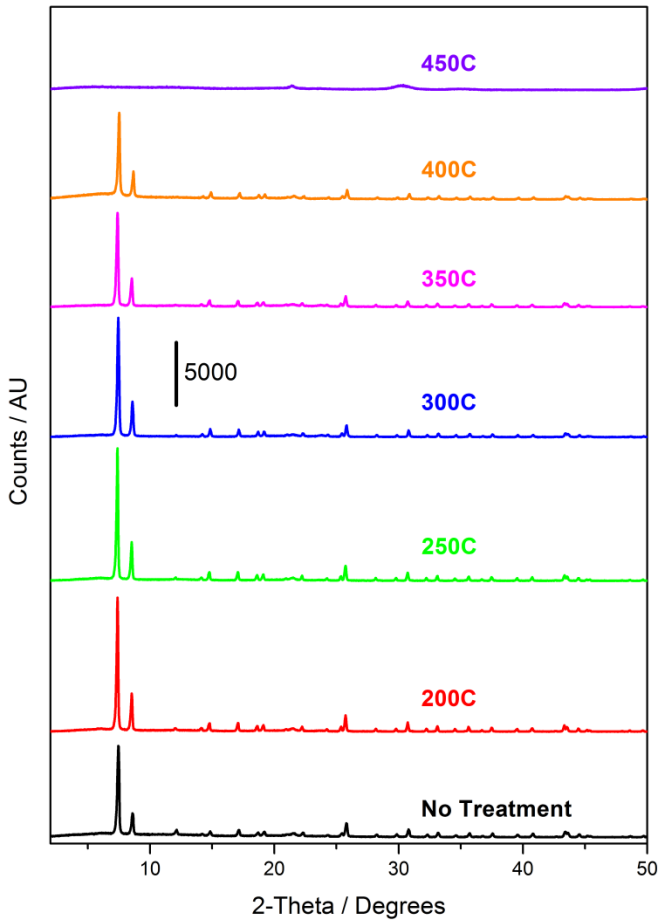

Figure S62: PXRD patterns recorded on UiO-66-220-2:1-2DMF after 12 hour exposures (in air) to the temperatures indicated on the figure. Monoclinic ZrO_2 begins to form after treatment at 450 °C, as evidenced by the emergence of broad and low intensity reflections at 30.3 and 35.1 2θ.

1.3.3. Thermal Stability Tests - Methanol Exchanged Samples Synthesized at 220 °C

Figures S63-S67 present the results of thermal stability tests performed on methanol exchanged samples synthesized at 220 °C with BDC:Zr ratios of 1:1, 5:4, 3:2, 7:4, and 2:1 respectively:

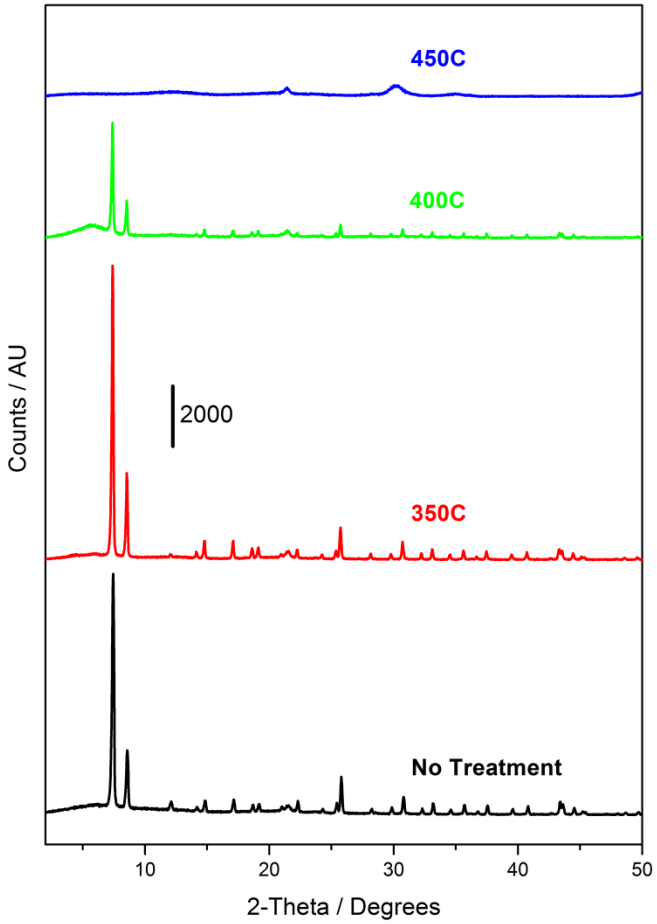

Figure S63: PXRD patterns recorded on UiO-66-220-1:1-MeOH after 12 hour exposures (in air) to the temperatures indicated on the figure. Monoclinic ZrO_2 begins to form after treatment at 450 °C, as evidenced by the emergence of broad and low intensity reflections at 30.3 and 35.1 2θ.

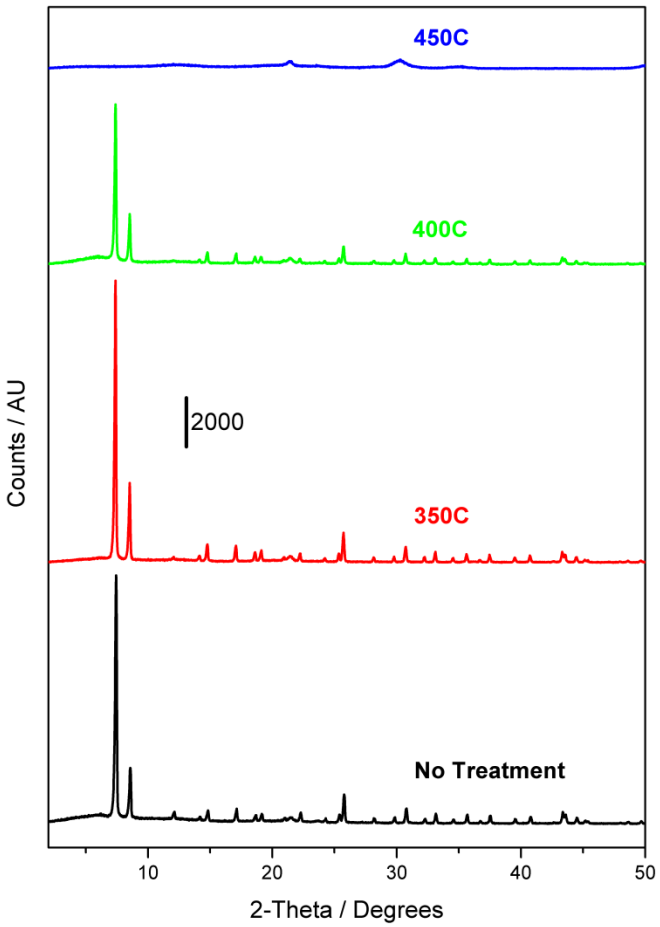

Figure S64: PXRD patterns recorded on UiO-66-220-5:4-MeOH after 12 hour exposures (in air) to the temperatures indicated on the figure. Monoclinic ZrO_2 begins to form after treatment at 450 °C, as evidenced by the emergence of broad and low intensity reflections at 30.3 and 35.1 2θ.

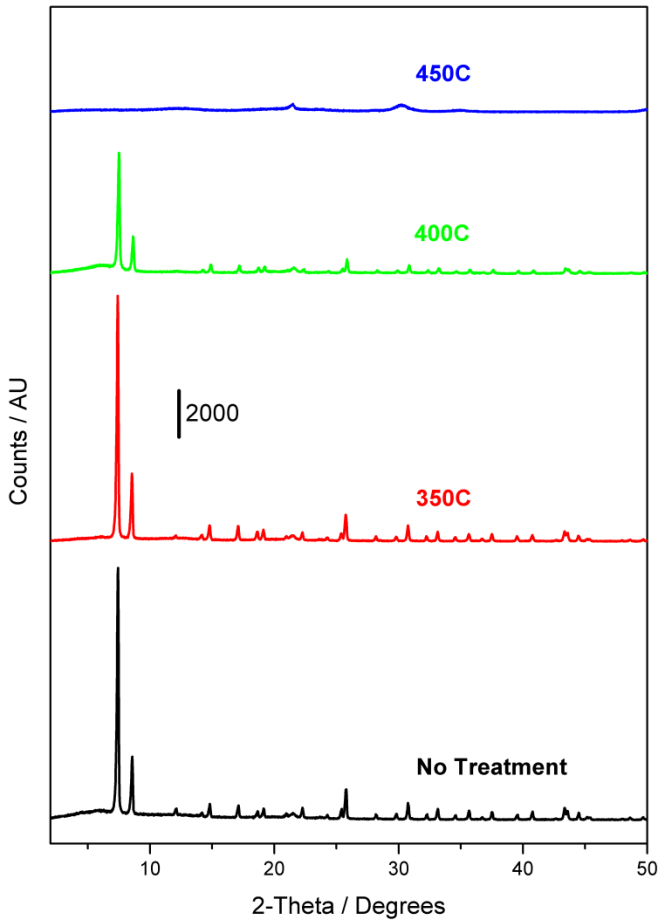

Figure S65: PXRD patterns recorded on UiO-66-220-3:2-MeOH after 12 hour exposures (in air) to the temperatures indicated on the figure. Monoclinic ZrO_2 begins to form after treatment at 450 °C, as evidenced by the emergence of broad and low intensity reflections at 30.3 and 35.1 2θ.

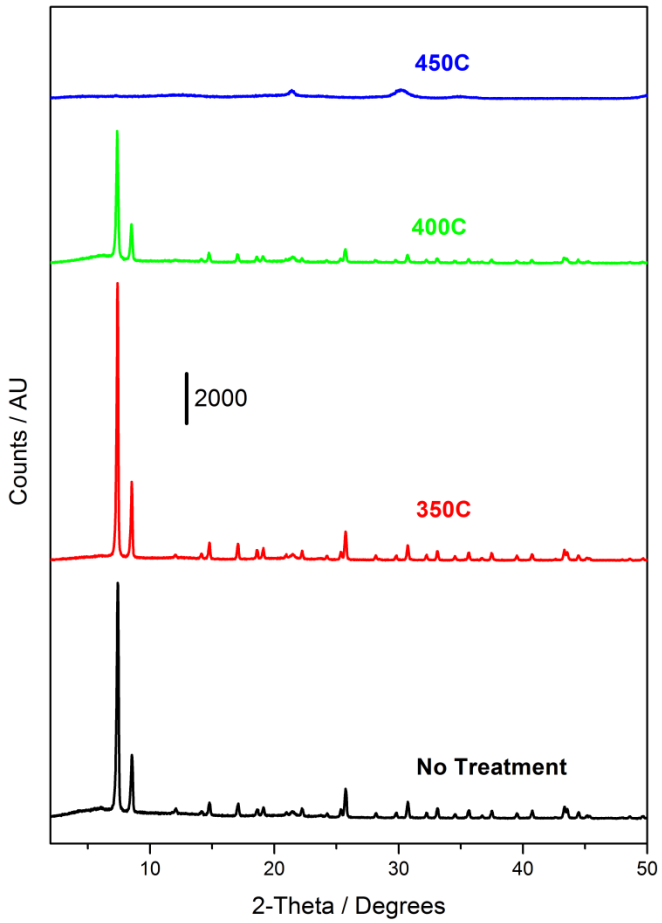

Figure S66: PXRD patterns recorded on UiO-66-220-7:4-MeOH after 12 hour exposures (in air) to the temperatures indicated on the figure. Monoclinic ZrO_2 begins to form after treatment at 450 °C, as evidenced by the emergence of broad and low intensity reflections at 30.3 and 35.1 2θ.

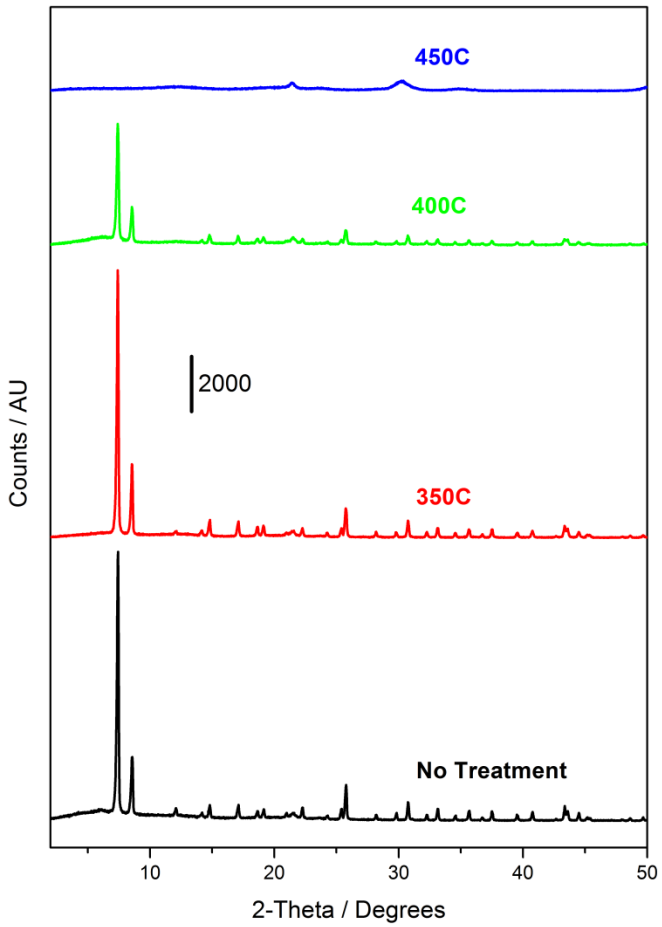

Figure S67: PXRD patterns recorded on UiO-66-220-2:1-MeOH after 12 hour exposures (in air) to the temperatures indicated on the figure. Monoclinic ZrO_2 begins to form after treatment at 450 °C, as evidenced by the emergence of broad and low intensity reflections at 30.3 and 35.1 2θ.

2. Full Range (2θ = 2-50) PXRD Patterns

Displayed in **Figures S68-S73** are the full (2θ = 2-50) range of the PXRD patterns presented in **Figures S3-S8** in section D:

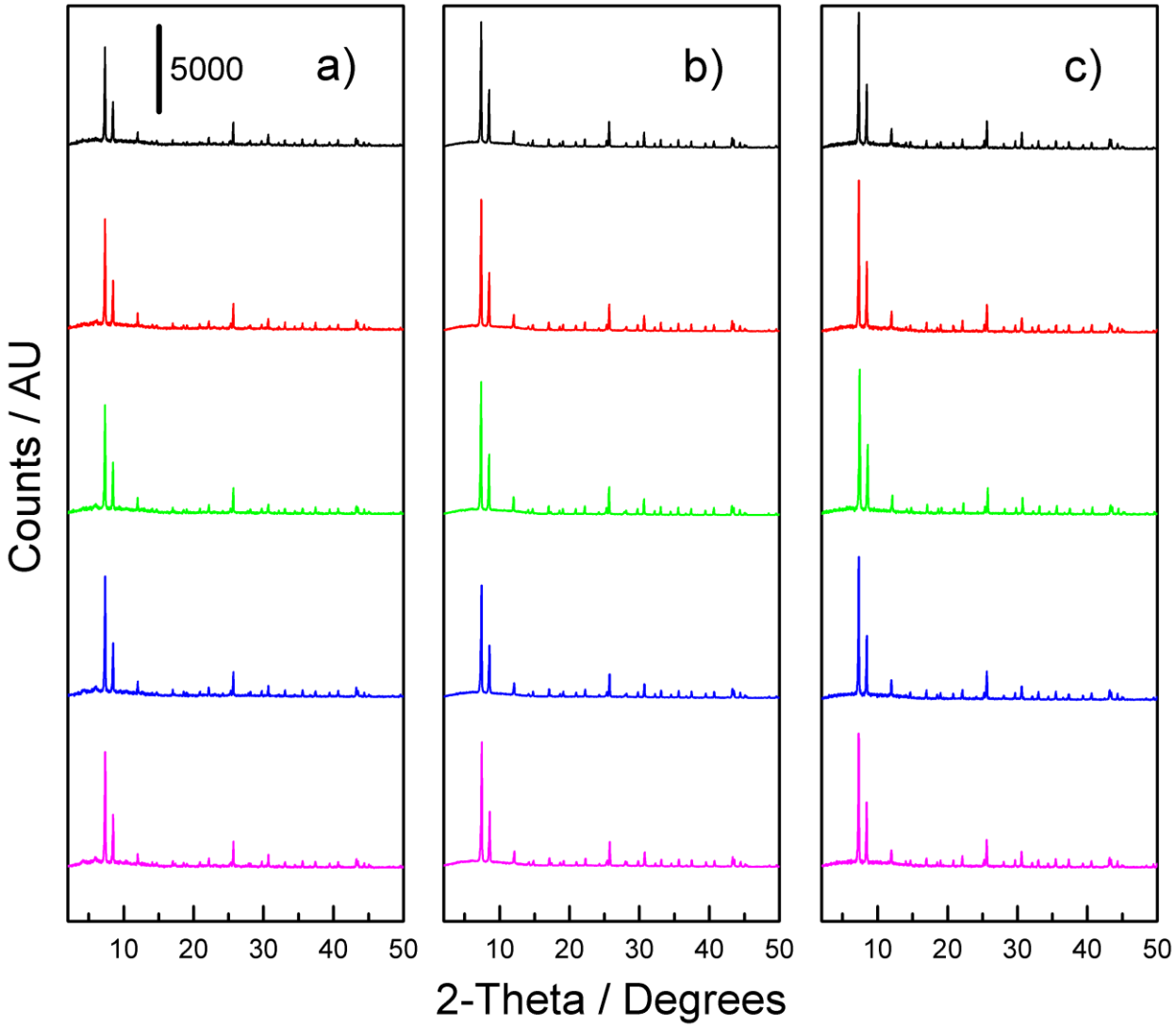

Figure S68: PXRD patterns recorded on crude (unwashed) UiO-66 samples synthesized at: a) 100 °C, b) 160 °C, and c) 220 °C. Throughout the figure, the BDC:Zr ratio used in the synthesis is represented by the color of the curve: 1:1 (black), 5:4 (red), 3:2 (green), 7:4 (blue), and 2:1 (magenta). The same y-scale is applied to all three plots.

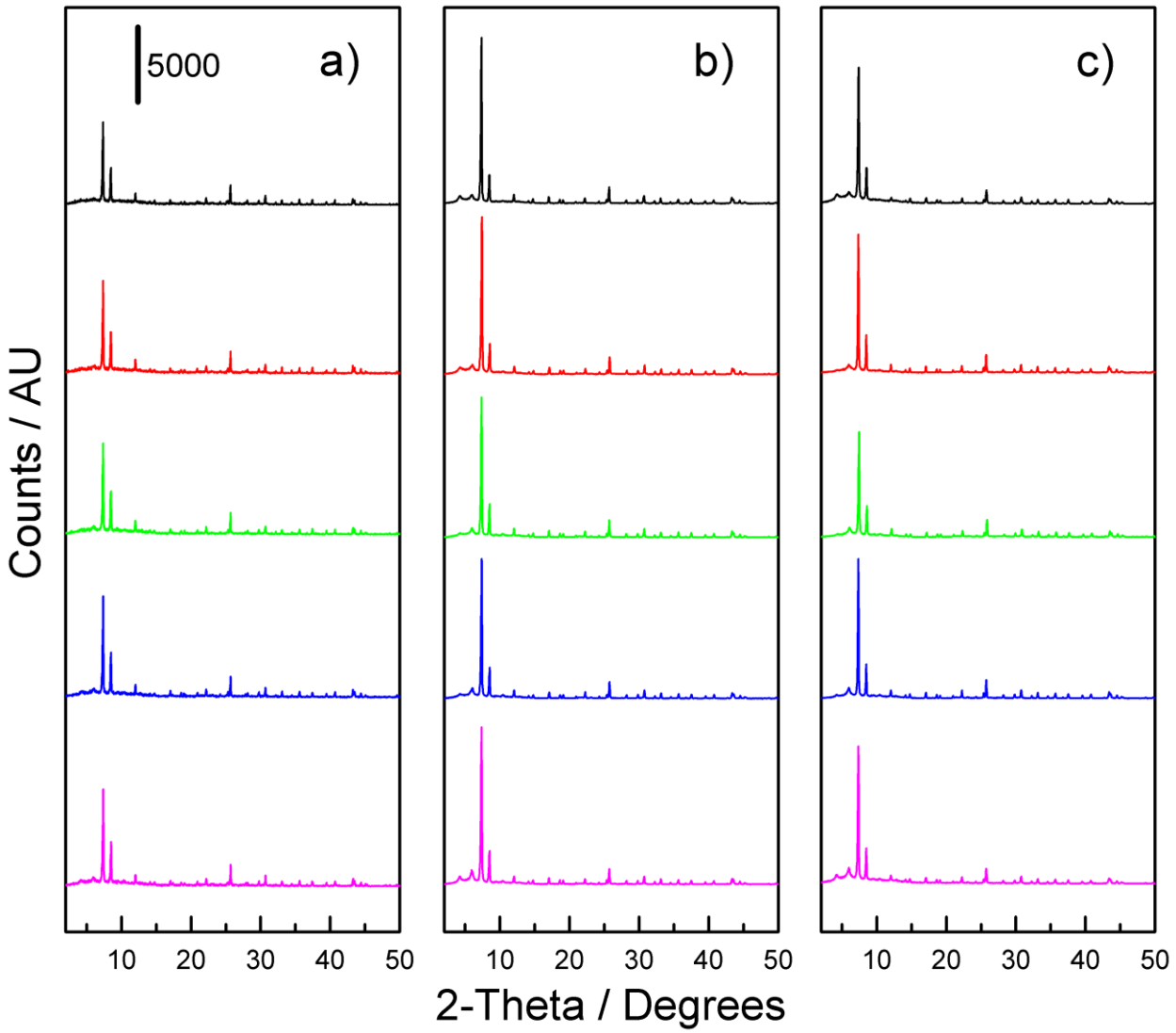

Figure S69: PXRD patterns recorded on UiO-66 samples synthesized at 100 °C: a) Crude (unwashed), b) Twice DMF washed, and c) Methanol Exchanged. Throughout the figure, the BDC:Zr ratio used in the synthesis is represented by the color of the curve: 1:1 (black), 5:4 (red), 3:2 (green), 7:4 (blue), and 2:1 (magenta). The same y-scale is applied to all three plots.

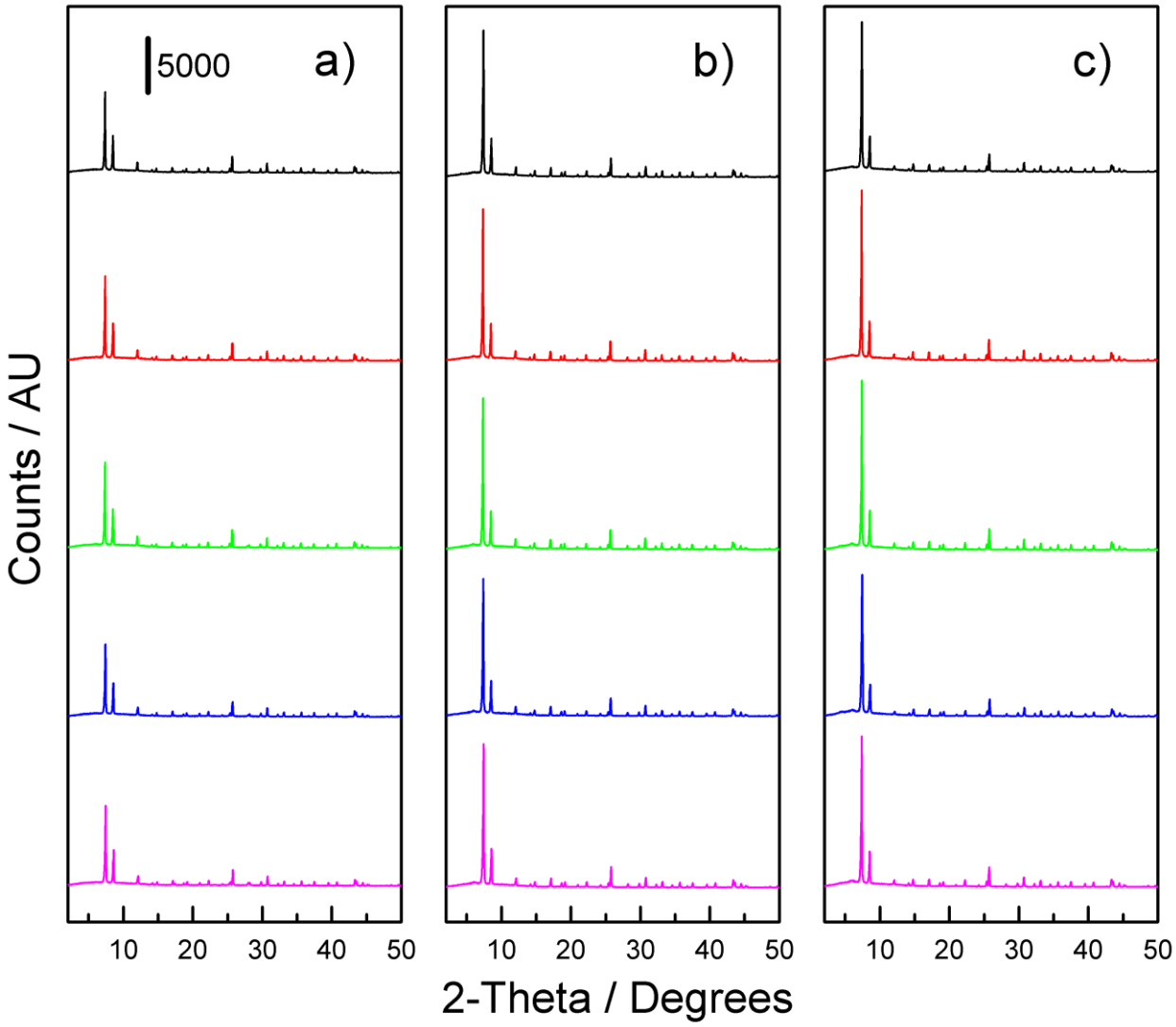

Figure S70: PXRD patterns recorded on UiO-66 samples synthesized at 160 °C: a) Crude (unwashed), b) Twice DMF washed, and c) Methanol Exchanged. Throughout the figure, the BDC:Zr ratio used in the synthesis is represented by the color of the curve: 1:1 (black), 5:4 (red), 3:2 (green), 7:4 (blue), and 2:1 (magenta). The same y-scale is applied to all three plots.

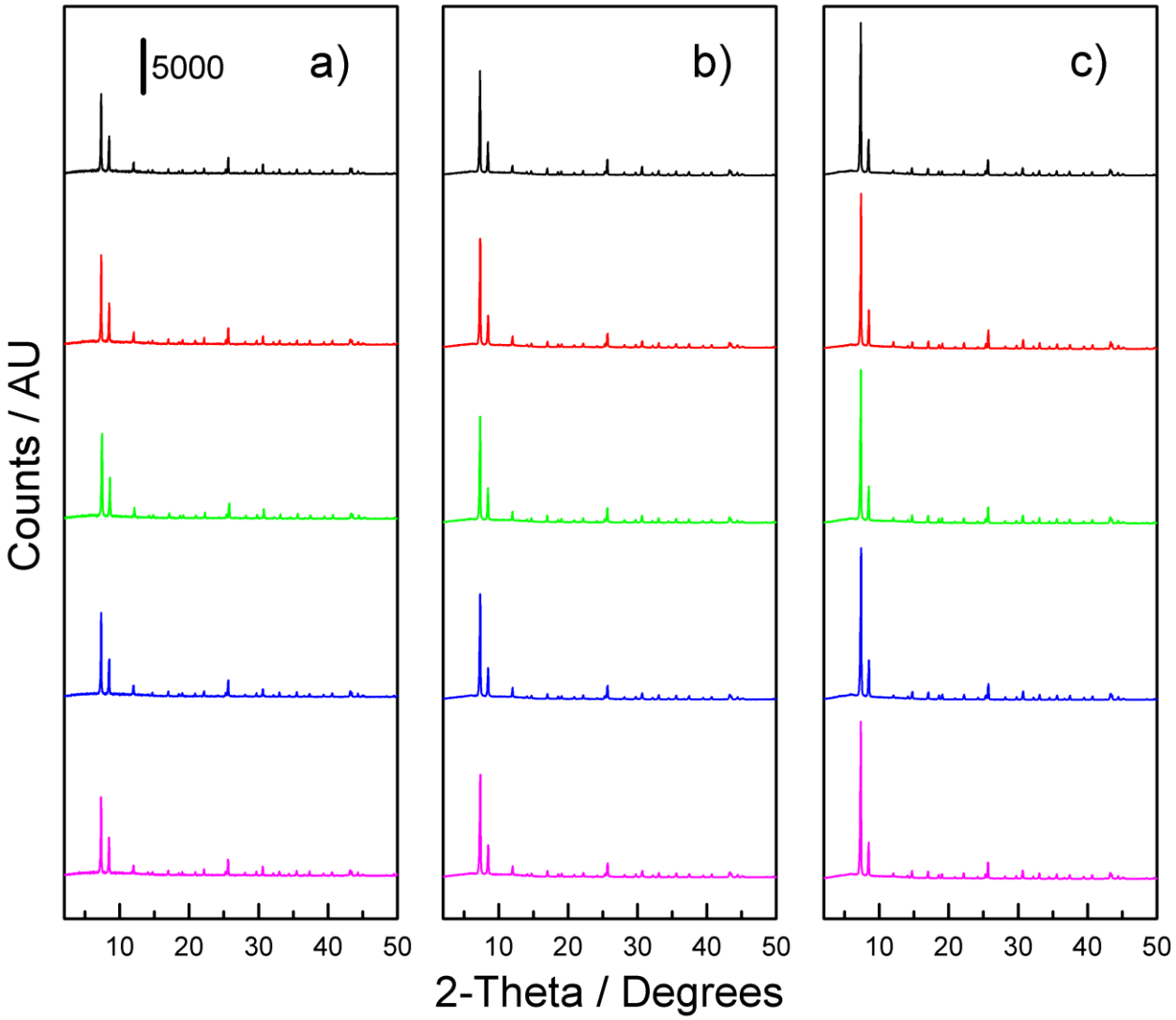

Figure S71: PXRD patterns recorded on UiO-66 samples synthesized at 220 °C: a) Crude (unwashed), b) Twice DMF washed, and c) Methanol Exchanged. Throughout the figure, the BDC:Zr ratio used in the synthesis is represented by the color of the curve: 1:1 (black), 5:4 (red), 3:2 (green), 7:4 (blue), and 2:1 (magenta). The same y-scale is applied to all three plots.

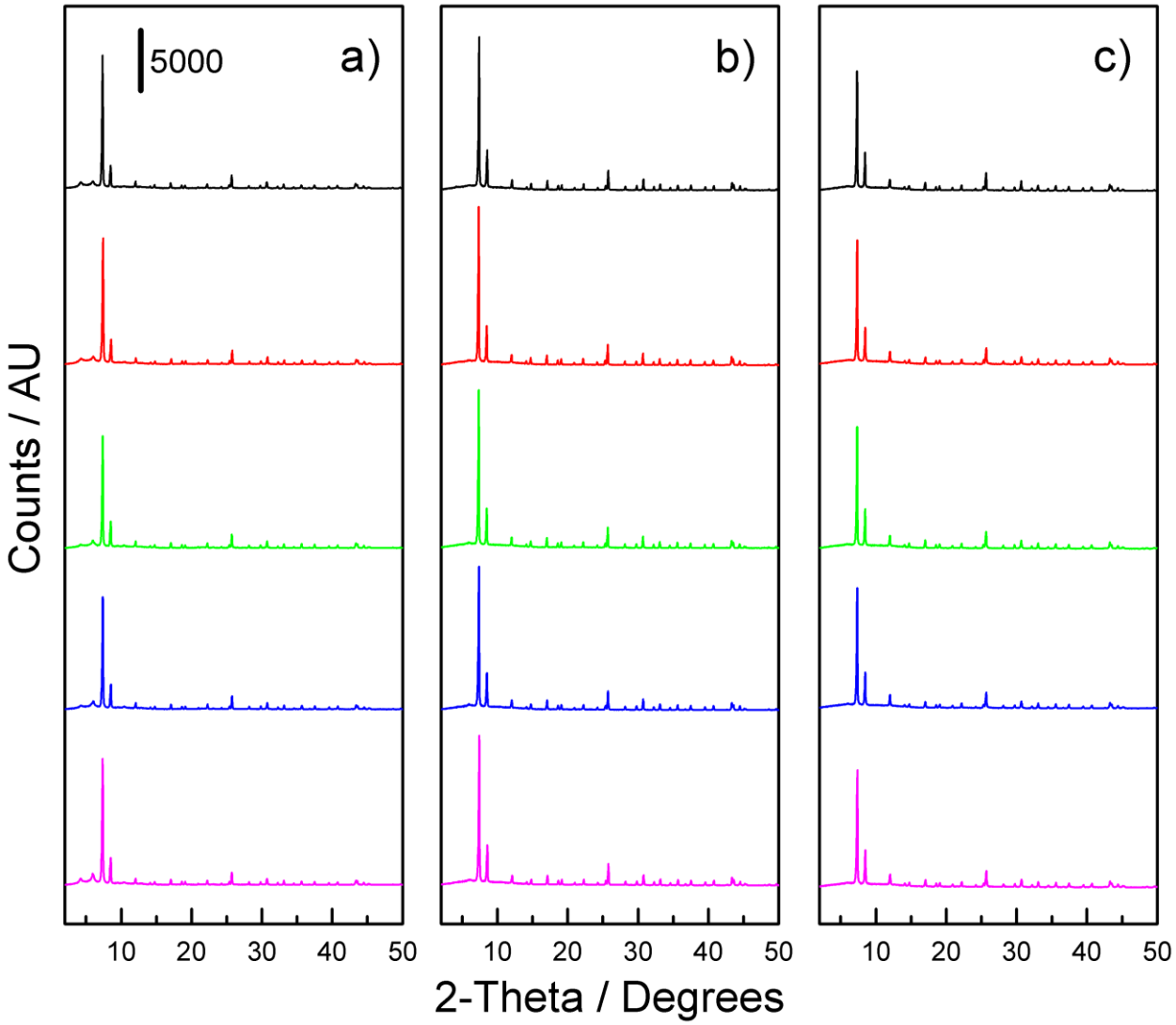

Figure S72: PXRD patterns recorded on twice DMF washed UiO-66 samples synthesized at: a) 100 °C, b) 160 °C, and c) 220 °C. Throughout the figure, the BDC:Zr ratio used in the synthesis is represented by the color of the curve: 1:1 (black), 5:4 (red), 3:2 (green), 7:4 (blue), and 2:1 (magenta). The same y-scale is applied to all three plots.

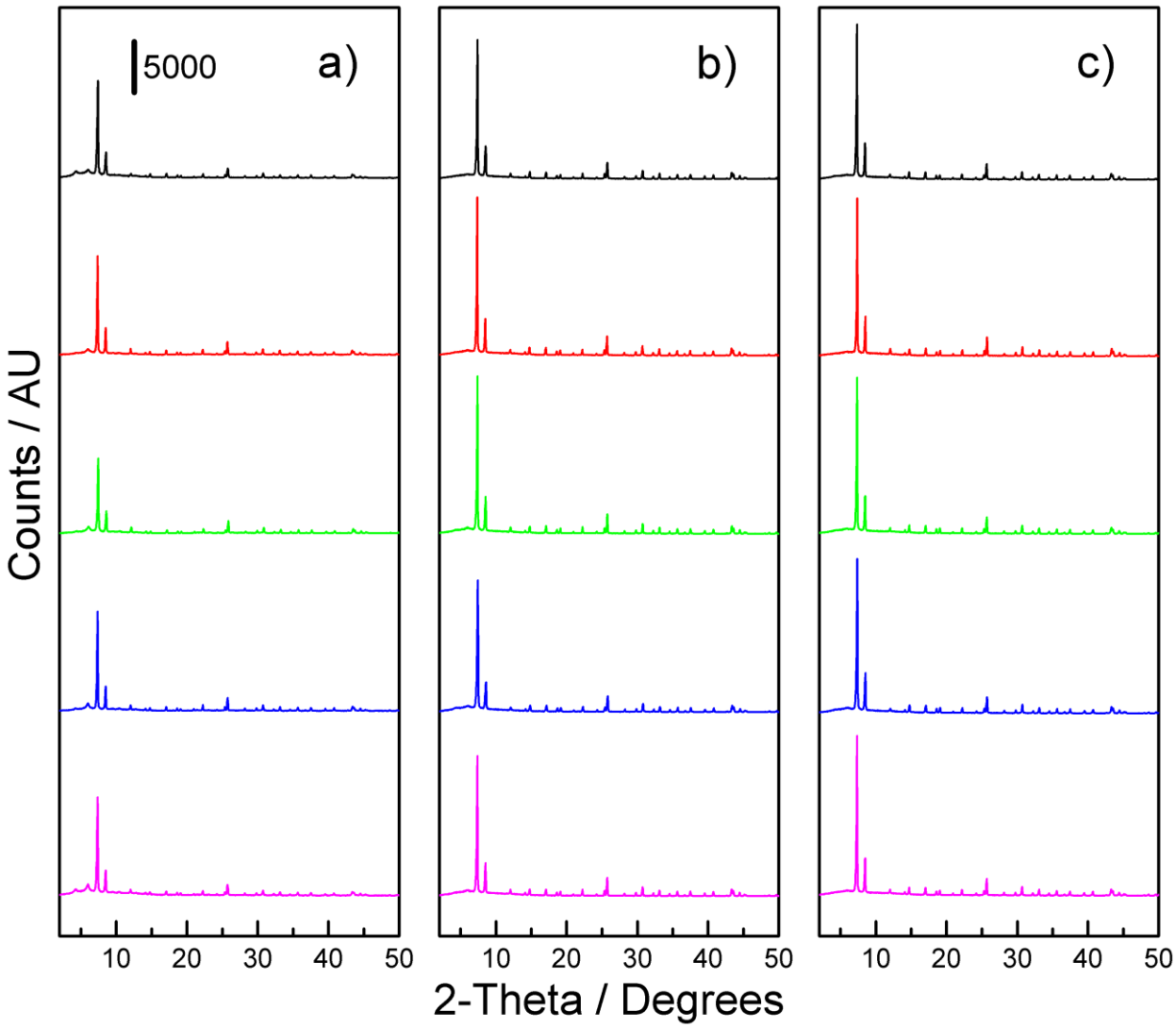

Figure S73: PXRD patterns recorded on methanol exchanged UiO-66 samples synthesized at: a) 100 °C, b) 160 °C, and c) 220 °C. Throughout the figure, the BDC:Zr ratio used in the synthesis is represented by the color of the curve: 1:1 (black), 5:4 (red), 3:2 (green), 7:4 (blue), and 2:1 (magenta). The same y-scale is applied to all three plots.

3. Following the Effect of Washing via TGA-DSC

Table of Content

3.1. Results on Samples Synthesized at 100 °C

Figures S74, S75, S76, S77, and S78 display the results obtained on samples synthesized with BDC:Zr ratios of 1:1, 5:4, 3:2, 7:4, and 2:1 respectively.

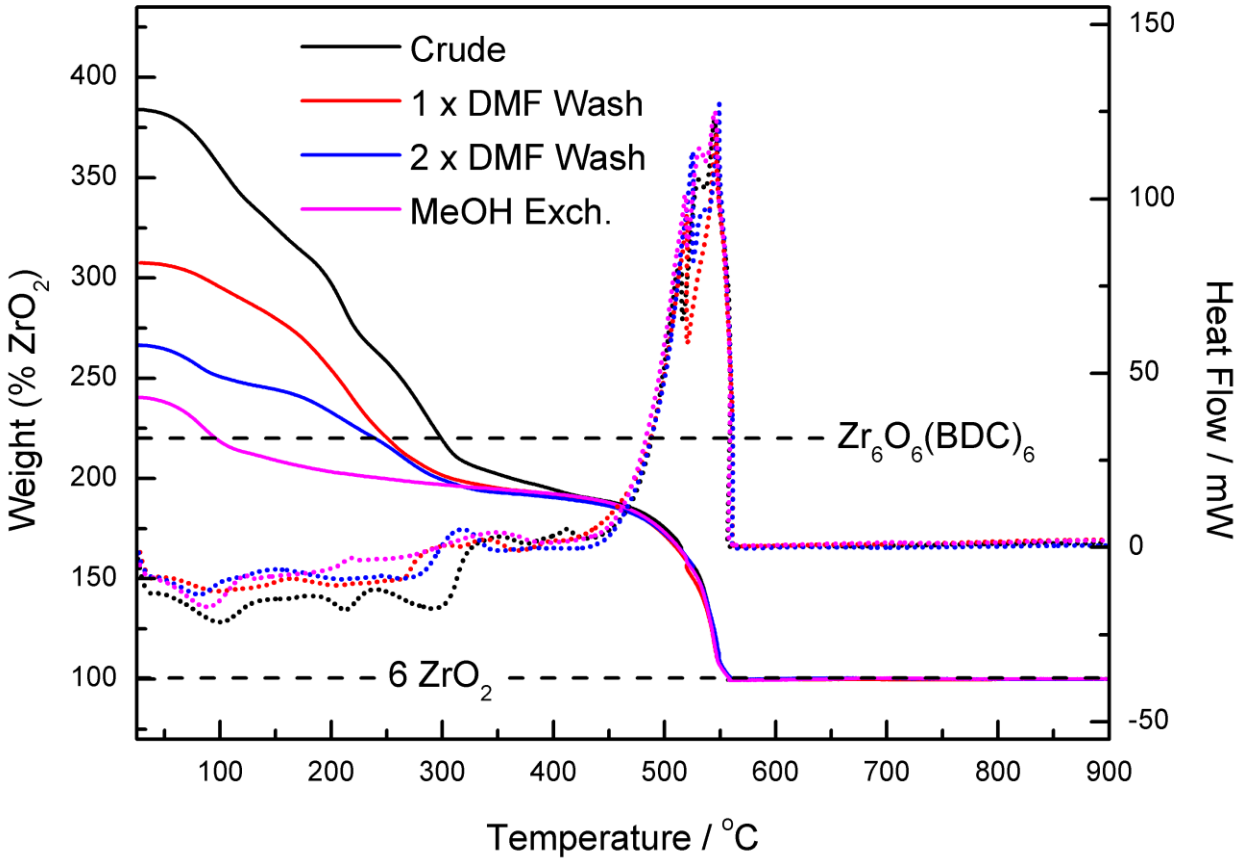

Figure S74: TGA curves (relative to ZrO_2, solid lines) and DSC signals (dotted lines) obtained on UiO-66-100-1:1 at various states of washing (explained on the legend). The position of the theoretical TGA plateau is marked by the horizontal dashed line labelled "Zr_6O_6 $(BDC)_6$".

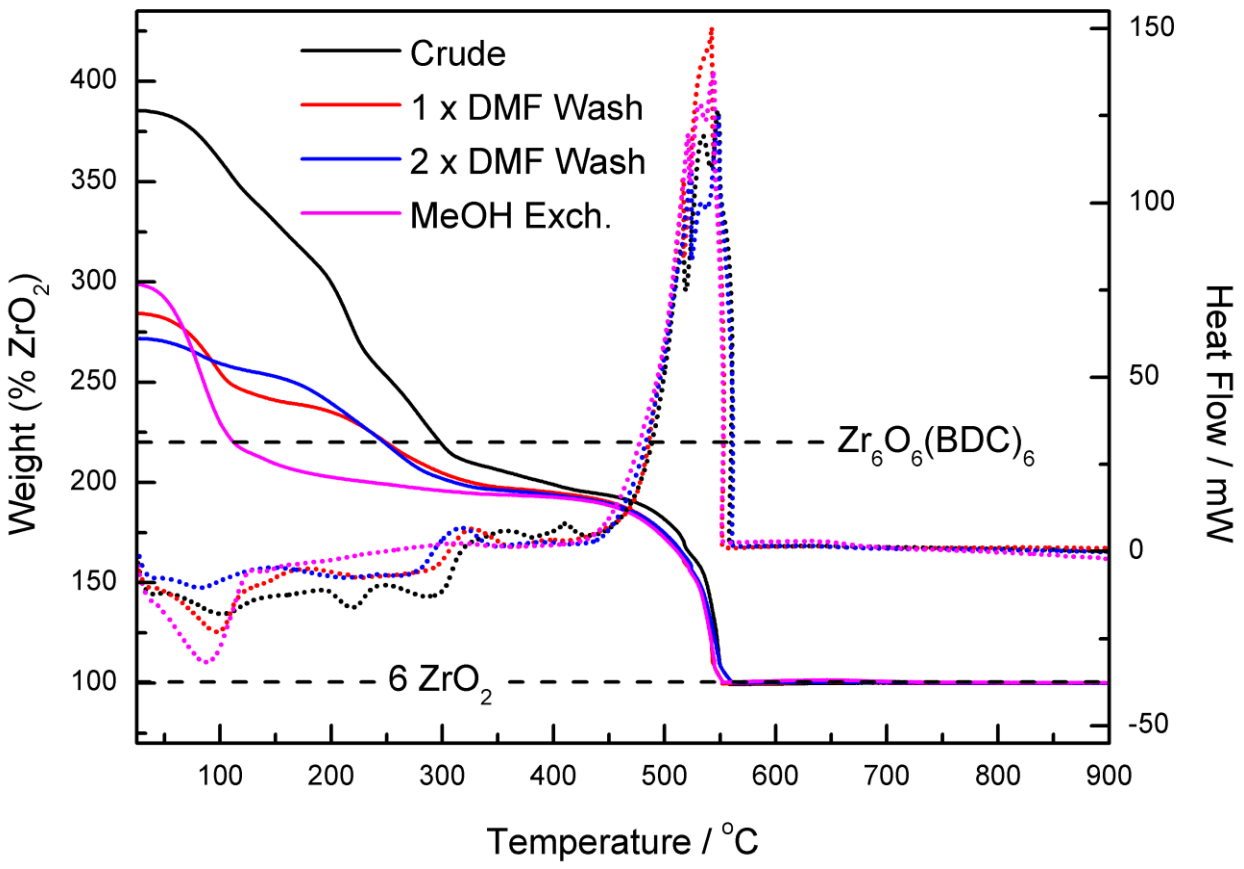

Figure S75: TGA curves (relative to ZrO_2, solid lines) and DSC signals (dotted lines) obtained on UiO-66-100-5:4 at various states of washing (explained on the legend). The position of the theoretical TGA plateau is marked by the horizontal dashed line labelled "Zr_6O_6 $(BDC)_6$".

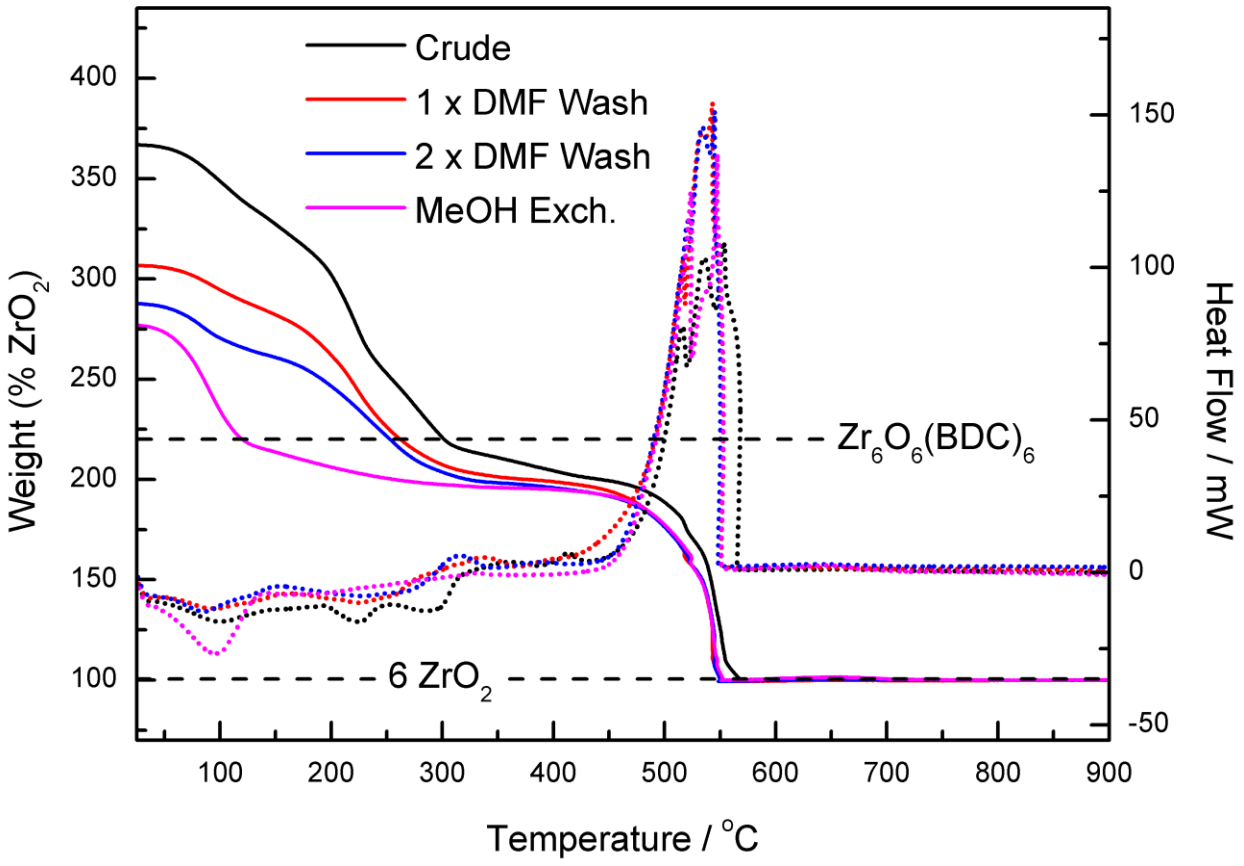

Figure S76: TGA curves (relative to ZrO_2, solid lines) and DSC signals (dotted lines) obtained on UiO-66-100-3:2 at various states of washing (explained on the legend). The position of the theoretical TGA plateau is marked by the horizontal dashed line labelled "Zr_6O_6 $(BDC)_6$".

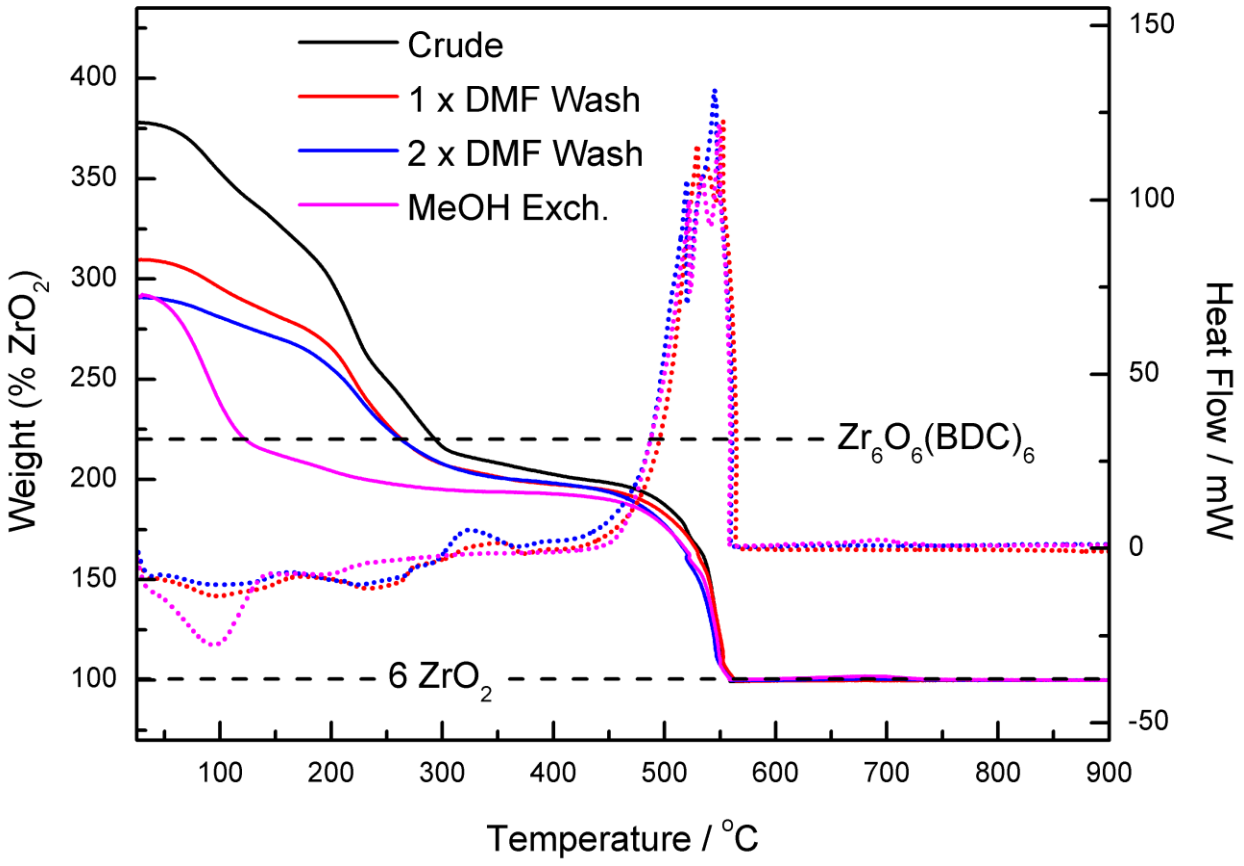

Figure S77: TGA curves (relative to ZrO_2, solid lines) and DSC signals (dotted lines) obtained on UiO-66-100-7:4 at various states of washing (explained on the legend). The position of the theoretical TGA plateau is marked by the horizontal dashed line labelled "Zr_6O_6 $(BDC)_6$".

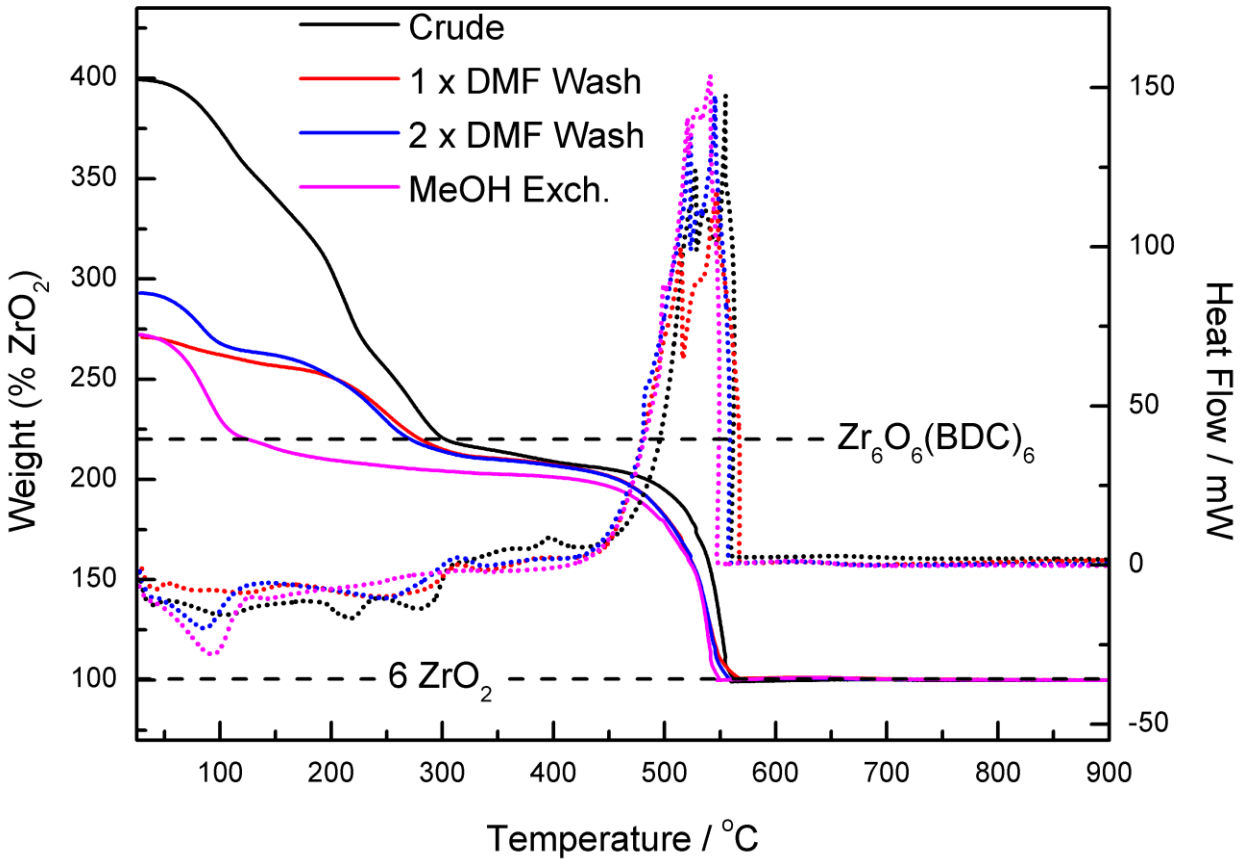

Figure S78: TGA curves (relative to ZrO_2, solid lines) and DSC signals (dotted lines) obtained on UiO-66-100-2:1 at various states of washing (explained on the legend). The position of the theoretical TGA plateau is marked by the horizontal dashed line labelled "Zr_6O_6 $(BDC)_6$".

3.2. Results on Samples Synthesized at 160 °C

Figures S79, S80, S81, S82, and S83 display the results obtained on samples synthesized with BDC:Zr ratios of 1:1, 5:4, 3:2, 7:4, and 2:1 respectively.

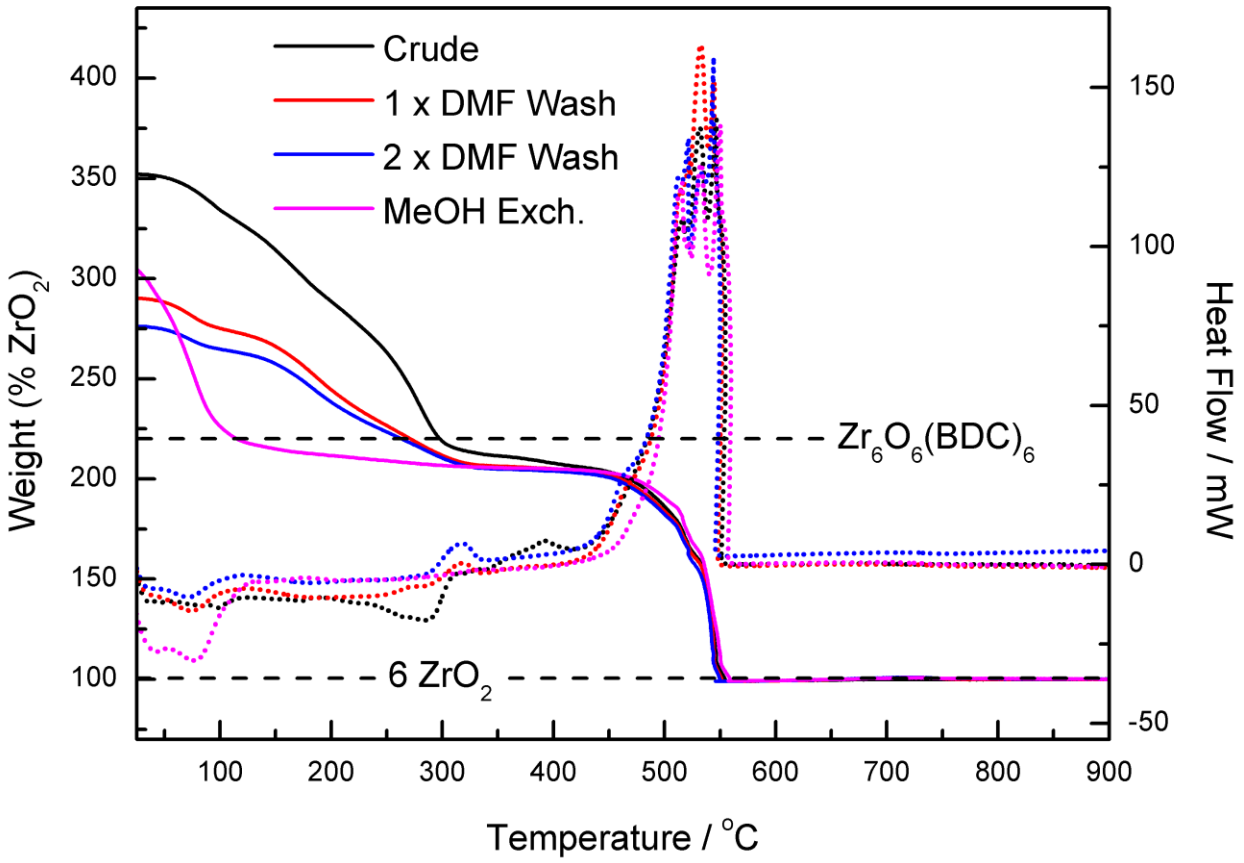

Figure S79: TGA curves (relative to ZrO_2, solid lines) and DSC signals (dotted lines) obtained on UiO-66-160-1:1 at various states of washing (explained on the legend). The position of the theoretical TGA plateau is marked by the horizontal dashed line labelled "Zr_6O_6 $(BDC)_6$".

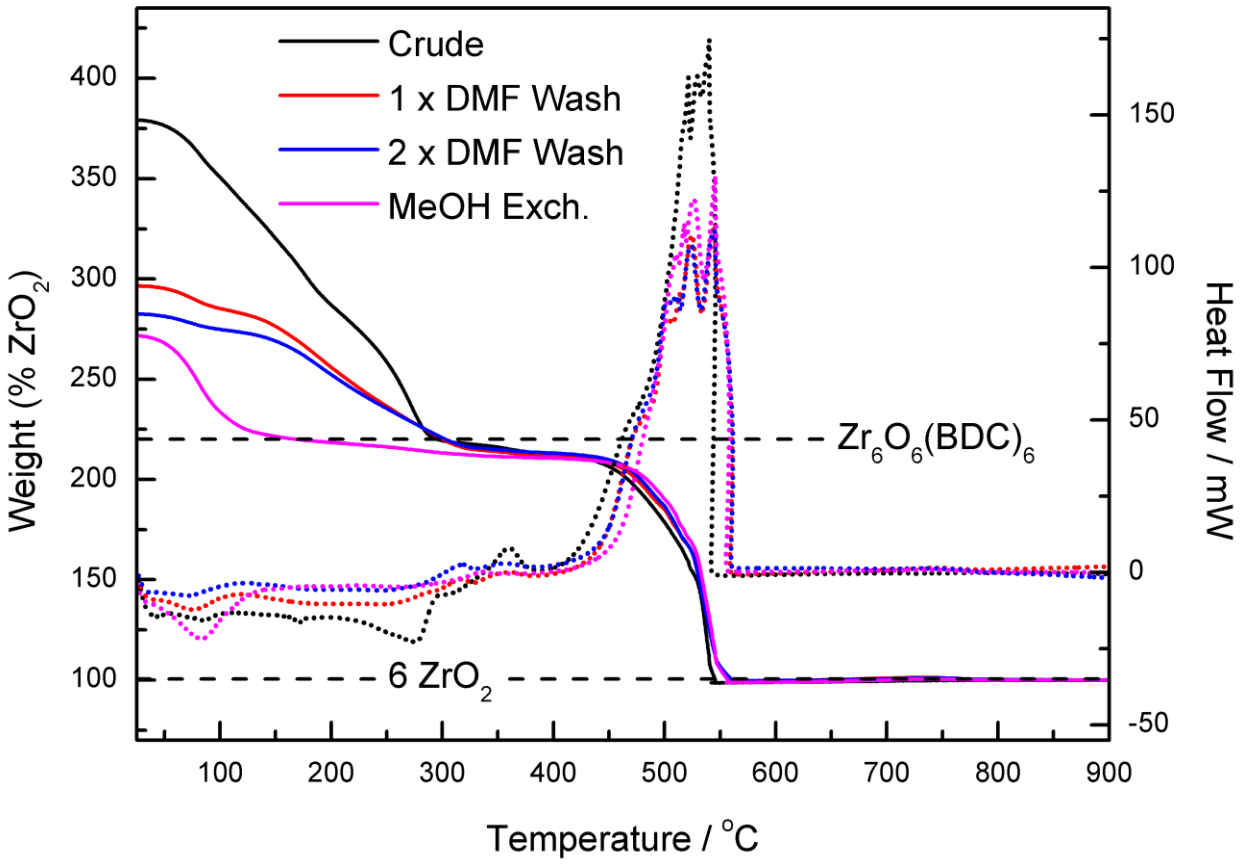

Figure S80: TGA curves (relative to ZrO_2, solid lines) and DSC signals (dotted lines) obtained on UiO-66-160-5:4 at various states of washing (explained on the legend). The position of the theoretical TGA plateau is marked by the horizontal dashed line labelled "Zr_6O_6 $(BDC)_6$".

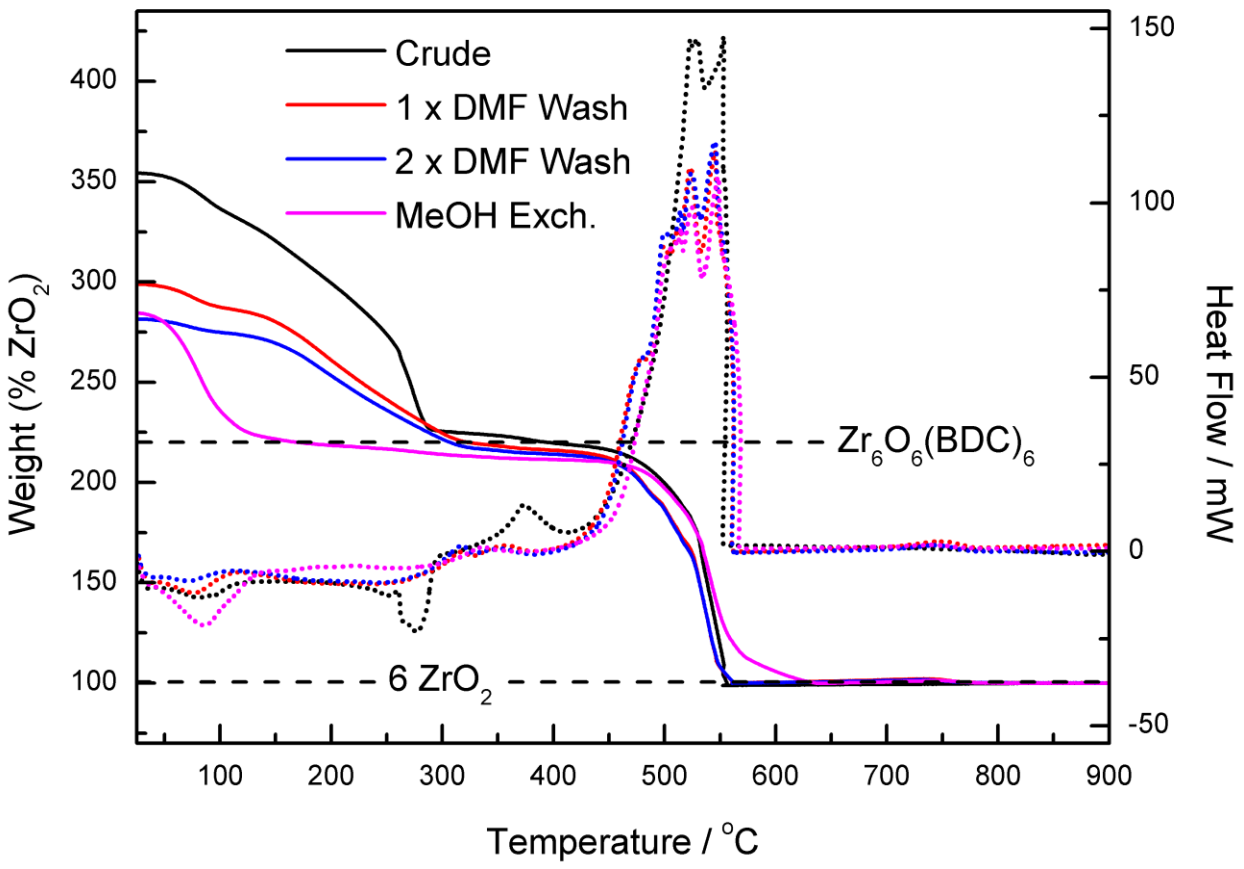

Figure S81: TGA curves (relative to ZrO_2, solid lines) and DSC signals (dotted lines) obtained on UiO-66-160-3:2 at various states of washing (explained on the legend). The position of the theoretical TGA plateau is marked by the horizontal dashed line labelled "Zr_6O_6 $(BDC)_6$".

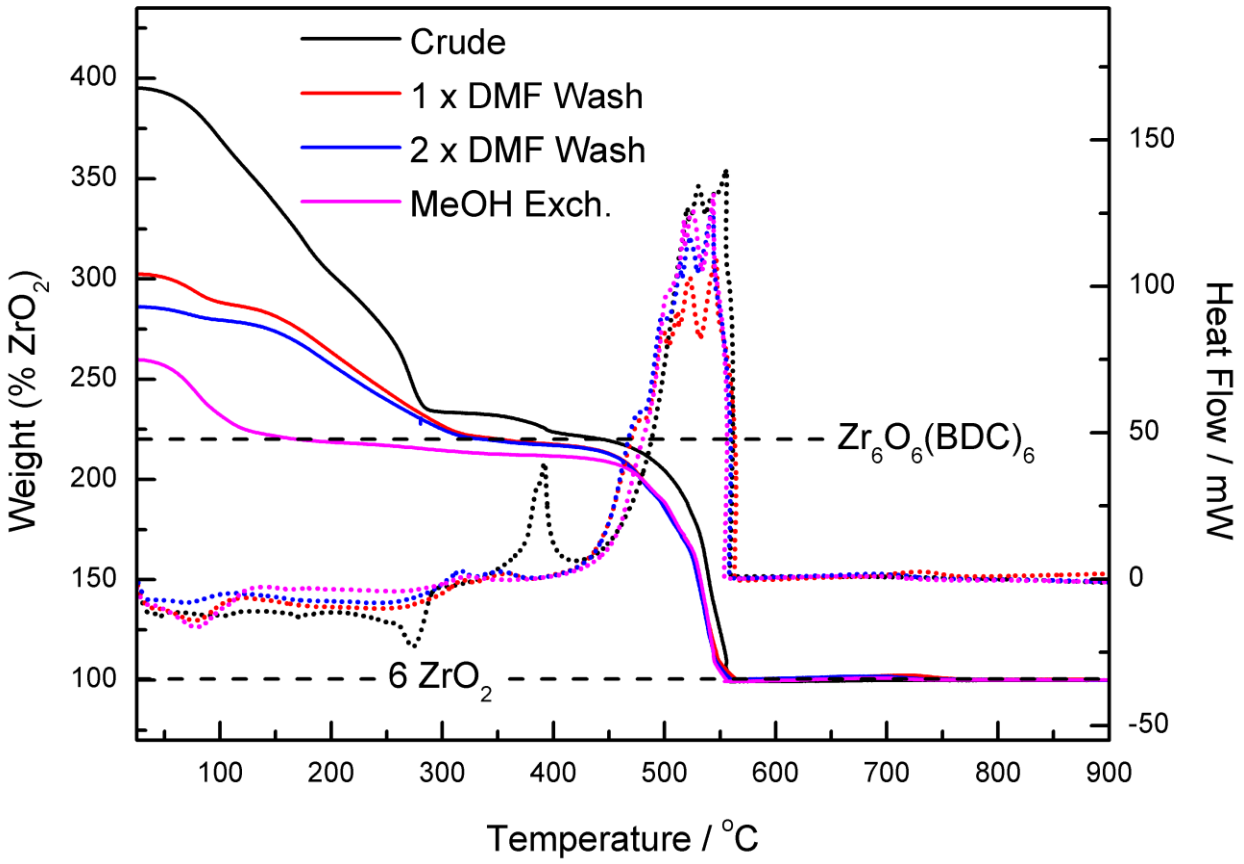

Figure S82: TGA curves (relative to ZrO_2, solid lines) and DSC signals (dotted lines) obtained on UiO-66-160-7:4 at various states of washing (explained on the legend). The position of the theoretical TGA plateau is marked by the horizontal dashed line labelled "Zr_6O_6 $(BDC)_6$".

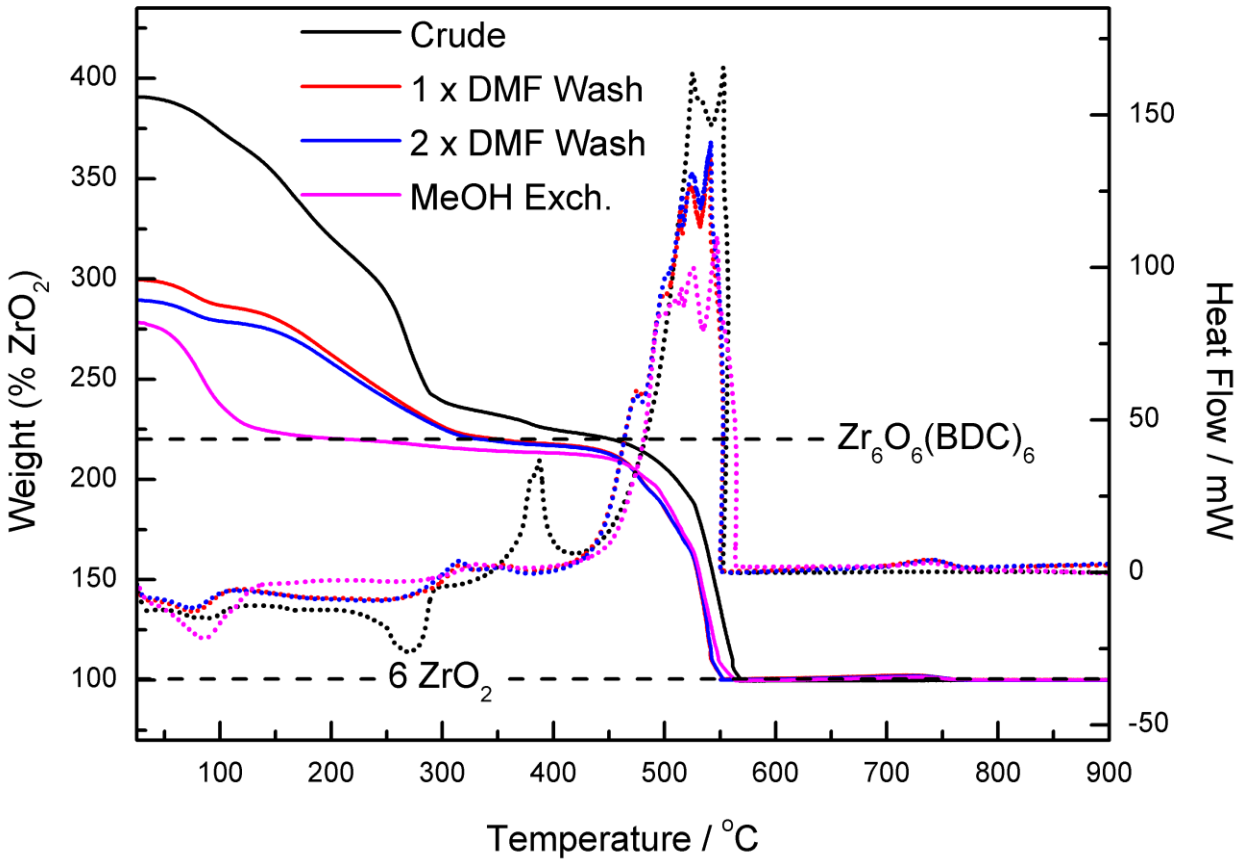

Figure S83: TGA curves (relative to ZrO_2, solid lines) and DSC signals (dotted lines) obtained on UiO-66-160-2:1 at various states of washing (explained on the legend). The position of the theoretical TGA plateau is marked by the horizontal dashed line labelled "Zr_6O_6 $(BDC)_6$".

3.3. Results on Samples Synthesized at 220 °C

Figures S84, S85, S86, S87, and S88 display the results obtained on samples synthesized with BDC:Zr ratios of 1:1, 5:4, 3:2, 7:4, and 2:1 respectively.

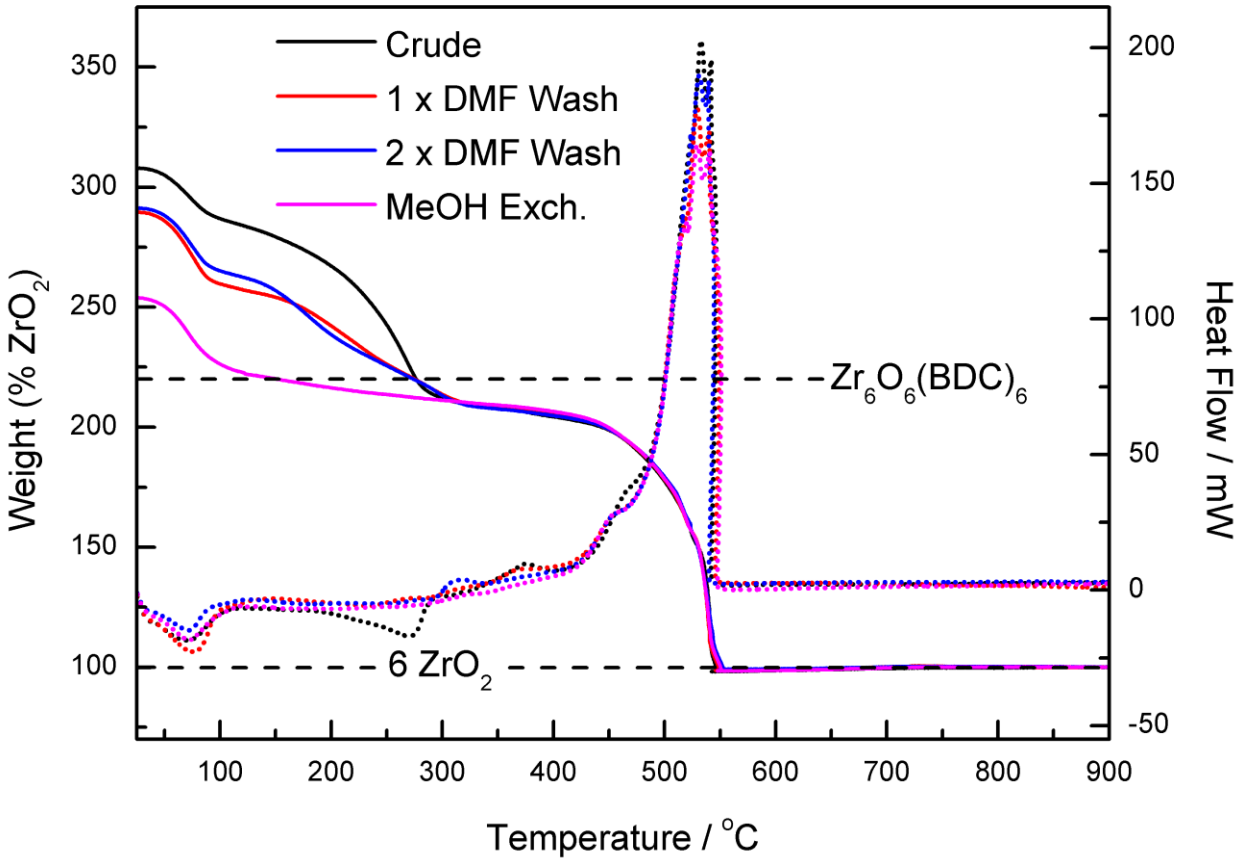

Figure S84: TGA curves (relative to ZrO_2, solid lines) and DSC signals (dotted lines) obtained on UiO-66-220-1:1 at various states of washing (explained on the legend). The position of the theoretical TGA plateau is marked by the horizontal dashed line labelled "Zr_6O_6 $(BDC)_6$".

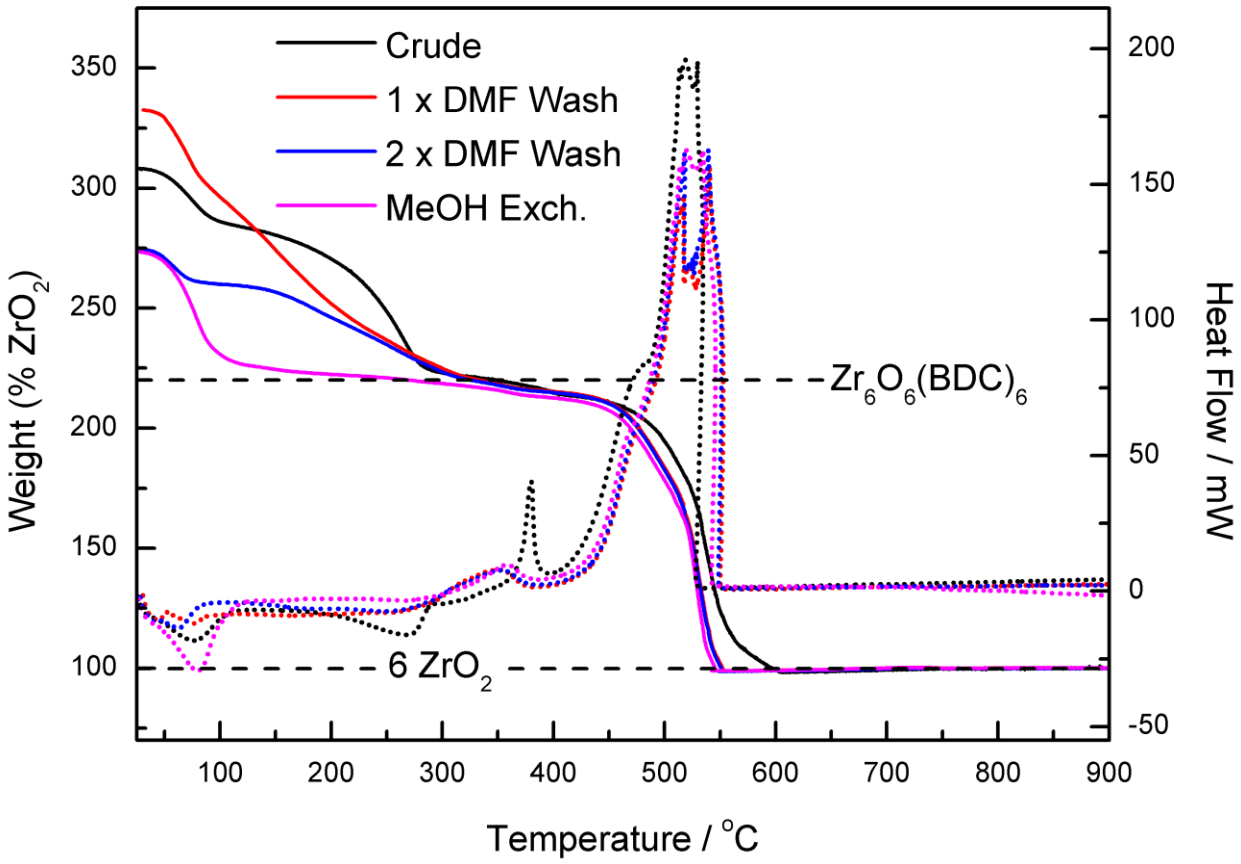

Figure S85: TGA curves (relative to ZrO_2, solid lines) and DSC signals (dotted lines) obtained on UiO-66-220-5:4 at various states of washing (explained on the legend). The position of the theoretical TGA plateau is marked by the horizontal dashed line labelled "Zr_6O_6 $(BDC)_6$".

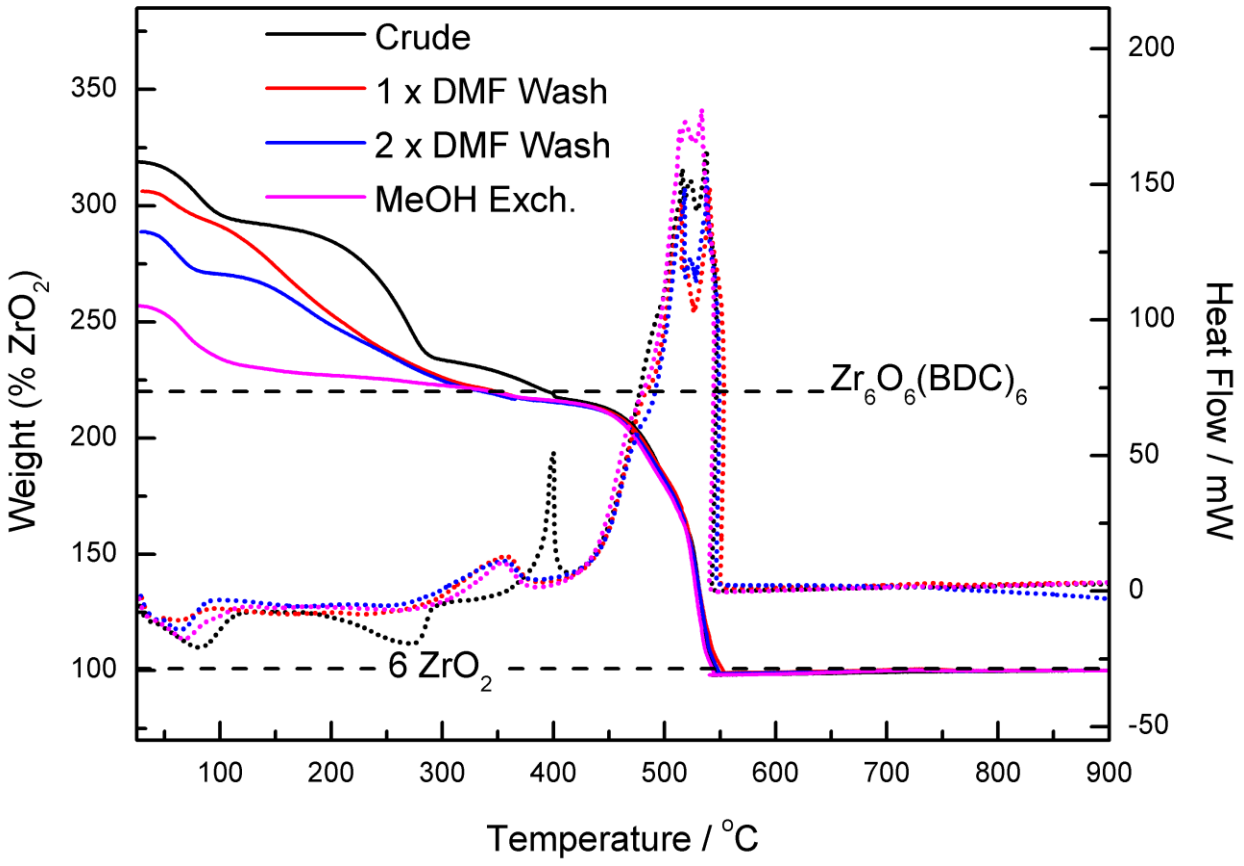

Figure S86: TGA curves (relative to ZrO_2, solid lines) and DSC signals (dotted lines) obtained on UiO-66-220-3:2 at various states of washing (explained on the legend). The position of the theoretical TGA plateau is marked by the horizontal dashed line labelled "Zr_6O_6 $(BDC)_6$".

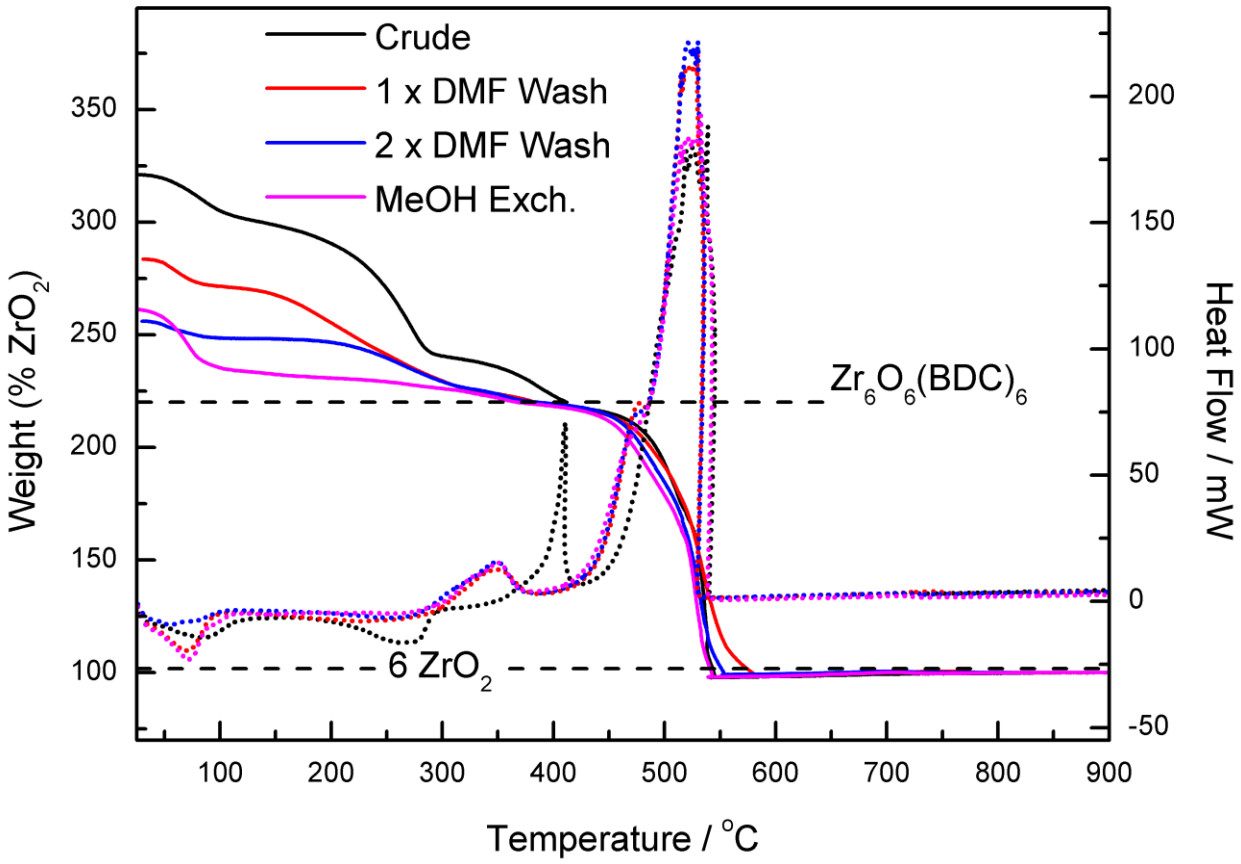

Figure S87: TGA curves (relative to ZrO_2, solid lines) and DSC signals (dotted lines) obtained on UiO-66-220-7:4 at various states of washing (explained on the legend). The position of the theoretical TGA plateau is marked by the horizontal dashed line labelled "Zr_6O_6 $(BDC)_6$".

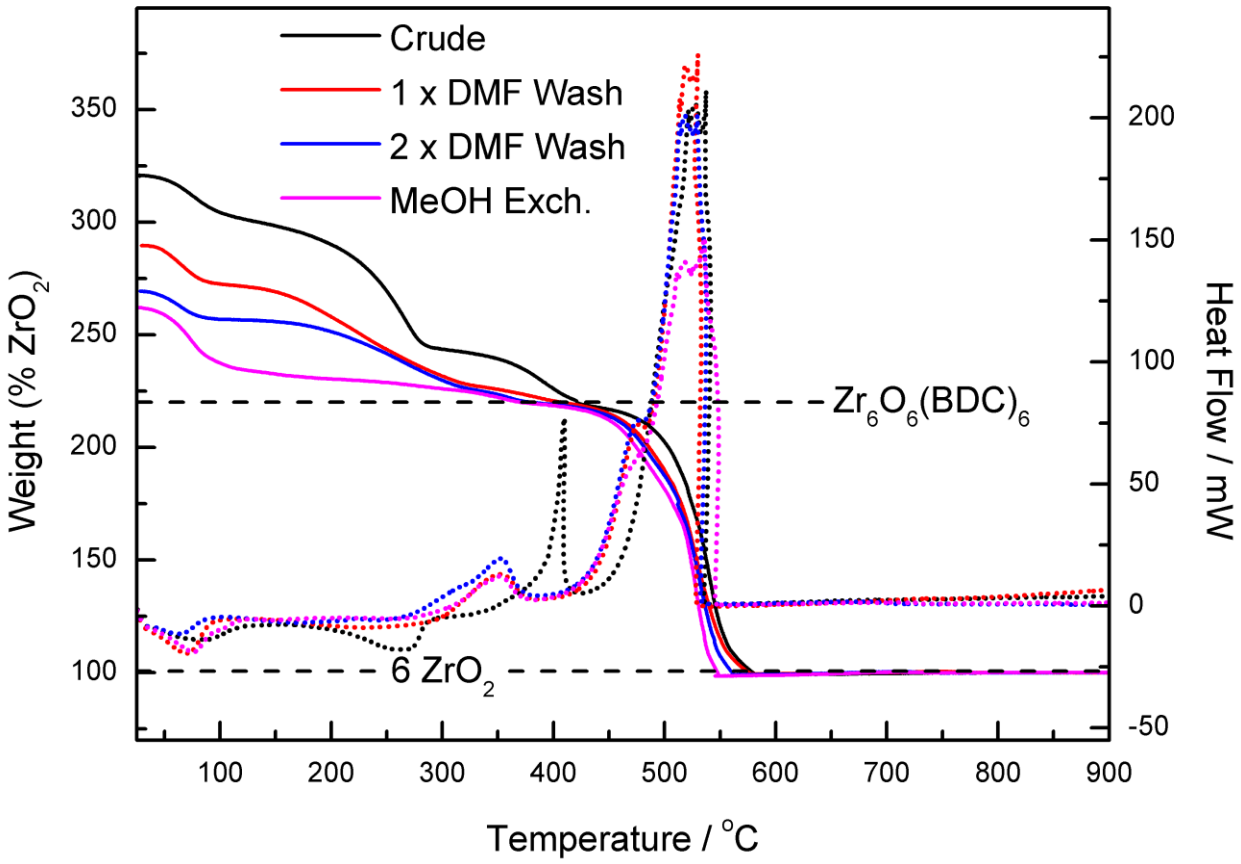

Figure S88: TGA curves (relative to ZrO_2, solid lines) and DSC signals (dotted lines) obtained on UiO-66-220-2:1 at various states of washing (explained on the legend). The position of the theoretical TGA plateau is marked by the horizontal dashed line labelled "Zr_6O_6 $(BDC)_6$".

4. Following Methanol Exchange and Activation via Dissolution / Liquid ^{1}H NMR

Table of Content

4.1. Results on Samples Synthesized at 100 °C

Figures S89, S90, S91, S92, and S93 display the results obtained on samples synthesized with BDC:Zr ratios of 1:1, 5:4, 3:2, 7:4, and 2:1 respectively

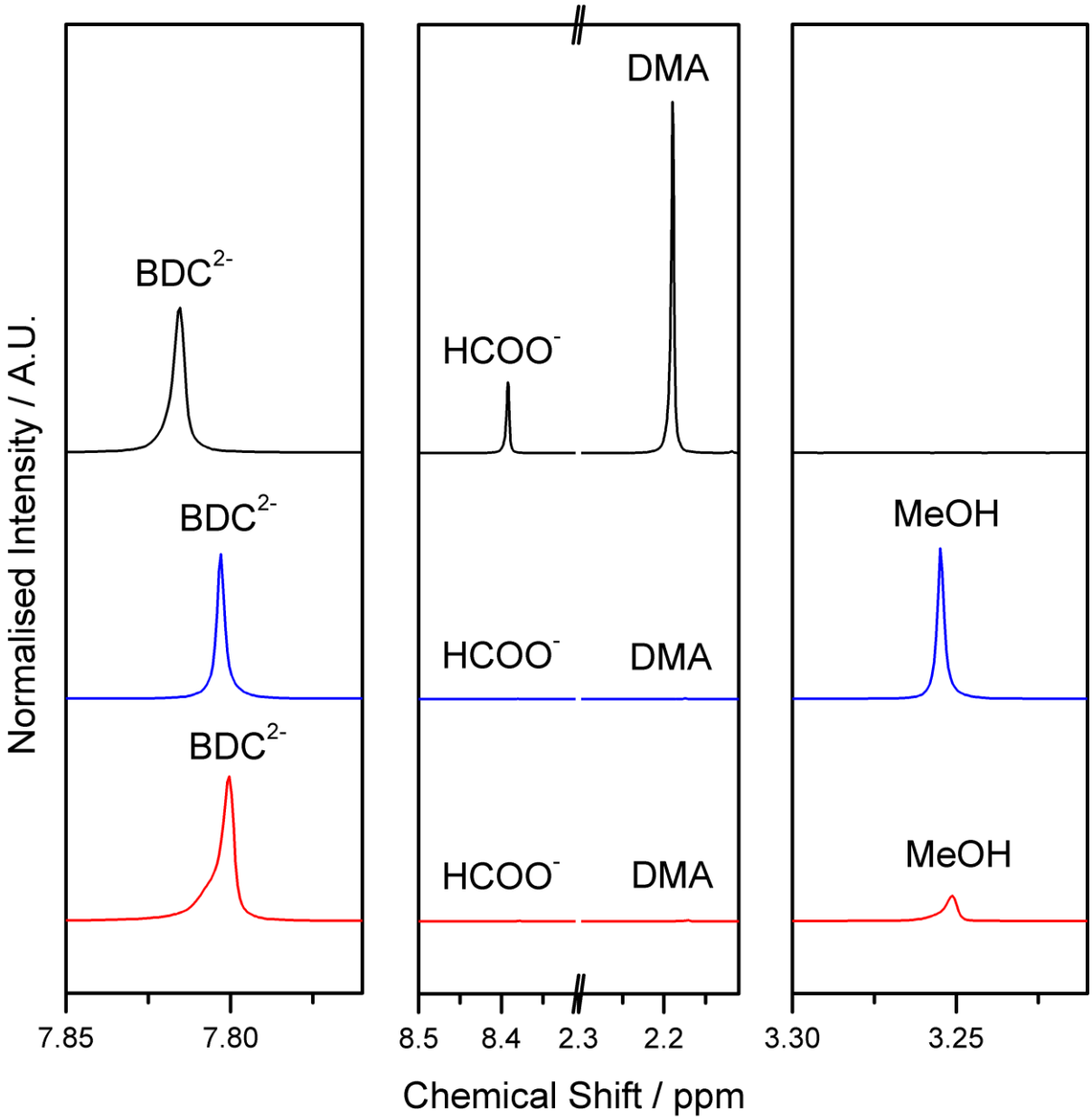

Figure S89: Liquid ^{1}H NMR spectra of digested (1M NaOH in D_2O for 24 hours) samples of UiO-66-100-1:1. Black: 2xDMF washed; blue: methanol exchanged; red: methanol exchanged sample after activation at 150 °C for 2 hours under vacuum. All normalized to the BDC^{2-} signal. Legend: BDC^{2-} = benzene-1,4-dicarboxylate, $HCOO^{-}$ = Formate, DMA = dimethylamine, MeOH = Methanol. The instability of chemical shifts is due to the use of the HDO signal as reference.

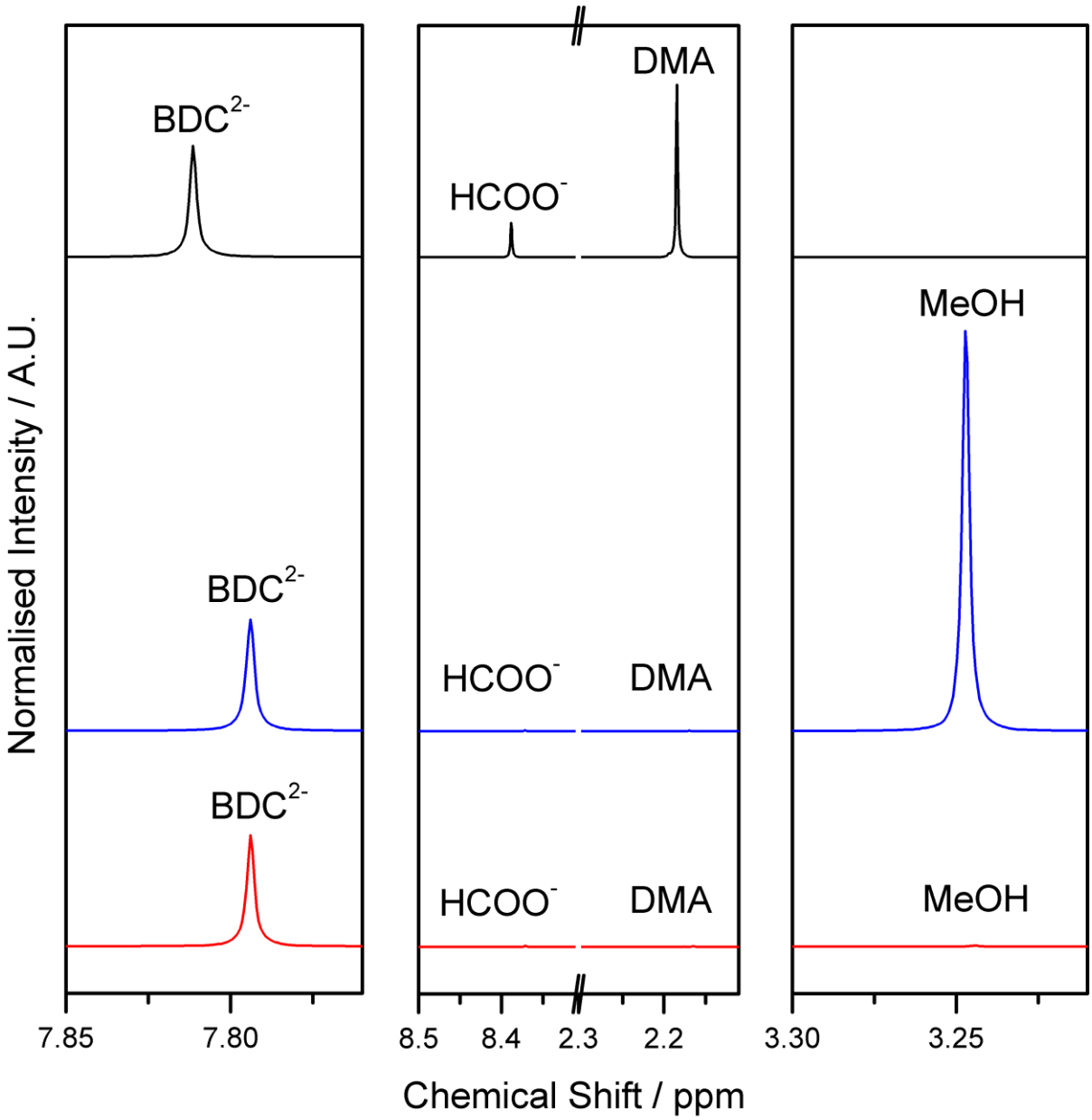

Figure S90: Liquid ^{1}H NMR spectra of digested (1M NaOH in D_2O for 24 hours) samples of UiO-66-100-5:4. Black: 2xDMF washed; blue: methanol exchanged; red: methanol exchanged sample after activation at 150 °C for 2 hours under vacuum. All normalized to the BDC^{2-} signal. Legend: BDC^{2-} = benzene-1,4-dicarboxylate, $HCOO^{-}$ = Formate, DMA = dimethylamine, MeOH = Methanol. The instability of chemical shifts is due to the use of the HDO signal as reference.

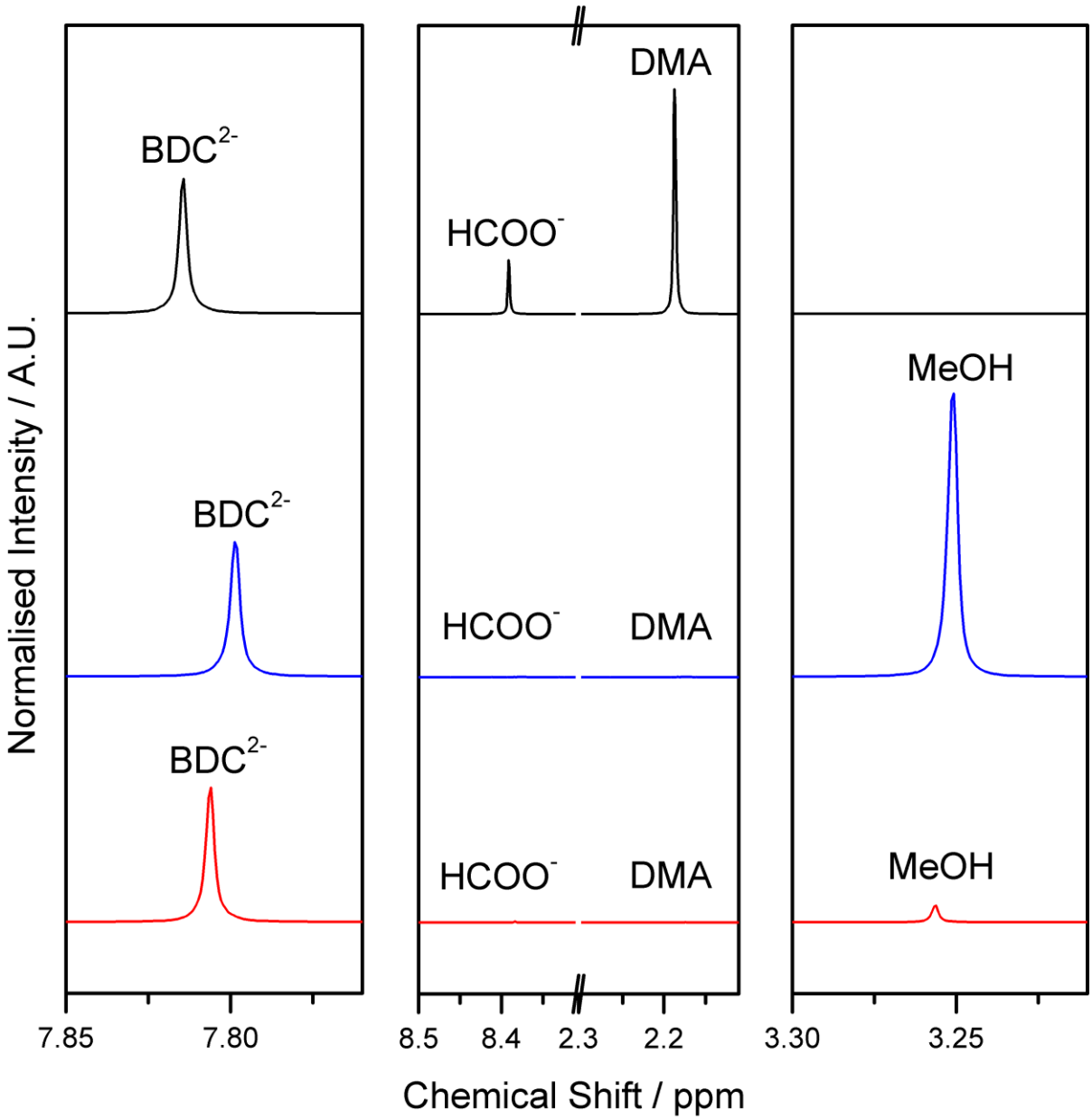

Figure S91: Liquid ^{1}H NMR spectra of digested (1M NaOH in D_2O for 24 hours) samples of UiO-66-100-3:2. Black: 2xDMF washed; blue: methanol exchanged; red: methanol exchanged sample after activation at 150 °C for 2 hours under vacuum. All normalized to the BDC^{2-} signal. Legend: BDC^{2-} = benzene-1,4-dicarboxylate, $HCOO^{-}$ = Formate, DMA = dimethylamine, MeOH = Methanol. The instability of chemical shifts is due to the use of the HDO signal as reference.

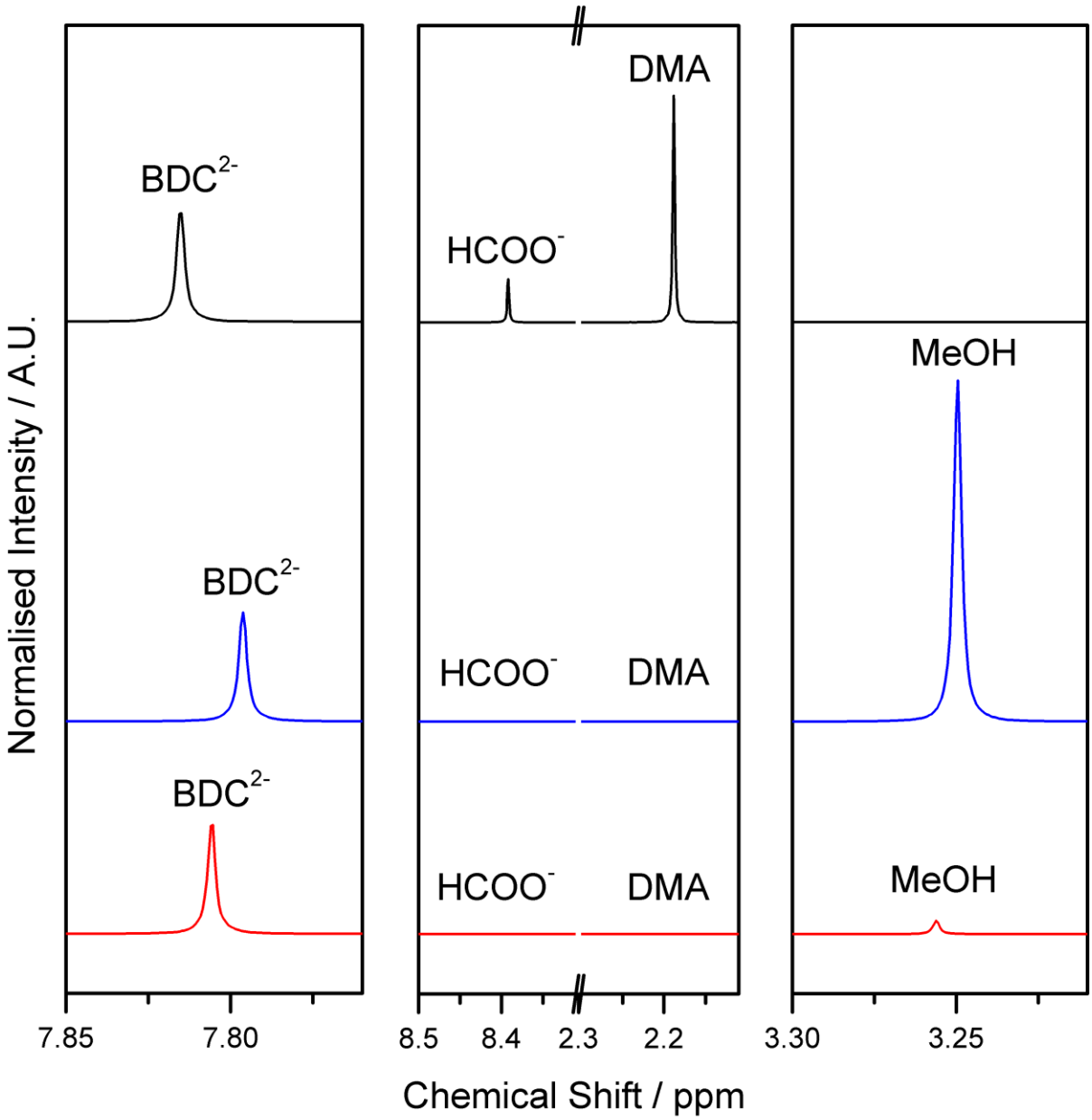

Figure S92: Liquid ^{1}H NMR spectra of digested (1M NaOH in D_2O for 24 hours) samples of UiO-66-100-7:4. Black: 2xDMF washed; blue: methanol exchanged; red: methanol exchanged sample after activation at 150 °C for 2 hours under vacuum. All normalized to the BDC^{2-} signal. Legend: BDC^{2-} = benzene-1,4-dicarboxylate, $HCOO^{-}$ = Formate, DMA = dimethylamine, MeOH = Methanol. The instability of chemical shifts is due to the use of the HDO signal as reference.

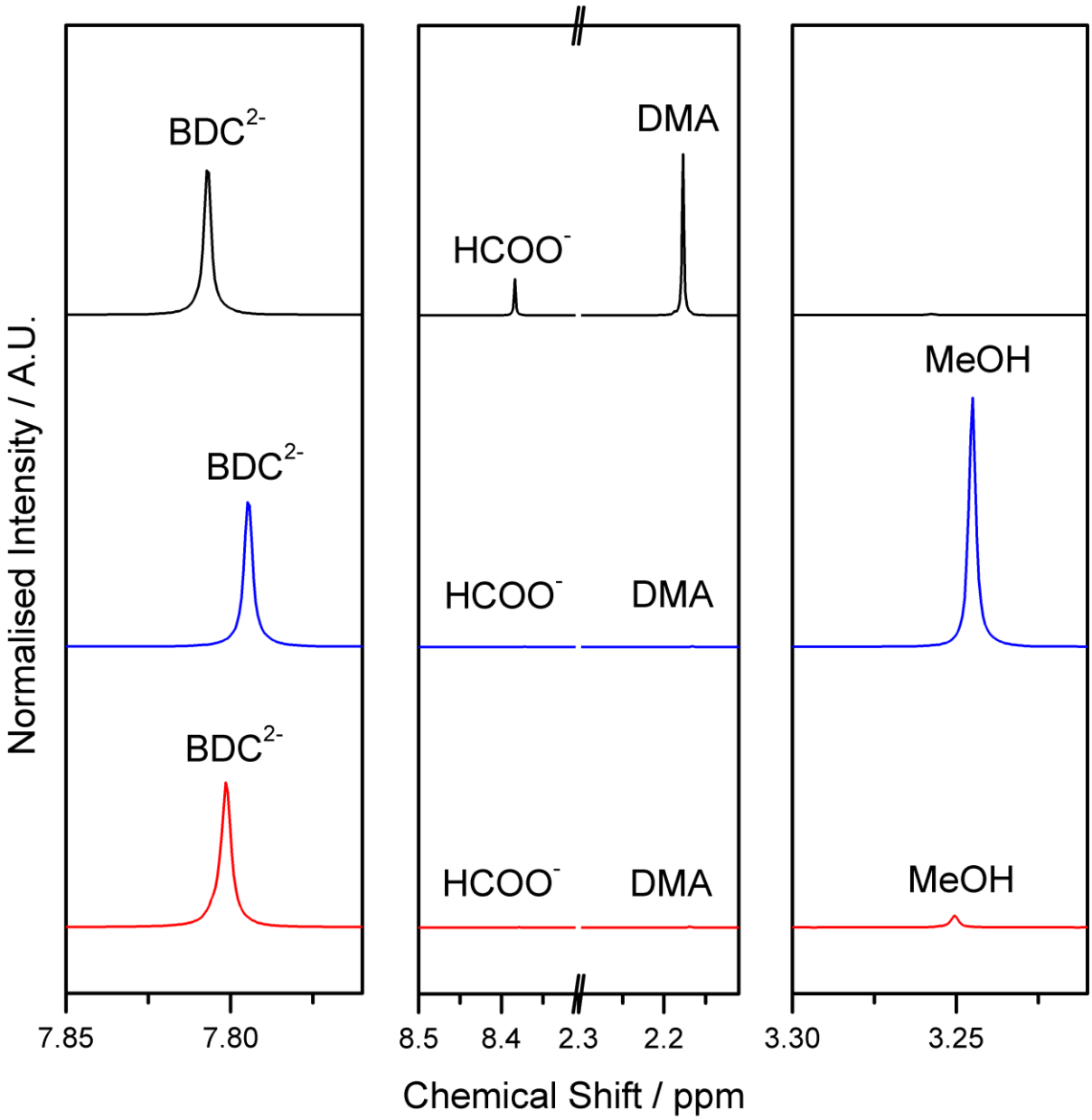

Figure S93: Liquid ^{1}H NMR spectra of digested (1M NaOH in D_2O for 24 hours) samples of UiO-66-100-2:1. Black: 2xDMF washed; blue: methanol exchanged; red: methanol exchanged sample after activation at 150 °C for 2 hours under vacuum. All normalized to the BDC^{2-} signal. Legend: BDC^{2-} = benzene-1,4-dicarboxylate, $HCOO^{-}$ = Formate, DMA = dimethylamine, MeOH = Methanol. The instability of chemical shifts is due to the use of the HDO signal as reference.

4.2. Results on Samples Synthesized at 160 °C

Figures S94, S95, S96, S97, and S98 display the results obtained on samples synthesized with BDC:Zr ratios of 1:1, 5:4, 3:2, 7:4, and 2:1 respectively.

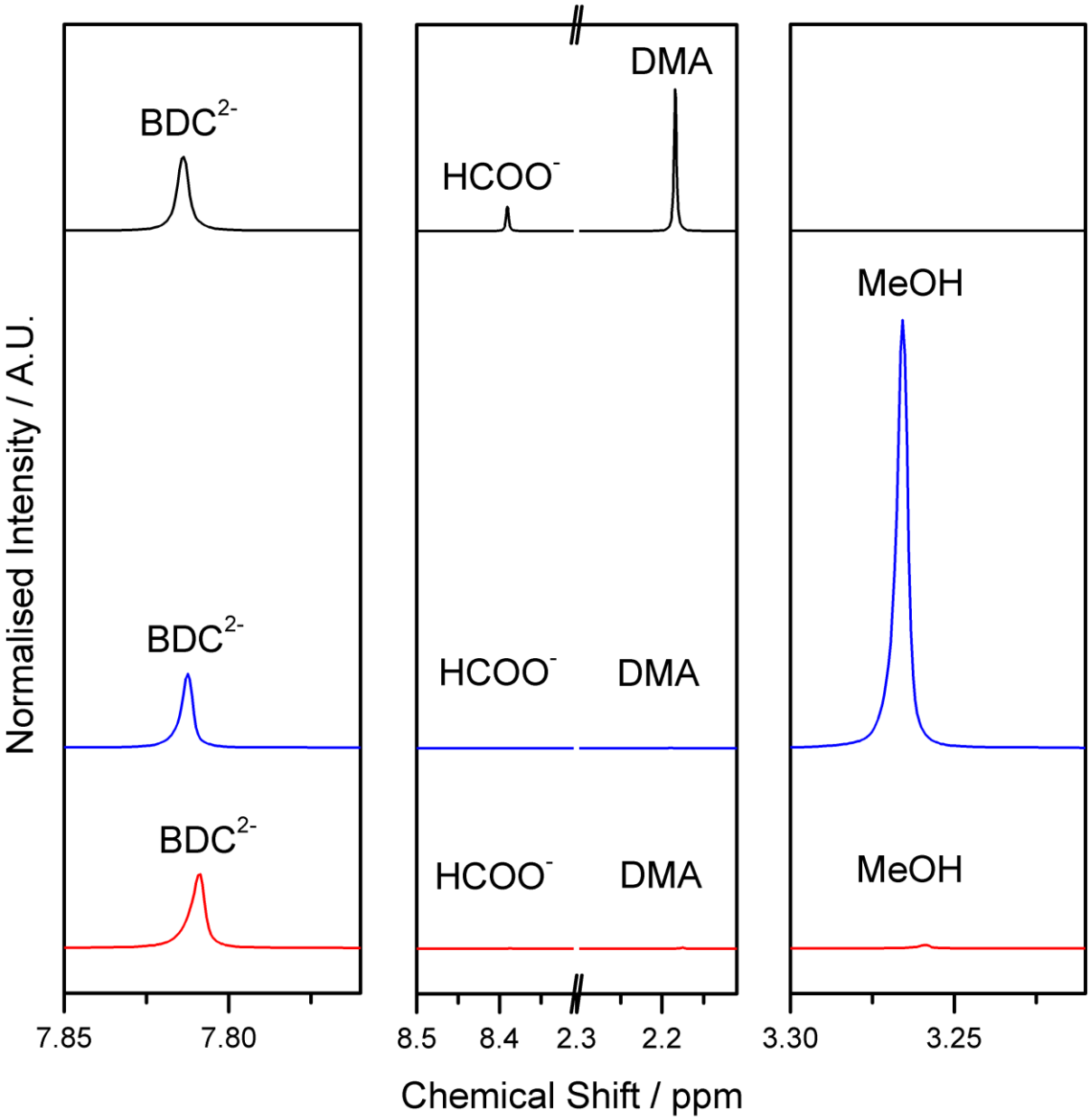

Figure S94: Liquid ^{1}H NMR spectra of digested (1M NaOH in D_2O for 24 hours) samples of UiO-66-160-1:1. Black: 2xDMF washed; blue: methanol exchanged; red: methanol exchanged sample after activation at 150 °C for 2 hours under vacuum. All normalized to the BDC^{2-} signal. Legend: BDC^{2-} = benzene-1,4-dicarboxylate, $HCOO^{-}$ = Formate, DMA = dimethylamine, MeOH = Methanol. The instability of chemical shifts is due to the use of the HDO signal as reference.

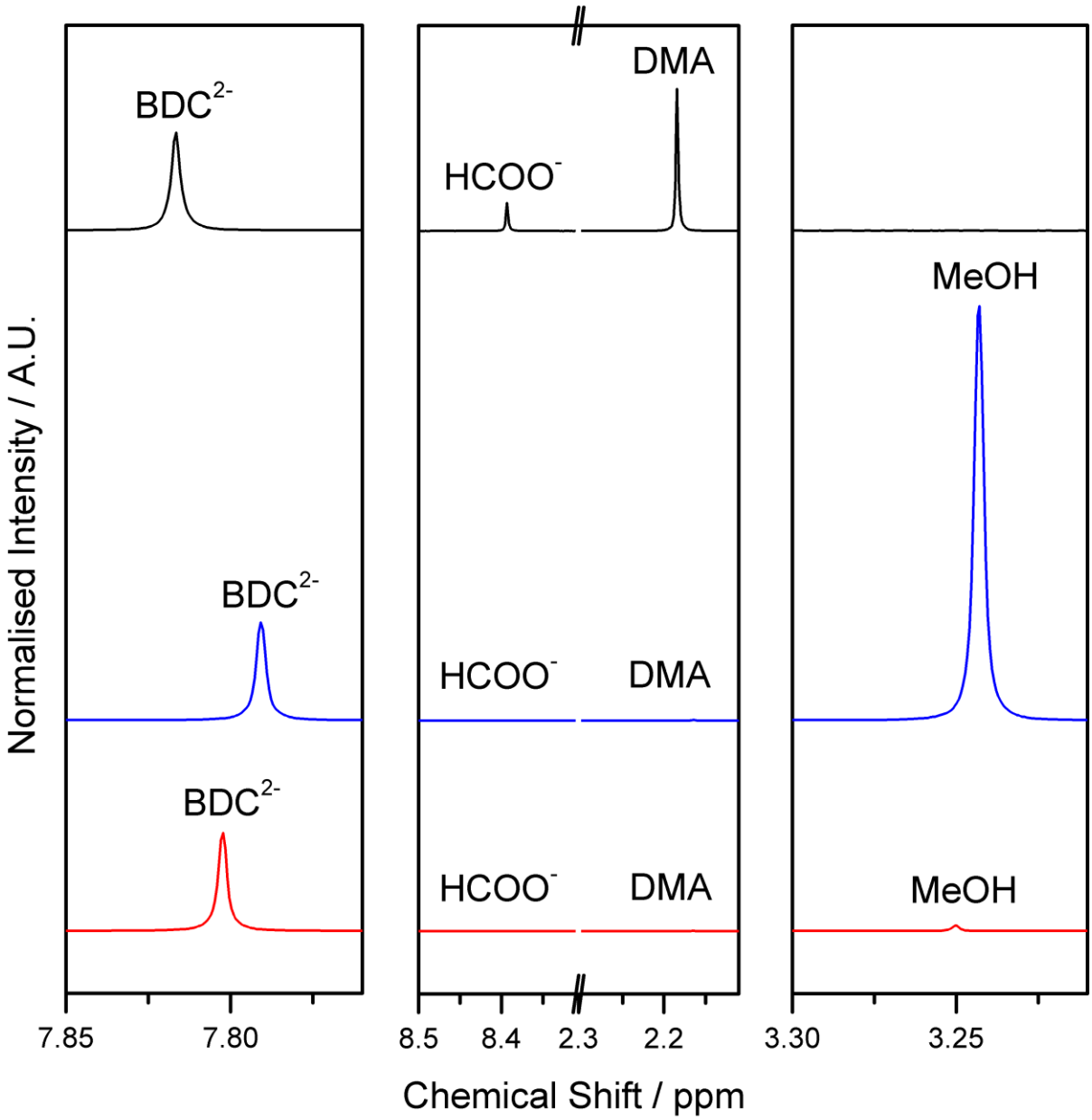

Figure S95: Liquid ^{1}H NMR spectra of digested (1M NaOH in D_2O for 24 hours) samples of UiO-66-160-5:4. Black: 2xDMF washed; blue: methanol exchanged; red: methanol exchanged sample after activation at 150 °C for 2 hours under vacuum. All normalized to the BDC^{2-} signal. Legend: BDC^{2-} = benzene-1,4-dicarboxylate, $HCOO^{-}$ = Formate, DMA = dimethylamine, MeOH = Methanol. The instability of chemical shifts is due to the use of the HDO signal as reference.

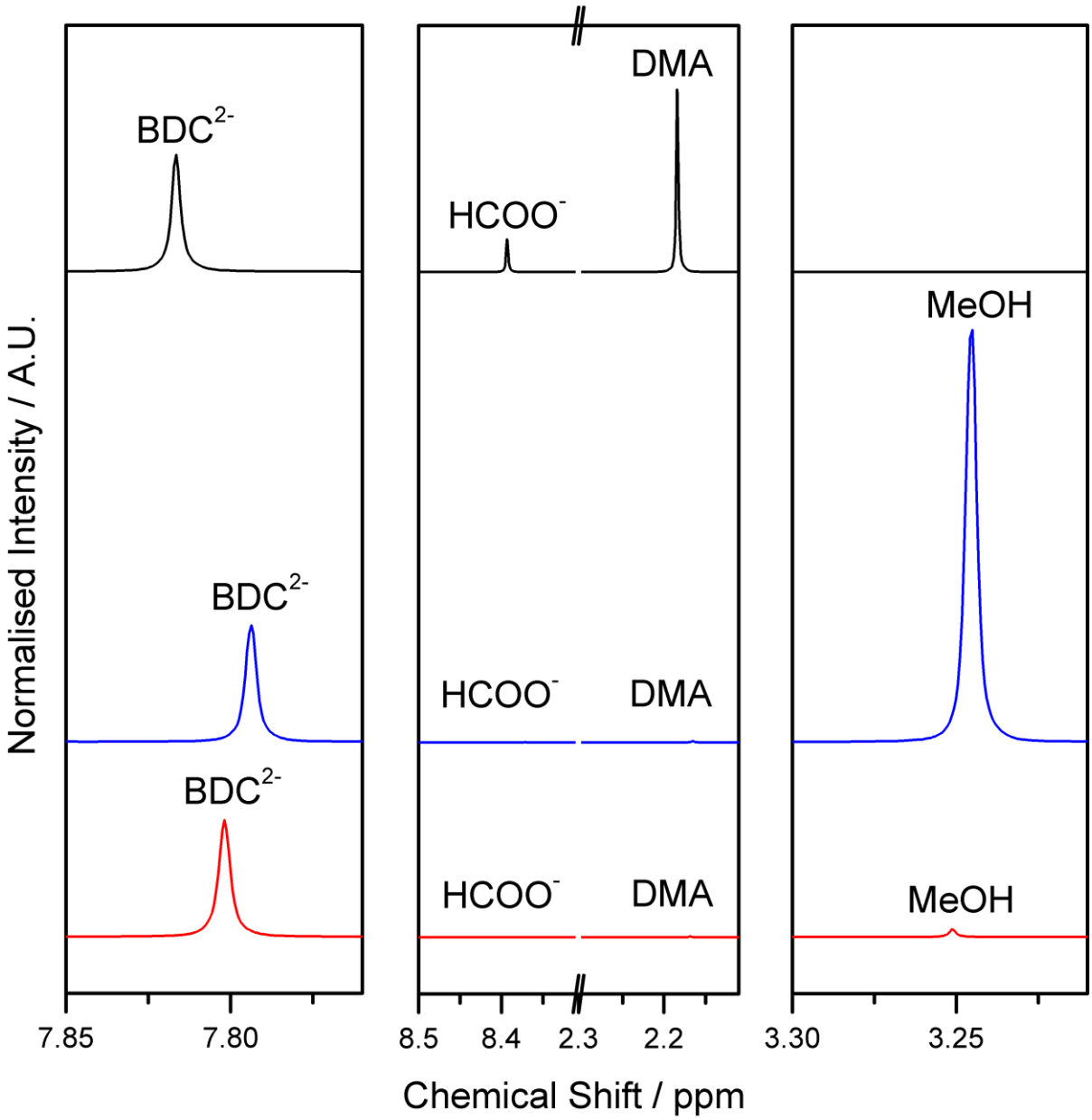

Figure S96: Liquid ^{1}H NMR spectra of digested (1M NaOH in D_2O for 24 hours) samples of UiO-66-160-3:2. Black: 2xDMF washed; blue: methanol exchanged; red: methanol exchanged sample after activation at 150 °C for 2 hours under vacuum. All normalized to the BDC^{2-} signal. Legend: BDC^{2-} = benzene-1,4-dicarboxylate, $HCOO^{-}$ = Formate, DMA = dimethylamine, MeOH = Methanol. The instability of chemical shifts is due to the use of the HDO signal as reference.

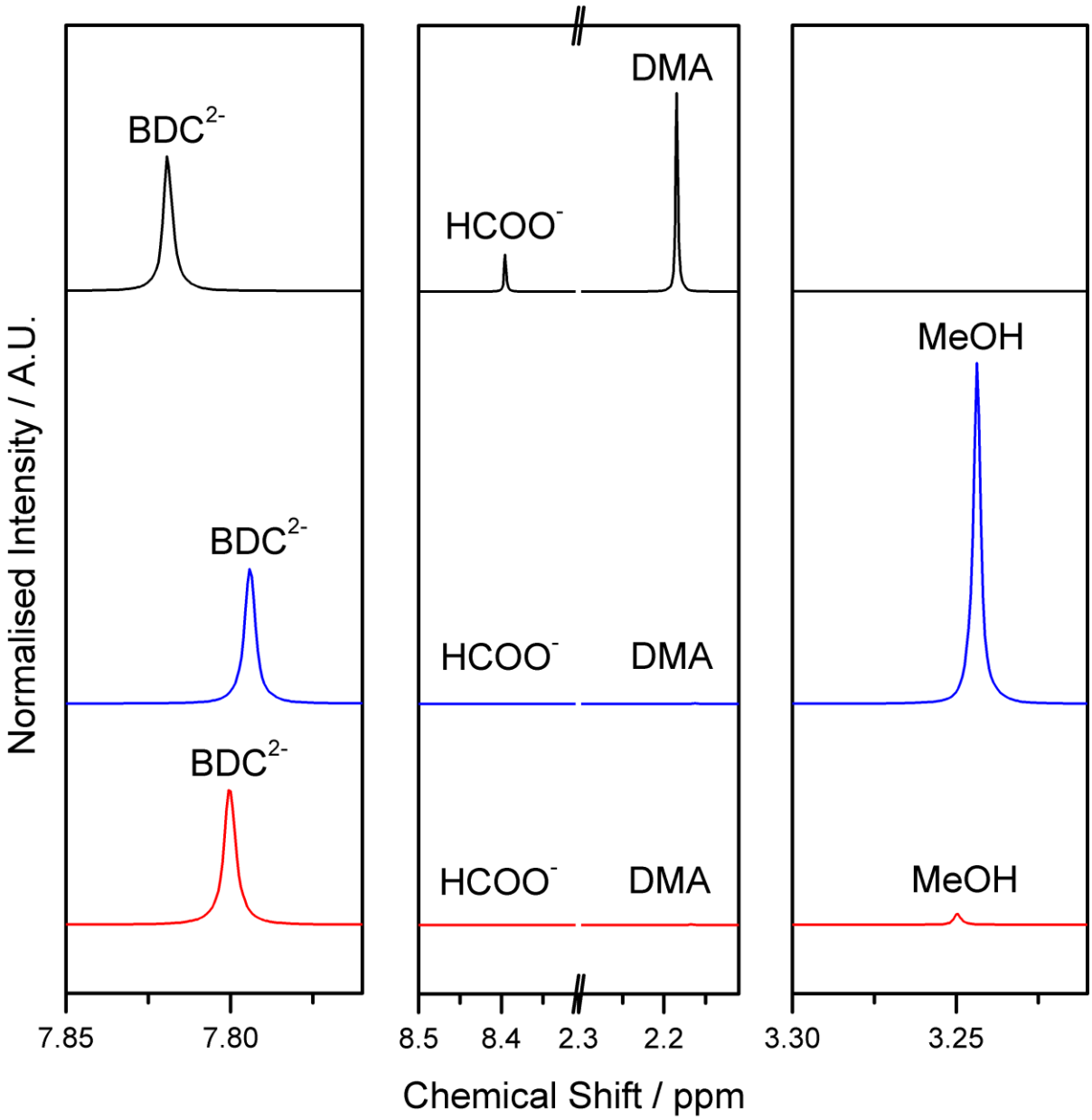

Figure S97: Liquid ^{1}H NMR spectra of digested (1M NaOH in D_2O for 24 hours) samples of UiO-66-160-7:4. Black: 2xDMF washed; blue: methanol exchanged; red: methanol exchanged sample after activation at 150 °C for 2 hours under vacuum. All normalized to the BDC^{2-} signal. Legend: BDC^{2-} = benzene-1,4-dicarboxylate, $HCOO^{-}$ = Formate, DMA = dimethylamine, MeOH = Methanol. The instability of chemical shifts is due to the use of the HDO signal as reference.

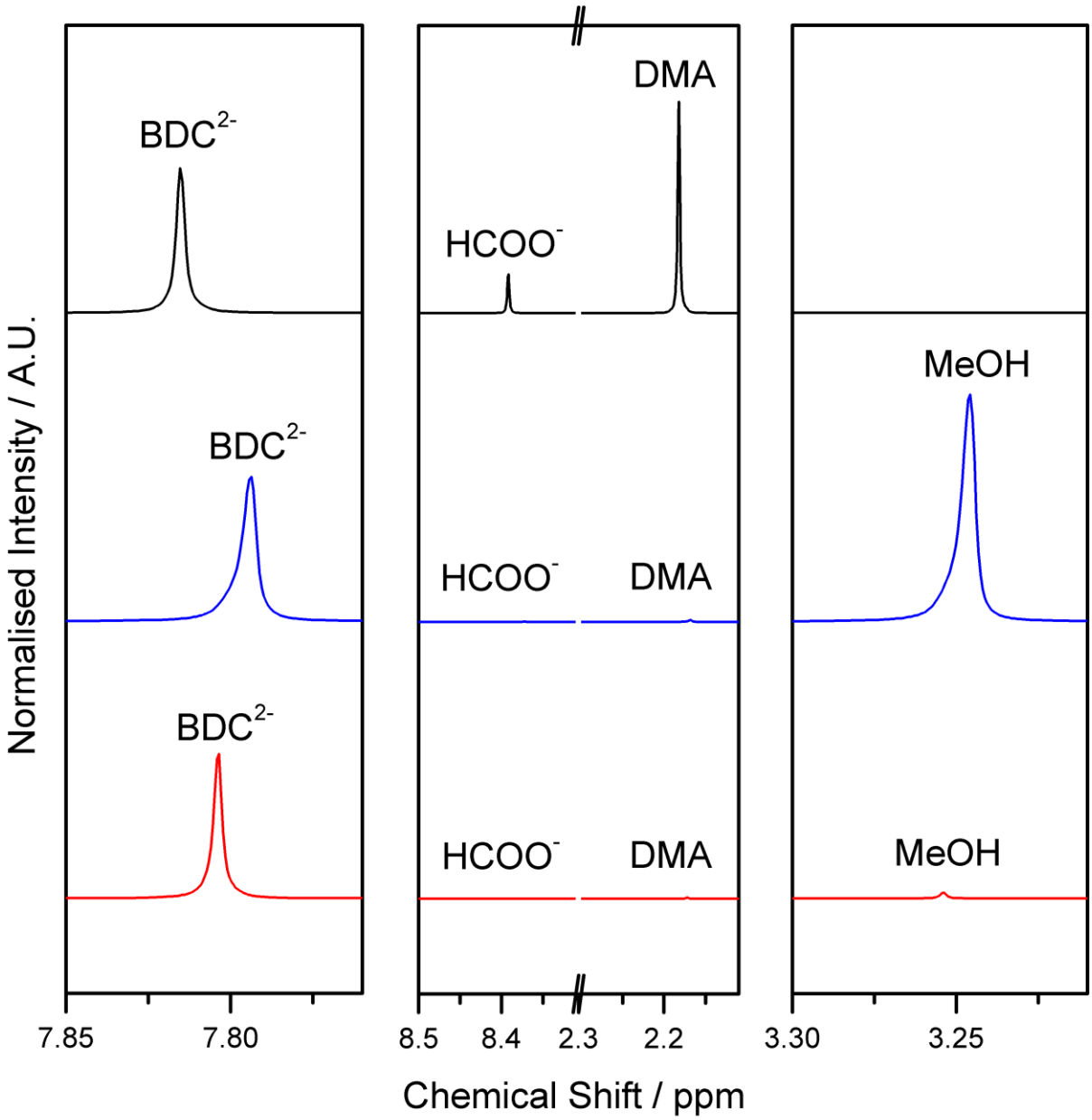

Figure S98: Liquid ^{1}H NMR spectra of digested (1M NaOH in D_2O for 24 hours) samples of UiO-66-160-2:1. Black: 2xDMF washed; blue: methanol exchanged; red: methanol exchanged sample after activation at 150 °C for 2 hours under vacuum. All normalized to the BDC^{2-} signal. Legend: BDC^{2-} = benzene-1,4-dicarboxylate, $HCOO^{-}$ = Formate, DMA = dimethylamine, MeOH = Methanol. The instability of chemical shifts is due to the use of the HDO signal as reference.

4.3. Results on Samples Synthesized at 220 °C

Figures S99, S100, S101, S102, and S103 display the results obtained on samples synthesized with BDC:Zr ratios of 1:1, 5:4, 3:2, 7:4, and 2:1 respectively.

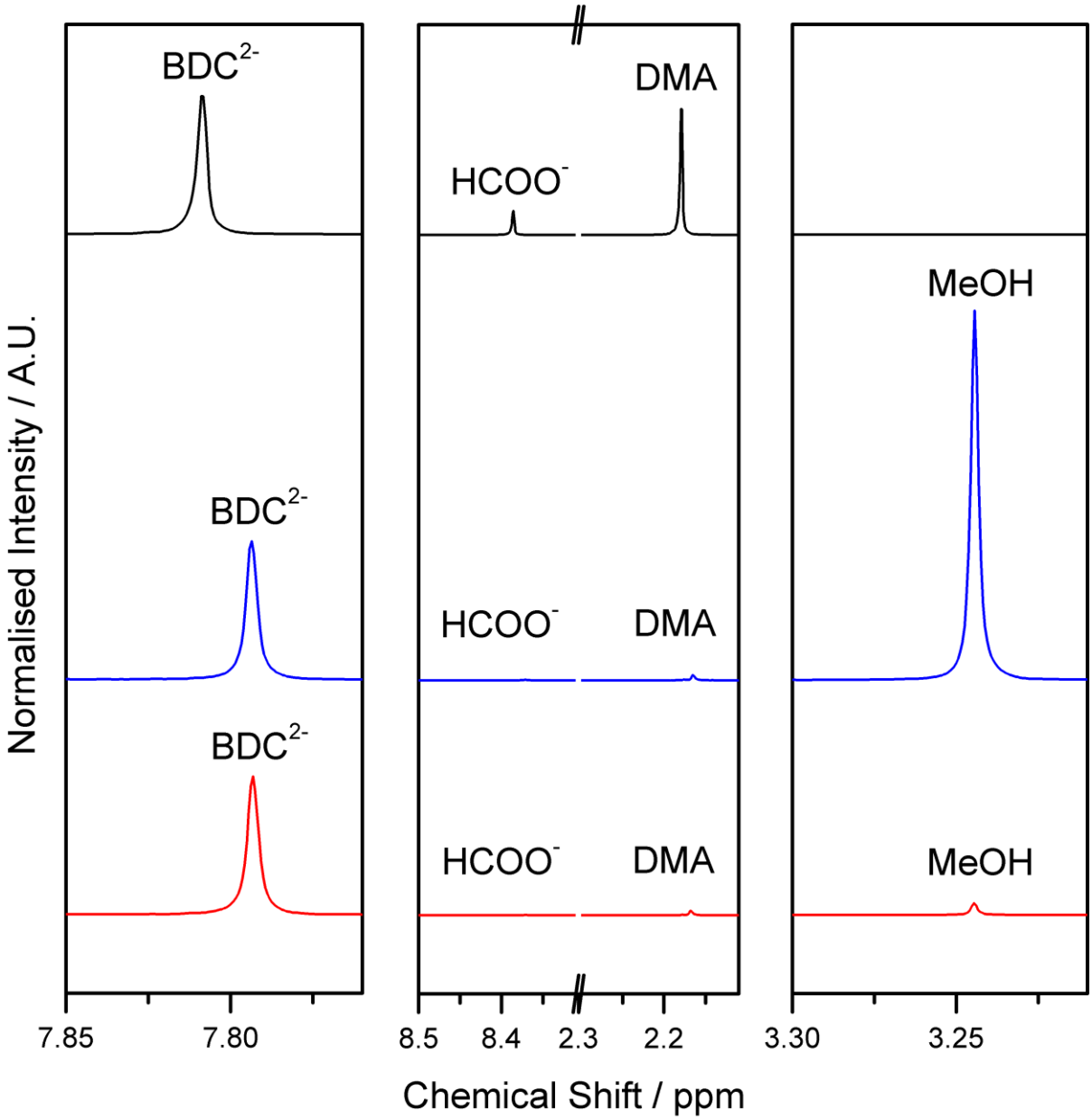

Figure S99: Liquid ^{1}H NMR spectra of digested (1M NaOH in D_2O for 24 hours) samples of UiO-66-220-1:1. Black: 2xDMF washed; blue: methanol exchanged; red: methanol exchanged sample after activation at 150 °C for 2 hours under vacuum. All normalized to the BDC^{2-} signal. Legend: BDC^{2-} = benzene-1,4-dicarboxylate, $HCOO^{-}$ = Formate, DMA = dimethylamine, MeOH = Methanol. The instability of chemical shifts is due to the use of the HDO signal as reference.

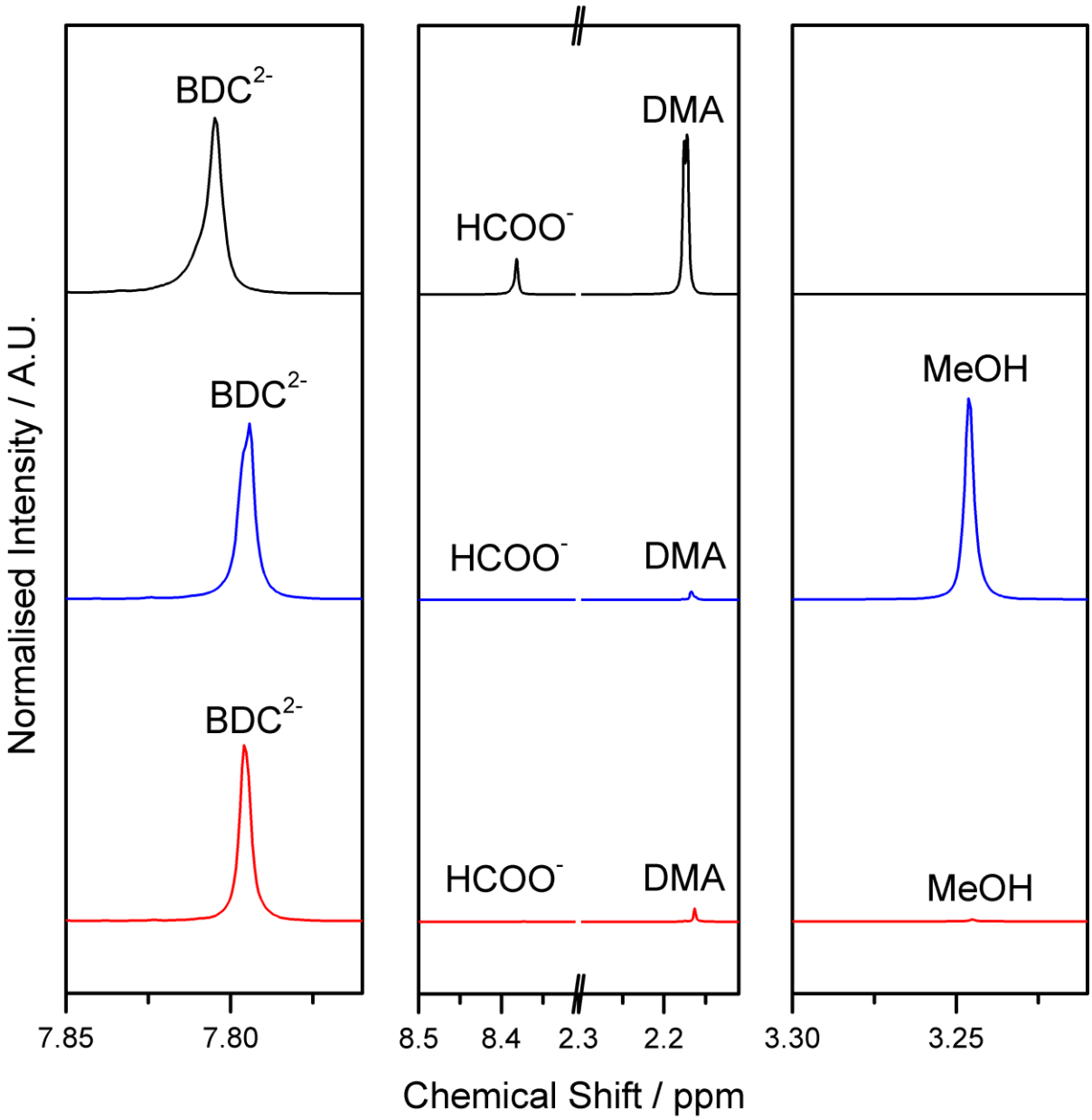

Figure S100: Liquid ^{1}H NMR spectra of digested (1M NaOH in D_2O for 24 hours) samples of UiO-66-220-5:4. Black: 2xDMF washed; blue: methanol exchanged; red: methanol exchanged sample after activation at 150 °C for 2 hours under vacuum. All normalized to the BDC^{2-} signal. Legend: BDC^{2-} = benzene-1,4-dicarboxylate, $HCOO^{-}$ = Formate, DMA = dimethylamine, MeOH = Methanol. The instability of chemical shifts is due to the use of the HDO signal as reference.

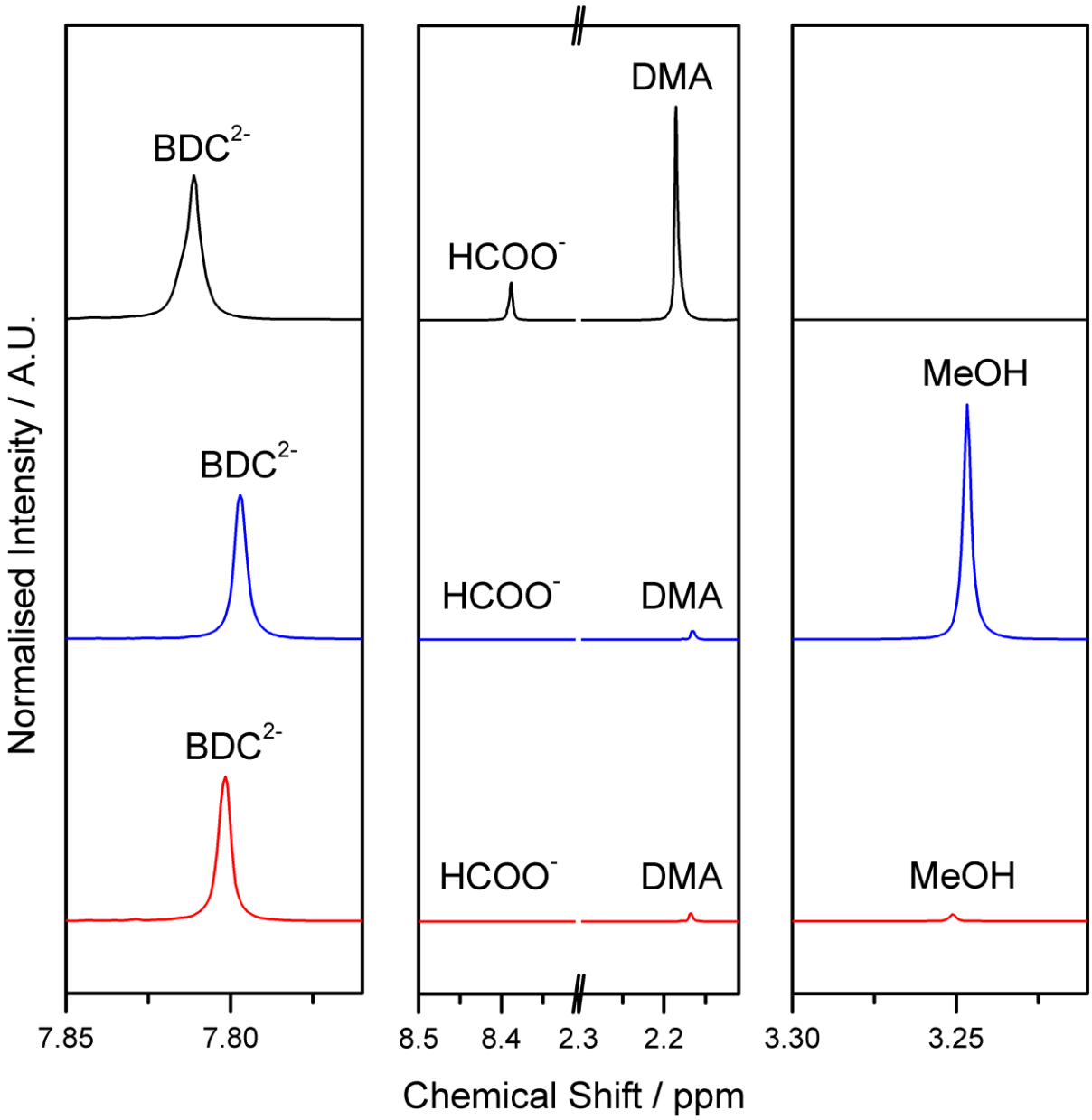

Figure S101: Liquid ^{1}H NMR spectra of digested (1M NaOH in D_2O for 24 hours) samples of UiO-66-220-3:2. Black: 2xDMF washed; blue: methanol exchanged; red: methanol exchanged sample after activation at 150 °C for 2 hours under vacuum. All normalized to the BDC^{2-} signal. Legend: BDC^{2-} = benzene-1,4-dicarboxylate, $HCOO^{-}$ = Formate, DMA = dimethylamine, MeOH = Methanol. The instability of chemical shifts is due to the use of the HDO signal as reference.

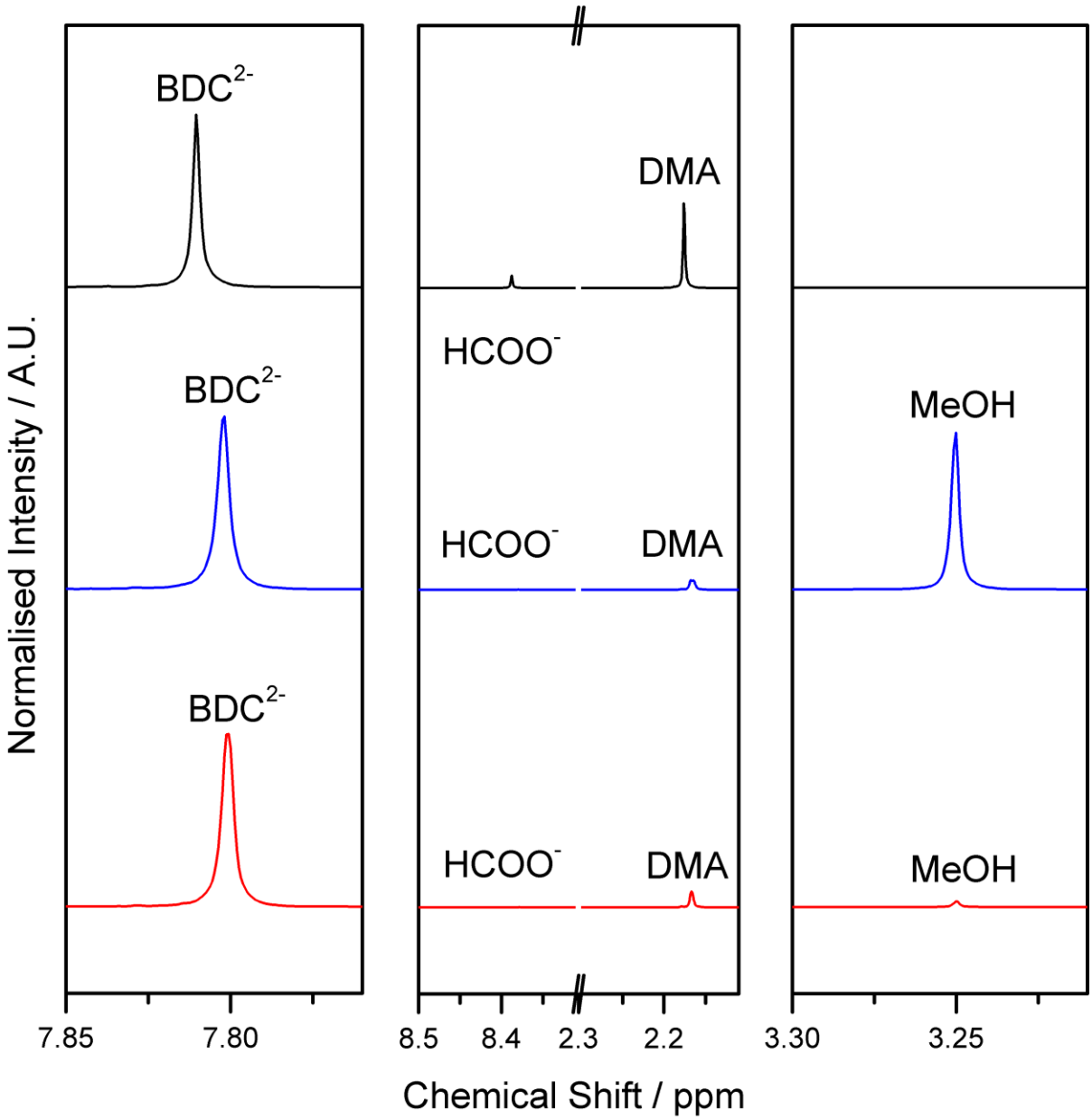

Figure S102: Liquid ^{1}H NMR spectra of digested (1M NaOH in D_2O for 24 hours) samples of UiO-66-220-7:4. Black: 2xDMF washed; blue: methanol exchanged; red: methanol exchanged sample after activation at 150 °C for 2 hours under vacuum. All normalized to the BDC^{2-} signal. Legend: BDC^{2-} = benzene-1,4-dicarboxylate, $HCOO^{-}$ = Formate, DMA = dimethylamine, MeOH = Methanol. The instability of chemical shifts is due to the use of the HDO signal as reference.

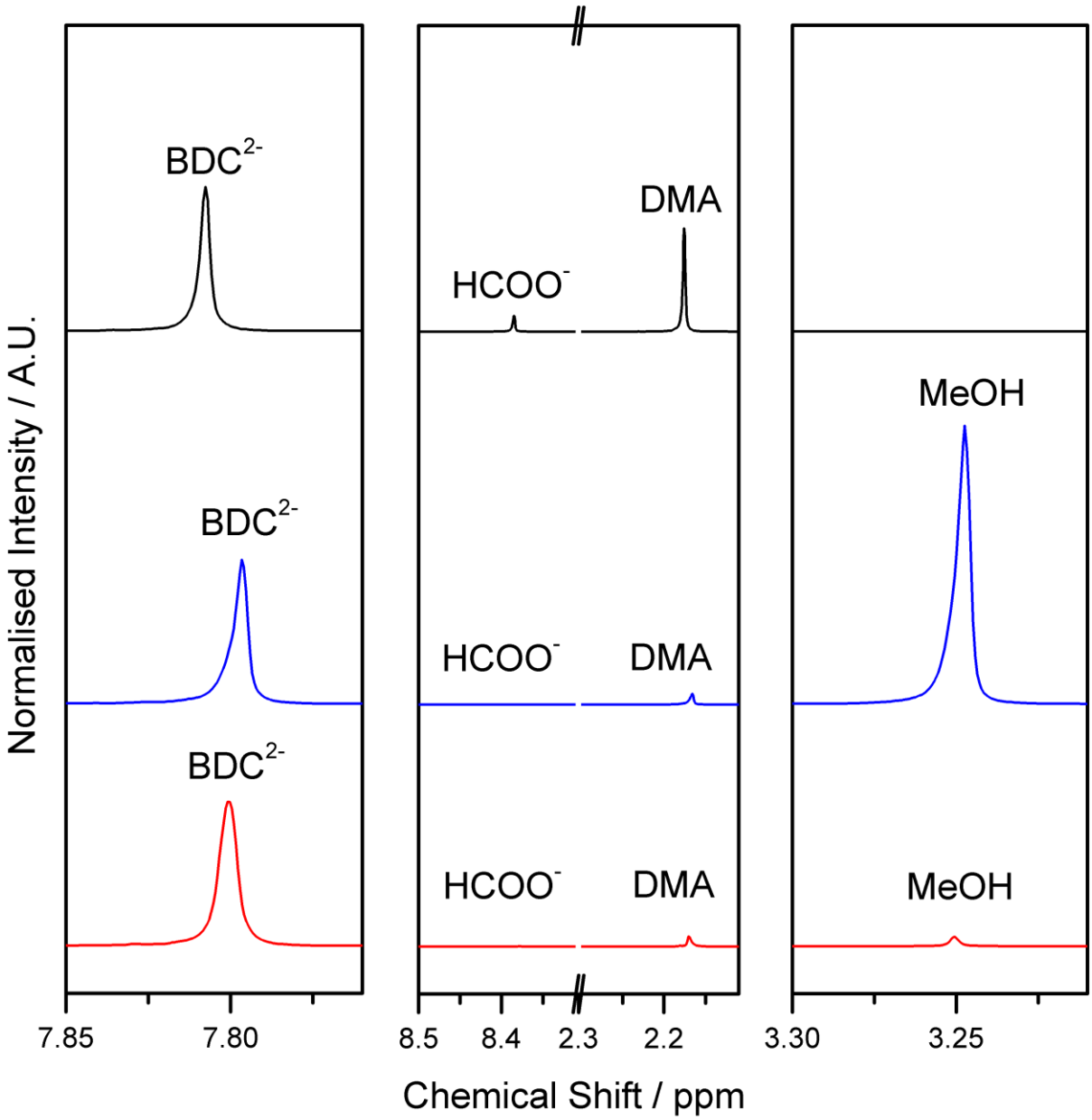

Figure S103: Liquid ^{1}H NMR spectra of digested (1M NaOH in D_2O for 24 hours) samples of UiO-66-220-2:1. Black: 2xDMF washed; blue: methanol exchanged; red: methanol exchanged sample after activation at 150 °C for 2 hours under vacuum. All normalized to the BDC^{2-} signal. Legend: BDC^{2-} = benzene-1,4-dicarboxylate, $HCOO^{-}$ = Formate, DMA = dimethylamine, MeOH = Methanol. The instability of chemical shifts is due to the use of the HDO signal as reference.

L) References

(1) Walton, K. S.; Snurr, R. Q. *J. Am. Chem. Soc.* **2007**, *129*, 8552-8556.
(2) Dovesi, R.; Orlando, R.; Erba, A.; Zicovich-Wilson, C. M.; Civalleri, B.; Casassa, S.; Maschio, L.; Ferrabone, M.; De La Pierre, M.; D'Arco, P.; Noël, Y.; Causà, M.; Rérat, M.; Kirtman, B. *Int. J. Quantum Chem.* **2014**, n/a-n/a.
(3) Valenzano, L.; Civalleri, B.; Chavan, S.; Bordiga, S.; Nilsen, M. H.; Jakobsen, S.; Lillerud, K. P.; Lamberti, C. *Chem. Mater.* **2011**, *23*, 1700-1718.
(4) Maschio, L.; Kirtman, B.; Rerat, M.; Orlando, R.; Dovesi, R. *J. Chem. Phys.* **2013**, *139*.
(5) Katz, M. J.; Brown, Z. J.; Colon, Y. J.; Siu, P. W.; Scheidt, K. A.; Snurr, R. Q.; Hupp, J. T.; Farha, O. K. *Chem. Commun.* **2013**, *49*, 9449-9451.
(6) a) Cavka, J. H.; Jakobsen, S.; Olsbye, U.; Guillou, N.; Lamberti, C.; Bordiga, S.; Lillerud, K. P. *J. Am. Chem. Soc.* **2008**, *130*, 13850-13851; b) Shearer, G. C.; Forselv, S.; Chavan, S.; Bordiga, S.; Mathisen, K.; Bjorgen, M.; Svelle, S.; Lillerud, K. P. *Top. Catal.* **2013**, *56*, 770-782.